ICE FLOE COLLISION UNDER WAVE ACTION IN THE MARGINAL ICE ZONE

LONGJUN GAO

ICE FLOE COLLISION UNDER WAVE ACTION IN THE MARGINAL ICE ZONE

BY

©LONGJUN GAO

A THESIS SUBMITTED TO THE SCHOOL OF GRADUATE
STUDIES IN PARTIAL FULFILMENT OF THE
REQUIREMENTS FOR THE DEGREE OF
MASTER OF ENGINEERING

FACULTY OF ENGINEERING AND APPLIED SCIENCE
MEMORIAL UNIVERSITY OF NEWFOUNDLAND

DECEMBER, 1991

ST. JOHN'S NEWFOUNDLAND CANADA

ISBN 0-315-73329-2

This thesis is dedicated to

my mother

Abstract

This thesis describes a research program to study ice floe collisions under wave action in the Marginal Ice Zone (MIZ). The primary objective of this program was to develop a new interpretation approach for the phenomenon of ice floe collisions in the MIZ and to obtain the floe collision frequency.

The ice floe field was considered to be random while the floe motion was modelled as a stochastic process. A new concept of floe spacing distributions was developed in order to study collision behavior by probability theory. From the aerial photographs of the LIMEX'89 field experiments, and by using probability plot test, ice floe edge distance distributions and centre distance distributions were derived. Both were shown to display Lognormal Distributions.

By analysing water particle displacements in a wave field, a floe collision criterion was obtained. With this criterion, floe collisions were related to floe centre distance, floe edge distance, wave amplitude, and wave period. The floe spacing distributions were introduced into this criterion and the collision probability for a floe during one wave cycle was obtained. Valuable results such as the frequency of collision events within an ice floe field and the number of collisions of one floe during a time period could be derived from this collision probability.

The same procedures were repeated to obtain floe spacing distributions and collision probabilities in different horizontal directions. The results showed that in

two different horizontal directions only small differences existed between the floe spacing distributions, and between the collision probabilities. Ice floe collisions, as well as wave scattering mechanism, made the ice floe field evenly distributed. Eccentric collisions made the collision events happened without dominant directions.

The acceleration data from the LIMEX'89 were analysed to find the number of collision events of the measured ice floes. Predictions of collision frequencies from floe-wave conditions and from acceleration data were significantly different. However, the difference became smaller after the dimensional effects of the floes were considered. The influences of winds were discussed and shown as the primary contribution to the results of higher wave amplitude with smaller collision frequency during a time period obtained from the acceleration data of LIMEX'89.

Acknowledgement

I would like to express my most sincere gratitude and appreciation to my supervisor Dr. Jack I. Clark, for his guidance throughout the research and the preparation of this thesis.

I would also like to express my sincere thanks to Dr. Greg Crocker of C-CORE, for many valuable discussions and useful suggestions. Additional advice and help from Mr. William Winsor are also gratefully acknowledged.

I wish to thank Dr. Leonard M. Lye for his assistance for preparing this thesis. Help from the staff at Centre for Computer Aided Engineering and Ocean Engineering Information Centre is gratefully acknowledged. Helpful assistance of fellow graduate students at Faculty of Engineering and Applied Science is appreciated.

I also like to take this opportunity to acknowledge the financial support through Dr. Clark's research grant, Graduate Studies Fellowship of Memorial University of Newfoundland, and Department Support of Faculty of Engineering and Applied Science, which made this work possible.

The photographic data and ice motion data used in this thesis are from the records of LIMEX'89 phase two conducted from the MV *Terra Nordica*. I would like to thank all the personnel involved in this experiment.

Finally, my dedication is due to my wife Xiang Min, for her constant encouragement and support.

Contents

Page

List of Figures

Page

Page

List of Tables

Symbols

A	Distance from an object to the lens, the flight altitude of the helicopter
B	Distance from the image to camera lens
a	Wave amplitude
C	Ice floe concentration
c	Subscript referring to ice floe centre distance
D	Ice floe diameter
E	Kinetic energy of an ice floe
E_o	Wave energy in open sea
E_m	Kinetic energy of an ice floe with mean diameter
E_x	Wave energy at a penetration distance x
e	Grid dimension *or* Subscript referring to ice floe edge distance
F	Flexural rigidity of ice
$F(z)$	Probability of standard normal variate z
f	Focal length of camera lens
G	Collision probability of two adjacent ice floes during one wave cycle
g	Gravitational acceleration
H_i	Ice Floe dimension in y axis at ith grid
h	Ice thickness

i	Grid order in x axis *or*
	Image height
k	Wave number
L	Ice floe edge distance
L_1, L_2	Edge distances between a small ice mass and two adjacent
	floes
l	Ice floe centre distance
l_m	Mean distance between two water particles
l_1	Horizontal displacement of particle 1
l_2	Horizontal displacement of particle 2
l_3	Instantaneous distance between two water particles
l_c	Relative distance change between two water particles
l_{cm}	The maximum distance change between two ice floes
M	Average floe mass
m	The number of ice floe collisions within an area during
	a period of time
m_o	Linear magnification to describe image size
N	Ice floe number in an area
n	The number of collisions of one ice floe during
	a period of time
o	Length of an object
P	Probability
p	Probability Density Function (PDF)
$p(L)$	Probability Density Function of ice floe edge distance

$p(l)$	Probability Density Function of ice centre distance
$p(l, L)$	Joint probability density function
R	Length ratio of projected pictures to the slides *or* Probability plot correlation coefficient
S	Scale of real length to image length on the projected pictures
T	Wave period
T_p	Wave peak period
t	Time
t_o	Time period
v	The maximum water particle velocity on wave surface
X	Time parameter set for a stochastic process
$\bar{x}$	x coordinate of floe geometric centre
$\bar{y}$	y coordinate of floe geometric centre
z	Standard normal variate
α	Frequency dependent attenuation coefficient
γ	The rank in Blom's plotting position
η	Scale parameter of Weibull distribution
λ	Wave length
μ	Mean of a variable x, or $x^{1/3}$, or $\ln(x)$
μ_x	Mean of Lognormal distribution for variable x
ξ	Shape parameter of Weibull distribution
ρ	Density of sea water
ρ_i	Density of ice
σ	Standard deviation of a variable x, or $x^{1/3}$, or $\ln(x)$

σ_x	Standard deviation of Lognormal distribution for variable x
Ω	The number of values in Blom's plotting position
ω	Wave angular frequency

Chapter 1

Introduction

1.1 Objective and Motivation

The purpose of this research is to obtain the ice floe spacing distributions and to determine the ice floe collision frequency under wave action in the Marginal Ice Zone where the discontinuous ice field meets and interacts with the ocean swell.

Ice floe collision is one of the most active physical processes in the Marginal Ice Zone. This information is required to provide better understanding of the importance of mechanical abrasion and degradation in relation to melting of the ice cover. Earlier studies (LIMEX'89) indicated that the thickness of the ice floes near the ice margin was similar to the thickness of the floes well removed from the edge. This suggests that mechanical degradation as a result of ice floe collisions is a dominant mechanism in comparison to thinning of the ice as a result of melting at either the top or the bottom of the floes.

Ice floe collisions influence the lateral deterioration of ice floes and contribute to the floe size and shape distributions. Through floe collisions, wave energy passing

through the ice floe field is attenuated. This knowledge is important for predicting the environmental loading forces on offshore structures. The potential of an oil spill always accompanies offshore oil industry development. The presence of pack ice will most certainly hinder clean-up efforts. Ice is an excellent containment and transport agent for oil, and the dispersion processes are slow by comparison with the open water process. Therefore, it is necessary to study wave-ice interaction for predicting the dispersal of an oil slick in the Marginal Ice Zone. The knowledge of ice floe collisions is also relevant to vessel movements through cold oceans. The present study can provide insight to the investigation of under-sea acoustic noise in the vicinity of the Marginal Ice Zone. Ice floe collision is one of the major physical processes generating noise in cold oceans. If a better understanding of wave-ice interaction is achieved, measurement of ambient sound may provide a convenient way of remote sensing some of the physical processes that occur over a wide expanse of the ocean surface.

This research is concentrated on ice floe collisions resulting from ocean swells, although other atmospheric and oceanographical factors such as air temperature, ice mechanical properties, winds, and ocean currents also affect floe collisions. The influences of these factors on ice floe collisions will be addressed briefly in relation to the importance of ocean swells.

1.2 The Marginal Ice Zone

The area between the minimum and maximum seasonal ice limits plus the region of the ice margin can be defined as the seasonal ice zone. This seasonal ice zone can be further divided into three main divisions: the Fast Ice Zone, the Shear Zone, and the Marginal Ice Zone. The Marginal Ice Zone forms a special transition zone between two different environments: ice cover and open ocean. The most noticeable feature of the open ocean is the presence of surface waves whose amplitude can be higher than 10 metres. In contrast, the Fast Ice Zone and the Shear Zone, have an almost continuous ice cover, and the vertical displacements of the ice cover are typically of the order of millimeters (Wadhams, 1986). The Marginal Ice Zone is a very dynamic zone where the ice-wave interaction plays an important role in the physical processes.

In the Marginal Ice Zone, sea ice can be subdivided into three characteristic zones: edge zone, transition zone, and interior zone in the direction from open water to the shore. In the edge zone, ice floes are about ten metres across and of uneven thickness. In the transition zone, ice floes are somewhat larger and smoother than those in the edge zone. In the interior zone, ice floe size can be over 100 metres (Squire, 1983a).

Some marginal ice zones have distinct ice floe distribution features such as the Labrador Ice Margin where bands and patches of ice floes are intermixed with bands and patches of open water. The Labrador Current forms a classic marginal ice zone exposed to the full force of the North Atlantic wave action. Ice which

forms in the Davis Strait is carried southward and joined by heavy floes from Foxe Channel coming out of Hudson Strait. The combined ice stream is carried south by the Labrador Current and reaches the east coast of Newfoundland (by January-February). Its extreme limits, attained by March-April, tend to coincide with the edge of the Current so that by the end of winter a wide seaward tongue of ice has formed off Newfoundland, corresponding to the eastward turn of the Labrador Current (Wadhams,1986). It was within this ice field that the LIMEX'89 experiment was conducted. Data from LIMEX'89 were utilized in the present study.

It is clear that the appearance of an Marginal Ice Zone is strongly influenced by local wave conditions in addition to other oceanographic and climatic factors. And the waves themselves are affected by the ice floes encountered during their passage through the floes. The waves in a continuous ice cover appear as flexural-gravity waves with dispersion behavior and amplitude different from their parent waves in open water. The scattering mechanism strongly influences waves in a discrete ice field. The ice floes tend to act as a low pass filter allowing low frequency waves to penetrate but inhibiting the propagation of higher frequencies (McKenna and Crocker, 1991).

1.3 The Phenomena of Ice Floe Collision

Large size ice floes tend to be broken into smaller ones through flexural failure induced by waves. The floes in turn modify the nature of the surface wave field. When the ratio of floe size to wave length is sufficiently small, the flexural response of the floe is negligible and the floe will move like a rigid body acted upon by ocean waves. Also, when this ratio is small enough, water particle-like motion occurs to the ice floe, which means the floe moves so as to exactly follow the motion of the ocean surface (Squire, 1983a; Lever et al, 1984; Wadhams and Cowan, 1984). Ice floes which occupy different positions, have alternate phases corresponding to the ocean waves. Under the action of ocean waves, the floes will collide with each other because of these phase differences.

The influence of wave action on floe collisions is clear and significant under certain environmental conditions. Even in a clearly diverging ice floe field, collisions can be intensive (McKenna and Crocker, 1991). The pack ice behaviour has been studied by treating the collision as an elastic collision between circular floes (Shen et al, 1987). However, several visual observations of floe collisions in the Marginal Ice Zone showed that the collisions were inelastic (Rottier, 1990; McKenna and Crocker, 1991). This is particularly true for LIMEX'89 which was carried out in April when the ice floes were close to melting temperature and quite ' soft '.

Ice floe collisions reduce floe size and cause wave energy losses. This can be certified by the brash ice mass among ice floes. Direct observations of ice floe damage during floe collisions confirm that ice floe collisions play an important role

in the process of ice growth, melt, and deterioration in and around the Marginal Ice Zone. Quite often a large amount of brash ice exists among ice floes. The form and structure of these brash ice masses indicate that most of them are not formed locally due to air temperature change. Instead they are formed by ice floe collisions. The impacts of neighbouring floes produce the brash ice and reduce the floe size (Rottier, 1990). Wave energy losses occur in this process due to collisions of the ice floes.

So far, no laboratory experiment of floe collisions has been performed. This is partly because of the fact that it is very difficult to chose a suitable model material to conduct the experiment under laboratory condition. Fortunately, a few field experiments have been carried out and they provide valuable information about ice-wave interaction in the Marginal Ice Zone. These field experiments were carried out in the North Atlantic Ocean off Newfoundland, the Bering Sea, and off Greenland (Wadhams et al, 1988; Eid et al, 1989; Rottier, 1990; McKenna and Crocker, 1991). They provide the ice floe morphology and the dynamic responses of ice floes to ocean waves, and form the basis for studying ice floe collision behaviour in the Marginal Ice Zone.

1.4 Proposed Approach to the Problem

The present study of ice floe collisions under wave action is restricted to small ice floes, with rigid bodies and perfect water particle-like motions acted upon by small amplitude waves in deep water. The ice floes therefore can be described by their size, thickness, concentration, and spacing distances. The ocean waves can be simply described by their amplitude and frequency. The mechanical and thermodynamic properties of ice floes are not involved in the following approach.

In order to obtain the ice floe collision frequency for a specific ice floe field, it is necessary to acquire continuous data of wave and ice floe conditions over the whole area. But, it is very difficult to measure the wave and ice floe parameters in this way. For the wave conditions and the motions of a few selected ice floes at some specific locations of an area, however, continuous measurements are possible and a time dependent process can be derived. Because floe size, thickness, shape and location are variable, any extrapolation of the results obtained from the limited number of measured floes is dangerous. For example, we can not obtain the number of floe collisions within an ice floe field simply by multiplying the collision number of a measured floe with the floe number (defining floe number as the number of floes) of the ice field. To solve the problem, an approach was developed to consider the movement of ice floes as a stochastic process and the ice floe field as a random field. Then the probability of collision occurrence under a significance level for limited number of floes was derived from probability theory. This probability could be extrapolated to get the collision frequency of the whole ice floe field during a period of time. A detailed discussion of this process can be found in the following

chapters.

Ice floe collision was demonstrated to occur when the changes in spacing distances between neighbouring floes, due to wave motion, became large enough. Through theoretical analysis, the ice floe collision criterion was obtained based on Airy Linear Wave Theory under the assumption that relatively small ice floes moved as water particles in a wave field. This criterion related floe collisions to ice floe spacing distances, wave amplitude, and wave frequency.

The field experiment LIMEX'89 provided valuable data for the present research. From the aerial photographs of the ice floe field, ice floe spacing distributions were derived. Combining the distributions and the floe collision criterion, one could acquire the collision probability for one floe in one wave cycle. The collision frequency within an ice floe field and the collision number of one floe during a specified time period were then derived.

Ice floe collision events were identified from the abnormal acceleration traces of LIMEX'89 ice motion package data. By counting the collision events, the collision frequencies of the packaged floes were derived. These collision frequencies could be then compared with the results from the approach based on floe spacing distributions and the collision criterion. The same procedures were repeated in different horizontal directions to find whether or not the floe spacing distributions and collision frequencies had dominant directions.

Chapter 2

Literature Review

2.1 Experiment of Ice-Wave Interaction in the Marginal Ice Zone

The penetration of ocean waves into icefields was recorded as early as the 1820's. The first navigators to encounter the Arctic and Antarctic ice margins noted waves and swells within ice fields at rather large distances from the ice cover edge. A series of observations were made later from ships, stations on ice cover, and permanent stations established on coasts. The results showed that longer period swells could penetrate through an ice field for greater distances than shorter period swells, and wave energy decayed as the waves penetrated the ice field. Efforts were made to get the attenuation rate and the wave behaviour in ice fields experimentally and theoretically. Mainly because of scaling and constitutive problems, few definite conclusions could be drawn from laboratory tank experiments. However, a number of such experiments were carried out (Ofuya and Reynolds, 1967; Henry, 1968; Wadhams, 1973). The achievements of the ice-wave interaction study were gained mainly by theoretical studies and field experiments.

Some conclusions were drawn from field experimentation during the last twenty years. Wadhams carried out a series of observations by sonar from a submerged submarine near the ice edge in the northern Greenland Sea (Wadhams 1972, 1978). Measurements also were conducted with an airborne laser profilometer off Newfoundland (Wadhams, 1975). All results showed an exponential wave decay with penetration distance, according to an equation of the form:

$$E_x = E_0 \exp(-\alpha x), \tag{2.1}$$

where α is a frequency dependent attenuation coefficient, E_x is the energy density of a spectral component centred at frequency ω at a penetration distance x, and E_0 is the original wave energy density in open sea.

A more complete series of ice-wave observations began in 1978 and involved several locations: North Atlantic Ocean off Newfoundland, the Bering Sea, and off east Greenland (Goodman et al, 1980; Squire and Moore, 1980; Wadhams et al, 1986; Wadhams et al, 1988; Eid et al, 1989; Rottier, 1990; McKenna and Crocker, 1991). Wave buoys were inserted into the open water between floes at different distances from the ice edge to measure the wave decay . The flexural, heave, surge and tilt responses of ice floes were obtained by putting accelerometers, strainmeters, gyros, and compasses onto the ice floes. The two kinds of measurements were combined to study ice-wave interaction in the Marginal Ice Zone. The thicknesses of the experimental floes were determined by coring, and floe size distributions and concentrations were derived from aerial photographs and video records from helicopters. The results of these experiments highlighted some regular patterns relating to: wave energy decay within an ice field, ice floe dynamic behaviour under

wave action, wave scattering among ice floes, wave penetration and reflection at ice edges, ice floe flexural properties, and ice floe collision behaviour under wave action.

To date the growth of ocean waves within an ice cover has received less attention. The wave growth by wind acting on the sea surface is severely hampered by a continuous ice cover, although not entirely inhibited (Crocker and Wadhams, 1988). Experiments were also conducted to study wave growth in discontinuous ice and these results showed that wave growth decreased rapidly as the percentage of the ocean covered by ice increased (Masson and LeBlond, 1989). It is reasonable to state that a large percentage of waves, measured within an ice field, is not generated locally, but has propagated to that point from the open ocean.

2.2 The Flexural-gravity Waves

Theoretical interest in flexural-gravity waves, or so called ice-coupled waves began over a century ago by Greenhill (Wadhams, 1988). He suggested that the ice could be represented by a thin elastic beam and derived a dispersion equation. Subsequently, many researchers have done extensive theoretical work on the theory of flexural-gravity waves (Wadhams, 1973, Squire and Allan, 1977; Mollo-Christensen, 1983; Weber, 1987). These works were concerned with propagation and attenuation of surface gravity waves through fields of pack ice.

If a small amplitude wave in deep water approaches a perfectly elastic ice sheet, a flexural-gravity wave will form in the ice-water system. The water motion is assumed inviscid, irrotational, and incompressible. The ice sheet motion is caused by the pressure field beneath it, and the ice sheet remains in contact with the water. The flexural-gravity waves of the ice-water system obey the same dispersion relation. Under the above assumption, there exist velocity potentials in water obeying Laplace's Equation. The motion of the ice sheet is described by elastic theory. The pressure underneath the ice sheet is represented by a linearized Bernoulli equation, since the displacements and velocities of water particles are assumed to be small. Through Laplace's Equation, this boundary problem was solved and the velocity potentials were obtained. The dispersion equation of this flexural-gravity wave can be written as (Wadhams, 1973):

$$Fk_n^5 + \rho g k_n - \omega^2(\rho_i h k_n + \rho) = 0 \tag{2.2}$$

where k is the wave number, ρ is the water density, ρ_i is the density of ice , h is the ice thickness, g is the gravitational acceleration, ω is the angular frequency, and F is the flexural rigidity of ice, (F is dependent on the Young's modulus of elasticity, Poisson's ratio, and ice-thickness).

Equation (2.2) has three physically feasible roots: one real, representing the propagating waves in the ice-water system, and two complex conjugates representing evanescent edge waves. Equation (2.2) is valid for all propagating waves in perfectly elastic floating ice sheets regardless of the mechanism of formation. Some important properties of flexural-gravity waves can be derived from this equation. The properties of flexural-gravity waves tend to those of water waves at long periods and/or for thin ice sheets. At shorter periods, however, they tend to those of pure flexural waves in thin elastic sheets.

Apart from its dispersion, the most important property of the flexural-gravity wave is the way in which the wave energy is shared between the ice and the water. For the ice-water system, the mean kinetic energy is equal to the potential energy, a result expected for a progressive wave. However, the energy is unequally divided between ice and water, and both ice and water have unequal time-average kinetic and potential energies. For short waves, most of the energy is transported by the ice; while for long waves, most of the energy translation occurs in the water. Ocean waves of all periods, except long swells, even transmitted perfectly from the water into the ice, display much lower amplitudes within the ice field. Only at very long swell periods does the flexural-gravity wave have an amplitude tending to its open

water parent.

Ice, however, is not a perfectly elastic material, but is viscoelastic, i.e. possesses creep properties. When exposed to an incident wave, each volume element of an ice floe passes through a cycle of alternating tension and compression. Part of the deformation thus induced is elastic, but it is accompanied by a time dependent plastic strain-creep. The creep process requires work, which involves the absorption of energy from the wave.

It is assumed that steady state creep occurs through all phases of the stress cycle, obeying the flow law of Glen. A further assumption is that the stress can be derived directly by linear elastic theory. Using the obtained stresses, the flow law is applied to calculate an energy dissipation rate, interpreted as a decay rate of the flexural-gravity wave with increasing penetration. Creep is thus seen as a small perturbation to a stress-strain situation dominated by elastic forces. Using these assumptions, Wadhams (1973) produced the solution for calculating the flexural-gravity wave decay with penetration distance. An important property of the flexural-gravity wave attenuation is that short period waves decay quicker than long period waves. The progressive attenuation through creep reduces the wave energy preferentially at the short periods. For example, a wave of 18 seconds showed little energy loss even after 1000 km of propagation for a typical 5 metres ice thickness of the Arctic ice cover. This might explain why only long period waves were recorded at locations far from the edges of fast ice.

Mollo-Christensen (1983) introduced compressive stress of the ice into the ice sheet motion equation. This stress was treated as a function of ice type, strain rate and temperature under otherwise steady conditions. Then through the same analysis as above, a solution was derived. In this solution, exists an item denoting the effect of compression of the ice. Under this effect the group velocity of the flexural-gravity wave can be reduced, and reach zero if the compressive stress is in excess of a critical value. This leads to a concentration of energy and a buckling of the ice. The required compressive stress can come from the effects of winds, surface currents , or even the radiation pressure of the wave itself against the upwind edge of the ice sheet. This approach was used to explain the ice rideup on shores. An observation of unusual waves of 1 metre amplitude and 18 seconds period at a location in the ice pack 560 km from the ice edge was also explained by this theory (Liu and Mollo-Christensen, 1988).

A different approach was to assume Newtonian creep and use a viscoelastic constitutive equation for ice from the start, instead of separating the analyses into an elastic analysis for propagation and a creep analysis for decay (Squire and Allan, 1977). A Maxwell-Voigt spring-dashpot model was used to represent sea ice behaviour under tension. Then the flexural rigidity of ice was replaced by a viscoelastic parameter, and a dispersion relation was derived. Two evanescent waves and a flexural-gravity wave were obtained, a situation almost like the elastic case of Wadhams. Instead of propagating with no energy loss, the waves decayed gradually in an exponential manner with distance into the ice.

Wave reflection and transmission at an ice edge are theoretically and practically important. As one expects, the thinner the sea ice or the longer the wave, the less the wave is affected by the ice cover , and the closer the transmission is perfect. Conversely, when the sea ice is very thick or the incoming waves have a very short period, very little wave energy enters the ice cover and most is reflected. This leads to short and choppy seas near the ice edge (Squire, 1983a). The reflection and transmission coefficients of the amplitude of surface displacements depend on ice thickness and wave period, as well as water depth, and to a less extent on the mechanical properties of the ice. By numerical experiments with six different ice models (Carstens and Rosdal, 1987), high reflection coefficients were only found for short period waves, while for waves with 10 second periods or more, reflection coefficients were less than 10 percent. The more flexible the ice, the less reflection.

The velocity potentials of the ice-wave system can not in themselves match at all water depths between the free surface domain and the ice-covered domain for getting reflection and transmission coefficients. The simplest approach to this problem is to match across the boundary only at water surface, on the grounds that most of the wave energy is found near the surface. In another solution, an infinity number of evanescent . ;odes are included in the solution and allow matching to be carried out by minimization of an integrated error term from surface to seafloor. Reflection and transmission are found to be markedly influenced by the inclusion of these modes (Fox and Squire, 1990).

2.3 Waves in a Discrete Ice Floe Field

Shore fast ice and vast ice floes are broken up due to wave induced flexural failure, which is the principal determinant of floe size distribution. A fracture criterion may be used to establish a limiting floe size distribution within the Marginal Ice Zone as a whole. There is a critical floe size, which is a function of wave height and length as well as ice thickness and strength, beyond which the floe is unstable and likely to break up (Squire, 1983a). In turn waves become more complicated and attenuate rapidly in the discrete ice floe field. The incident wave produces a forced response to the floating ice floe and thus generates a scattered wave field. The ice floes concerned in the present study are restricted to those whose dimension is small compared with wave length.

Wadhams (1973) approached this problem by considering only the reflections from a floe. The energy in the reflected portion was assumed to dissipate before reaching the preceding floe, which made the single scattering model. It was assumed that only the mismatch between the free sea surface and the elastic floe surface caused energy reflection. Then velocity potentials were obtained for each domain and matched at water surface and at a depth of one quarter of the wave length. This solution was used to explain the measurements showing that surface wave power spectrum decayed exponentially with distance into a discontinuous ice cover. The rate of decay was greater for higher frequency components of the wave spectrum. These components corresponded to shorter waves which were affected more by the presence of the ice. Attenuation coefficients of waves in a discrete ice floe field were

then obtained.

Most ice floe fields encountered in the Marginal Ice Zone are sufficiently concentrated for multiple scattering to be important. Assuming that reflected wave vectors experience the same reflection and transmission coefficients as the main forward wave vector, the scattering is incoherent, and a wave vector is allowed to suffer up to two reflections only, one gets the attenuation coefficient for multiple scattering. This coefficient is smaller than that for single scattering, because multi-reflections return some of the reflected energy to the forward propagating wave. The predicted coefficients of this model agreed well with several field observations. The fit was especially good for the phenomenon of the decrease of the coefficients with increasing wave periods which occurred in the mid-range of wind wave periods (Wadhams, 1973).

A theoretical model was developed by Rao and Vandiver (1987) for the calculation of the attenuation waves as they passed through a discrete ice field. The method produced a prediction of the attenuated wave spectrum after passage through a user selected distance from the ice edge. To determine the attenuation of waves, scattering was the only factor considered. The ice floe was modeled as a rigid, floating 2-D body in a plane wave field. Using the program NIIRID, they solved the time harmonic linear radiation problem and obtained the heave and sway exciting forces to a single floe. These were then used in a separate program to get the transmission and reflection coefficients. Conclusions similar to Wadhams' were found. For a wave frequency range of 0.05 to 0.25 Hz, floe diameter of 40 metres and

thickness of 0.2 metres, the attenuation went from zero to 90 percent . The single 2-D body result was ultimately extended to model a ice floe field. End effects were ignored and the 3-D problem was transformed into a 2-D problem by assuming that every point along a plane wave front encountered only one body. The attenuation due to a group of 3-D distributed floes was then considered the same as attenuation due to a 2-D body of equivalent width.

All the works for determining wave attenuation in an ice floe field were considered in the wave propagation direction, the 3-D scattering problem was simplified to a 2-D scattering problem. However, The directional surface spectrum is also modified by the presence of the ice cover (Wadhams et al, 1988). In the first few kilometres of ice cover, there is a tendency for the directional spectrum to narrow and become more perpendicular to the ice edge. This is because components travelling at angles other than 90 degrees suffer increased attenuation, as they have travelled a greater distance to reach the same point within the ice floe field. After this initial narrowing of the spectrum, the random scattering of waves from floe edges becomes more dominant than the attenuation of components travelling at non-normal angles and the overall effect is then to produce a more homogeneous directional spectrum.

Weber (1987) proposed an alternative theoretical treatment. It was not based on progressive scattering of incoming waves from ice floes. Instead, the ice field was modelled as a highly viscous Newtonian fluid overlying a slightly viscous (due to turbulent diffusion) rotating ocean. Although originally intended to model brash

ice, this second order theory worked well for appropriate values of eddy diffusion coefficient and the derived damping rate compared favorably with field data from the Bering Sea MIZEX of 1983.

2.4 Ice Floe Collision under Wave Action

The problem of ice floe collisions under wave action could be divided into three parts. The first is the problem of a single floating body in ocean waves. This leads to a basic understanding of the dynamic behaviour of a floating body in a wave field. The second is the problem of a pair of floes excited by wave forces. This will give us a picture of the relative movement of neighbouring floes and floe collision occurrence condition. Finally, an ice floe field is treated as a whole to consider the floe collision problem.

The problem of floating bodies under ocean waves has been studied extensively, experimentally and theoretically, principally connected with naval architecture. Even after considerable simplifying assumptions, complete solutions of the response of a freely floating body to wave forces are difficult to obtain. Wave-ice interaction is a subset of this floating body problem. A single ice floe under wave action displays all the usual rigid body motions: heave, surge, sway, roll, pitch, and yaw, but it will also bend and possibly break up. The response of ice floes and icebergs to ocean waves were studied primarily with an interest in wave induced flexural loads and the potential importance of waves as agents in ice floe breakup.

There are two distinct approaches in determining the motion of a floating body interacting with waves: Morison's equation and potential theory. Each method has been shown to be valid for a different domain of applicability. Morison's equation is used by offshore engineers wherever inertial and viscous forces dominate, whereas

potential theory is used when diffraction becomes significant. The two theories approach one another asymptotically in the inviscid, small body limit.

A potential theory approach which neglected viscosity was used to model the motion of the floes in the MIZ, and to calculate the wave loading beneath each floe due to the passing ocean waves by Squire (1983b). His results showed that floe motions were very small compared with water motion when the wave periods were short, whereas for long period waves the heave and sway responses were almost perfect but the roll was negligible. Here the dominant factor is the ratio of wave length to floe size. Wadhams and Cowan (1984) showed that small floes, 20 metres diameter or less, had an essentially perfect heave response, i.e. the floe moved so as to exactly follow the level of the ocean surface.

Lever et al (1984) studied the wave induced motion of ice bodies in regular wave conditions using models that were different in shape and surface roughness. Their results indicated that when the ratio of wavelength to characteristic body size was greater than 13, water particle-like motions occurred in all models. When this ratio was between 10 and 13, the occurrence of particle-like motions was dependent on the model shape. Wave diffraction and possible viscous force were thought to affect model behaviours as this ratio dropped below 10 and particle-like motion was not observed.

A theoretical nonlinear 3-D time-domain method for predicting the motion in waves, of a small (with respect to wave length) floating body of arbitrary shape,

was developed by NORDCO Limited (1989). The general equations of motion of a rigid body were applied and the wave forces were computed by a direct integration of pressures over the instantaneous wetted surfaces of the body. The scattering forces were estimated by the equivalent motion concept and the viscous forces were estimated by the application of appropriate semi-empirical drag coefficients with respect to the equivalent motion velocity . Their results indicated that when the ratio of wavelength to characteristic body size was less than 4, the motions were dominated by drifting; when this ratio was greater than 13, they had the same conclusion as Lever et al. When this ratio was in the range between 7 and 11, the motions were significantly affected by body submergence and wave overtaking.

Although the phenomenon of ice collision has been reported by some investigators (Martin and Becker, 1988; Winsor et al, 1989; Rottier, 1990; McKenna and Crocker, 1991), literature on the physical process and mechanical properties of ice floe collisions is limited. Attempts have been made to model pack ice behaviour in the Marginal Ice Zone by considering the elastic collision between floes (Shen et al, 1987). This model was used to investigate the role of collisions in momentum transfer through an ice floe field. The floes were assumed to be circular and perfectly elastic, and their motions were assumed to be random. Collisions between neighbouring floes were considered as being caused by the mean deformation field. Those collisions transferred momentum which produced the internal stresses in the deforming ice field. By equating the collisional energy losses to the deformation energy, a relationship between the stress and strain rate was quantified. They found that the collisional stresses were proportional to the square of floe diameter and

the square of the deformation rate. It was found that the collisional stresses were very small. Consequently, the resulting stress divergence was estimated to be much lower than the air stress typically encountered in the Marginal Ice Zone.

A floe collision model was developed by McKenna and Crocker (1990). They assumed the floe velocity in waves to be equal to that of a water particle at the position of the floe centre. By linear wave theory, collision velocity was derived for a pair of initially contacted neighbouring floes. It was also assumed that floe collisions were inelastic and that floes collided directly with the maximum wave induced velocity. Thin-layer fluid and constant stress models for contact pressures were used to estimate the upper bounds on floe size reduction and brash ice production which was the residue of the crushing process. The amount of energy, extracted from the wave field by this process, was also derived. It was concluded that collisions were important for determining the decrease in floe size. The reduction in wave energy with distance due to floe collisions was however considerably smaller than the total wave attenuation observed in practice, indicating that other mechanisms, for example wave scattering, by which waves were attenuated in an ice floe field, were more important.

Rottier (1990) proposed three mechanisms by which adjacent floes interacted as a result of forcing by ocean swells: collision between ice floes, compression of brash ice between floes, and shearing contact between floes. It was suggested that the first two event types were driven by relative surge of two adjacent floes, while the last one could be driven by a relative surge, heave, and pitching motions of the floes. A

model was developed in order to quantify the conditions that must be met for each of the processes to occur. This work was done under the assumption that each floe did not contribute significantly to the hydrodynamic velocity potential, regardless of the way it responded to that field. It was shown that the ratio of the mean wave height to the mean floe spacing is the dominant factor in the determination of the event rates of the first two mechanisms. This ratio was used to identify four regimes in which interaction events were (a) extremely unlikely, (b) highly dependent on wave height, (c) moderately dependent on wave height, and (d) in a ' saturated ' state where the event rate was almost independent of the wave height. The interaction model was extended to attempt to quantify the intensity with which these processes occurred in an appropriate manner in order to estimate how great a contribution to the ocean noise field each process might take. Correlation between the model output and ambient noise measurements indicated that some features of the ocean sound field were predicted well by this model.

McKenna and Crocker (1991) introduced the ice motion measurements taken during the Labrador Ice Margin Experiment 1989 (LIMEX'89) in detail. The ice motion data were interpreted to determine the causes and the frequency of collision between floes. Collision events were defined by the evidence of any contact between floes during a wave cycle, which was investigated by checking the acceleration data. They observed that the collisions were closely related to the wave cycle with some events being intermittent or continuous. It was found that local air temperature decreasing and local winds increasing would tend to increase the likelihood of collisions. Additionally, there was not a positive relation between collision frequency

and wave amplitude .

Chapter 3

Ice Floe Collisions under Wave Action

3.1 Floe Motion under Wave Action

The response of ice floes to surface waves forms one of the foundations of ice floe collision studies. As mentioned in Chapter 2, complete solutions are difficult to obtain even after considerable simplifying assumptions. In the present study, the ice floes concerned are restricted to *small* ones whose dimensions are small compared with the wave length. These small floes are stable and not broken up by wave induced flexural failure. They move as rigid bodies under wave action. The waves are those of small amplitude and frequency. Water is taken to be inviscid and incompressible with infinite depth, and its motion is taken to be irrotational and incompressible. The effects of added mass and non-unity response amplitude operators (RAO) are assumed to be negligible. Then floe motion is approximated by the movement of a water particle which is positioned at the floe centre, as if the floe were not there.

Added mass coefficients have been shown to vary with the kind of motions the floe may undergo. In general, they are also functions of wave frequency. In the Marginal Ice Zone, the ice floes are usually very shallow compared to the water depth, which means the influences of water depth on RAO and added mass need not to be involved in the present study of floe collision. The following work will be based on the assumption of infinite water depth. On the condition of aspect ratio $\lambda/D > 5$, where λ is wave length and D is characteristic floe size, the added mass coefficients are usually small (Bai, 1977). If this ratio rises up to $\lambda/D > 13$, a freely floating body responds to wave excitation closely, which means that the response amplitude operators are very close to unity for floe surge, heave, and pitch. This has been observed and computed by several researchers (for example Lever et al, 1984). When this ratio becomes smaller, however, response amplitude operators are non-unity and the floating bodies demonstrate less water particle-like motion. Wave diffraction and possible viscous forces begin to affect floating body behaviours as this ratio drops below 10 and water particle-like motion does not occur (Lever et al, 1984). The present study is based on the data provided by the field experiment LIMEX'89. The ice floe field encountered in LIMEX'89 was composed of relatively small ice floes. The mean diameter of the floes was about 10 metres, and the wave length was approximately 156 metres, giving the ratio of wavelength to floe diameter to be greater than 13. It is reasonable to assume that the effects of added mass and response amplitude operators are negligible and therefore ice floes move like water particles.

The assumption that a floe oscillates like a water particle forms one of the

foundations for further analysis of the ice floe collision problem. However, it must be borne in mind that the effects of added mass coefficients and response amplitude operators may be significant, particularly for those large floes under waves of high frequencies.

3.2 Floe Collision Criterion

It has been demonstrated that small ice floes move as water particles on surface waves under certain conditions. Therefore, a criterion for ice floe collision occurrence can be obtained through studying the kinetic behaviour of the floes. The relative position change of two neighbouring ice floes controls the floe collision occurrence. The critical conditions for collision occurrence follows the analysis of Airy Linear Wave Theory.

The effects of an ice floe's vertical movements in the following analysis can be ignored, since they only have little influence on floe collision behavior when Airy Linear Wave Theory is used to analyse the problem. For example, under the conditions of floe diameter of 10 metres and 0.1 Hz frequency wave, the vertical component of the differential velocity at two adjacent floe impact is always less than ten percent of the horizontal component (McKenna and Crocker 1990). Therefore, the following analysis is carried out only in a horizontal x direction, i.e. the wave propagation direction.

Let l_m be the mean distance between two surface water particles, l_1 the horizontal displacement of particle 1, l_2 the horizontal displacement of particle 2, l_3 the instantaneous distance between the two particles, as illustrated in Figure 3.1. Airy Wave Theory describes the horizontal displacements of these two water particles as :

$$l_1 = -a \sin(-\omega t) \tag{3.1}$$

$$l_2 = -a \sin(kl_m - \omega t) \tag{3.2}$$

where

a - wave amplitude,

k - wave number, $k = 2\pi/\lambda$,

λ - wave length,

ω - wave angular frequency, $\omega = 2\pi/T$,

T - wave period.

One can express the instantaneous distance between the two particles as:

$$l_3 = l_m - l_1 + l_2 \tag{3.3}$$

The relative distance change, l_c, of the two water particles in x direction is:

$$\begin{aligned} l_c &= l_m - l_3 \\ &= a \sin(kl_m - \omega t) - a \sin(-\omega t) \end{aligned} \tag{3.4}$$

It is this relative distance change l_c that we are interested in. The assumption has been made that ice floes move like water particles positioned at the floe centres. If we change l_m of the equations into l which represents the mean distance between two ice floe centres, the instantaneous spacing distance between the floe centres will also be governed by equation (3.3), and the relative distance change between them will follow equation (3.4). When l_c becomes large enough, which means that the two floes move close enough to each other, they will possibly collide with each other.

In order to obtain the maximum relative distance change of two adjacent floes

during a wave cycle, which will decide whether or not a collision occurs, it is necessary to differentiate the relative distance change l_c with time t:

$$\frac{\partial l_c}{\partial t} = -a\omega \cos(kl - \omega t) + a\omega \cos(\omega t) \tag{3.5}$$

Let $\frac{\partial l_c}{\partial t} = 0$ and the following results are derived:

$$\sin \frac{kl}{2} = 0 \tag{3.6}$$

$$\sin(\omega t - \frac{kl}{2}) = 0 \tag{3.7}$$

The first result leads to $l = 0$, which is meaningless. The second one leads to

$$t = \frac{kl}{2\omega} \tag{3.8}$$

and

$$t = \frac{(kl - 2\pi)}{2\omega} \tag{3.9}$$

Substitution of equation (3.8) and (3.9) into equation (3.4) gives the maximum relative distance change l_{cm} between the two floes as:

$$\begin{aligned} l_{cm} &= 2a \sin\frac{kl}{2} \\ &\simeq akl \end{aligned} \tag{3.10}$$

here kl is small since only small floes are considered and k is very small for ocean swell. Two neighboring floes may change their spacing distance as large as l_{cm} from their mean spacing distance at a moment during one wave cycle.

For two neighboring ice floes, we can define the edge distance as L, and the centre distance as l (Figure 3.2), and together they will be called floe spacing distances.

When the edge distance L is smaller than the maximum relative distance change l_{cm}, the two floes will collide with each other. The critical condition for collision occurrence can then be defined as:

$$L \leq l_{cm} = akl \tag{3.11}$$

or

$$\frac{L}{l} \leq ak \tag{3.12}$$

where ak is wave slope.

From the floe collision criterion of equation (3.12), it is clear that floe collision possibility increases as wave amplitude increases and wave length decreases, as long as response amplitude operators stay near unity. Floe collision also depends on the ratio of floe edge distance L and floe centre distance l: the smaller the L/l, the higher the likelihood of floe collision occurrence. Small edge distance L means that two adjacent floes are very close to each other. Large l means that the two floes sit apart a great distance and have a considerable phase difference, so that they have large relative distance change.

It must be kept in mind that although equation (3.12) provides a criterion to judge collision occurrence of two adjacent floes, it should not be used directly to describe the collision behavior of any individual floe during a period of time in a real ice floe field. Because the spacing distances between any two adjacent floes are not only the function of time, some other factors also influence these distances. They can be defined as stochastic processes which will be discussed in Chapter 4.

Therefore, if the spacing distances of two adjacent floes satisfy the collision criterion of equation (3.12) at a specific moment, it should not be concluded that they will keep colliding for a long time period at the frequency of the waves. The following simple fact demonstrates one of the reasons. After colliding, the two floes will touch each other and remain in contact for a short period of time. This means that they move as one single larger floe with a new centre different from either of the original two centres. This changes the movements of both the two floes.

In a real ice floe field, the centres of most adjacent floes are not in the line of the wave propagation direction. Instead most of them deviate somewhat from the wave propagation direction. When two floes meet the criterion at a moment in a wave field, they will collide with each other. Because of the centre line deviation, the collision will cause the floes not only to impact and be damaged, but also to rotate and drift obliquely. This mechanism changes the two floes' movements under wave action after collision. Then they may or may not collide during the next wave cycle. It is proposed that ice floe spacing distances are treated as stochastic processes and floe collisions in a real ice floe field are studied from the view of stochastic process and probability theory.

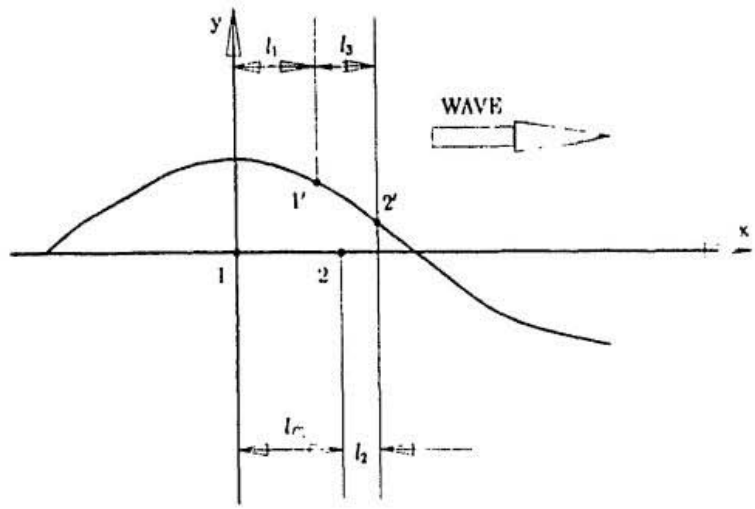

Figure 3.1: Water particle displacement on wave surface

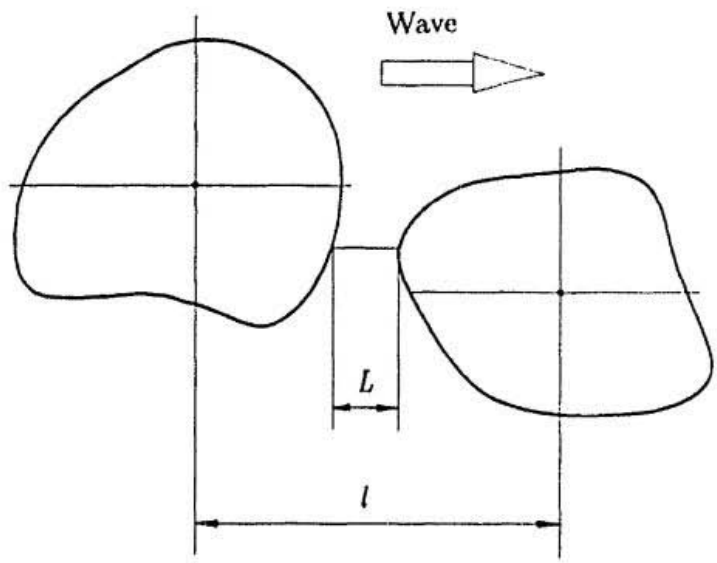

Figure 3.2: Edge and centre distances of ice floes

Chapter 4

Ice Floe Spacing Distribution

4.1 Definition of Ice Floe Spacing Distances

In chapter 3, the ice floe collision criterion under wave action was derived as equation (3.12). The ratio of floe edge distance L and centre distance l , as well as wave conditions, determine whether or not two adjacent floes will collide with each other in a wave field. Now the problem is how to use this criterion to describe the collision phenomena in a real ice floe field , i.e., how to obtain ice floe collision frequency from this criterion. To do this, floe edge distance L and centre distance l must be carefully defined and studied.

In a real ice floe field under wave action, floes move and change positions all the time. Their relative positions and spacing distances also change all the time. These distances are time dependent processes. As described in chapter 3, deviation of floe centre lines from the wave propagation direction makes the floe collision not a one-dimensional impact, but rather, one which is accompanied by floe rotation

and oblique drift. Furthermore, after entering into and propagating in an ice floe field, multiple reflections and scattering by ice floes cause ocean swells to be less one dimensional and become more like a three-dimensional wave field.

In an ice floe field, every floe is surrounded by other floes in different directions so that the ice floe spacing distances are multi-dimensional stochastic processes. For the study of floe collisions under wave action, it is reasonable to take the wave propagation direction as the direction in which ice floe spacing distances are defined. Even in the wave propagation direction, floe spacing distances are not only functions of time, but also one-dimensional stochastic processes. Then the floe spacing distances in the wave propagation direction can be defined as random variables $L(t)$ and $l(t)$:

$$L(t), t \in X \tag{4.1}$$

$$l(t), t \in X \tag{4.2}$$

here, X is a time parameter set. These stochastic processes are continuous parameter processes since X is the time interval having positive length.

4.2 Assumptions and Treatments for Ice Spacing Distribution

In chapter 3, ice floe edge distance L and centre distance l were used to describe the ice floe spacing conditions, and a floe collision criterion was obtained. Floe edge distance and centre distance were chosen with the assumption that the floes oscillate like water particles in a wave field. The distance between floe centres represents the phase difference of two adjacent floes. This phase difference produces the relative distance change of two floes, which may cause floe collisions. When a pair of adjacent floes have a maximum relative distance change, at a moment during a wave cycle, whether or not they collide with each other also depends on the edge distance between them. The edge distance represents the distance between the two floe edges in the wave propagation direction. If the maximum relative distance change is larger than the edge distance, a collision will occur. Otherwise, it will not. Here L and l are chosen to describe ice floes' relative movements which have been demonstrated as the determinants of floe collision occurrence along with wave conditions.

On the other hand, for an ideal ice floe field of uniform floe shape and size, floe size D and concentration C may be adequate to define the floe conditions for our purpose of floe collision studies. However, this is far from the real picture of an ice floe field in the Marginal Ice Zone where ice floes are very irregular in shape and different in size from each other. It is sometimes said that the floe size in the Marginal Ice Zone is in a range of several metres to tens of metres. Moreover there also exists a large number of smaller ice masses that are usually not counted as ice

floes. Most of this ice mass, which may be called brash, is broken away from ice floes as they are eroded, especially through the process of floe collisions. This brash may contain ice pieces smaller than several centimetres across or lumps of tens of centimetres across (Rottier, 1990). Furthermore, ice floe spacing distributions are random at any instant in a real ice floe field. Therefore, we can not use any dimension parameter D of a regular shape or floe concentration C to describe the critical conditions for floe collisions. For example, even if two pairs of floes have the same D and the same centre distance l, one may collide but the other may not, if they are set as illustrated in Figure 4.1. The key parameters to describe ice floe conditions are then chosen as l and L but not floe size D and concentration C, as long as D is not large enough to violate the assumption of water particle-like movement.

In the last section, ice floe edge distance L and centre distance l were defined in stochastic terms. If $L(t)$ and $l(t)$ can be obtained from some data for an ice floe field during a time period, we may analyse floe collisions in the ice floe field during the time period by the floe collision criterion with the aid of stochastic process theory. However, up to now there are not any field data available to be used for the purpose of obtaining $L(t)$ and $l(t)$. The limited data available on ice floe spacing distribution patterns are derived from aerial photographs and video tapes. They show only the floe spacing distributions of ice floe fields at some specific moments, but not the distributions of time variable. In other words, they give the pictures of ice floe spacing distributions in an area at the moments when the photographs or video tapes were taken. We do not know what kinds of floe distribution patterns

exist before or after these moments. Since floe edge distance and centre distance are the two key parameters in the floe collision study, an assumption must be made to get the two parameters from the limited available data. The assumption is that both the two stochastic processes are wide stationary stochastic processes, which means their mean functions do not change with time:

$$L(t) = L \tag{4.3}$$

$$l(t) = l \tag{4.4}$$

Ice floes always move in a wave field and their relative positions, which decide the floe edge distance and centre distance, are always changing as well. The aerial photographs can only show the floe distribution patterns of specific moments when the photographs were taken. For our case, the aerial photographs are from the field experiment LIMEX'89. A favourable factor for the above assumption is the high floe concentration and the relatively small ice floes (about 10 metres of mean diameter) in the ice floe field encountered during that experiment. There are tens of floes on one photograph and more than ten floes within one wave length. Among them, at the moment of photographing, each edge distance or centre distance possessed a value between the maximum and the minimum that a pair of floes might achieve under wave action. These distances are randomly distributed in space at any moment. Each distance changes with time, but by looking at the whole ice floe field, these distance distributions may be considered not to change with time. In other words, the edge distance distribution and centre distance distribution obtained from the aerial photographs may be regarded as mean distributions which

do not change with time, because of the large number of floes on one photograph and within one wave length. These arguments make the assumption of a wide stationary stochastic process reasonable for the present study.

The assumption of wide stationary stochastic processes must be restricted to an individual space subset and an individual time period. Obviously, ice floe spacing distributions change with different ice floe fields. Even within an ice floe field, the area may still be divided into several zones, with each having its own floe spacing distribution. For example, the ice floe condition at the edge of the field is different from that at the centre area of the field. Differences may also exist between the area where waves enter the ice field and the area where the waves exit the ice field. When we say that a floe spacing distribution does not change with time, we mean that it does not change with time during an individual time period. This time period should be long enough in comparison with the wave period, but short in comparison to the time required for a significant change of wave conditions and/or ice floe conditions.

Under the above assumption of a wide stationary stochastic processes, ice floe edge distance distributions and centre distance distributions obtained from aerial photographs are the mean distributions of the processes. They can represent the ice floe spacing characteristics for that surrounding area, for a time period before wave and ice floe conditions change significantly from the moment of photographing.

What has been mentioned before but not yet described clearly is that the floe

edge distances and centre distances considered are the distances in the direction of wave propagation. This is because waves are the only factor considered which cause floes to oscillate and collide with each other. Thus, it is a one-dimensional problem. One fact about real ice floe fields is that few adjacent floe centres align in the direction of wave propagation. Then l should not be taken as the distance in the cross centre line, but as the cosine projection of the cross centre distance in the wave propagation direction. And L should be taken as the shortest distance in the wave propagation direction between floe edges. See the sketch in Figure 3.2. From the view of inelastic floe collisions, it is reasonable to assume that a floe may at most hit two other floes (forward and backward of wave direction) during one wave cycle. Only one smallest l and one relevant L for one floe will be measured in the forward wave propagation direction, corresponding to the above assumption.

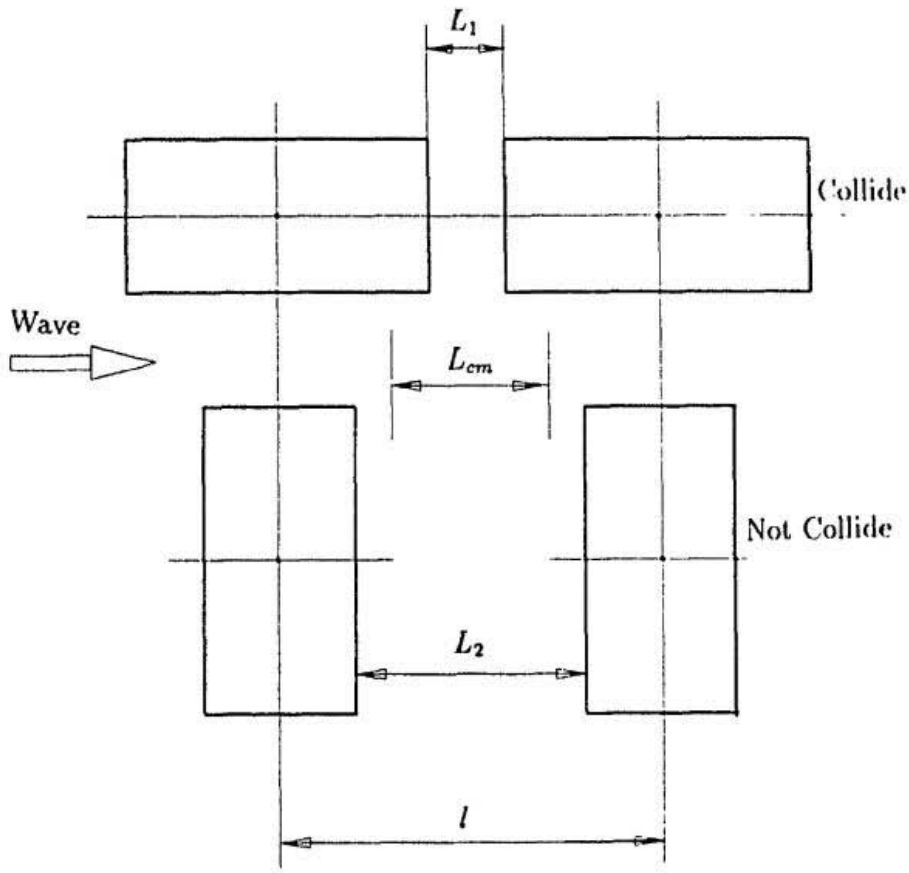

Figure 4.1: Sketch of key parameters of floe spacing conditions

4.3 LIMEX'89, the Labrador Ice Margin Experiment 1989

The Labrador Ice Margin Experiment 1989 (LIMEX'89) took place, as a two phase experiment, off the east coast of Newfoundland from March 4 to April 4, 1989 (Figure 4.2). The primary objective of LIMEX'89 was to establish a link between the status and evolution of ice and ocean properties in the economically important Labrador Marginal Ice Zone, with concurrent remotely sensed data, particularly Synthetic Aperture Radar imagery. Two ships, both supported by helicopters, served as research bases in the ice and at the ice margin for the surface programs.

The data dealt with here were from experiment 6 of LIMEX'89 phase two conducted from the MV *Terra Nordica* whose trajectory is shown in Figure 4.3. Programs for phase two included the extended studies of wave motion in ice, ice dispersion, quantitative wave observation, and ice physical and mechanical properties. Experiment 6 took place 200 kilometers northeast of the eastern coast of Newfoundland, in a water depth of approximately 300 metres on April 2 and 3, 1989. At that time, the outer extent of the pack ice was approximately 120 kilometers offshore of the test location, placing the experiment well within the pack ice as shown in Figure 4.4.

The ice encountered during the phase two of MV *Terra Nordica* was generally thin (median thickness 0.70 m), but heavily rafted. It was on average only about 1° to 2°C below the freezing point, and had a fairly high salt content (mean salinity $\approx$4.6 ppt). The floes were composed almost entirely of polycrystalline ice,

originating from brash and/or frazil and /or saturated snow. Only a few isolated layers of columnar ice were found (Crocker, 1990). Three ice motion packages, (numbered 3, 5, and 6)were fixed onto three ice floes and measured accelerations, tilt and rotational motions. From the obtained acceleration data, valuable information about ice floe collisions can be derived. This will be discussed in chapter 6 in detail. Here, attention is paid to the aerial photographs taken from a helicopter over the measured ice floe field during experiment 6 on April 2, 1989. The details of the photography work are in Appendix A. The aerial photographs of interest from experiment 6 are those of slide number 5400, 5404, 5412, 5416, and 5420 (Windsor, 1990). These photographs were taken from the helicopter down vertically onto the ice field. See Table 4.1 for the details of these 5 photographs. Figure 4.5 shows one of the photographs, slide 5400. The ice floe spacing distributions will be obtained from these aerial photographs by measuring spacing distances between floe centres and between floe edges and by probability plot tests.

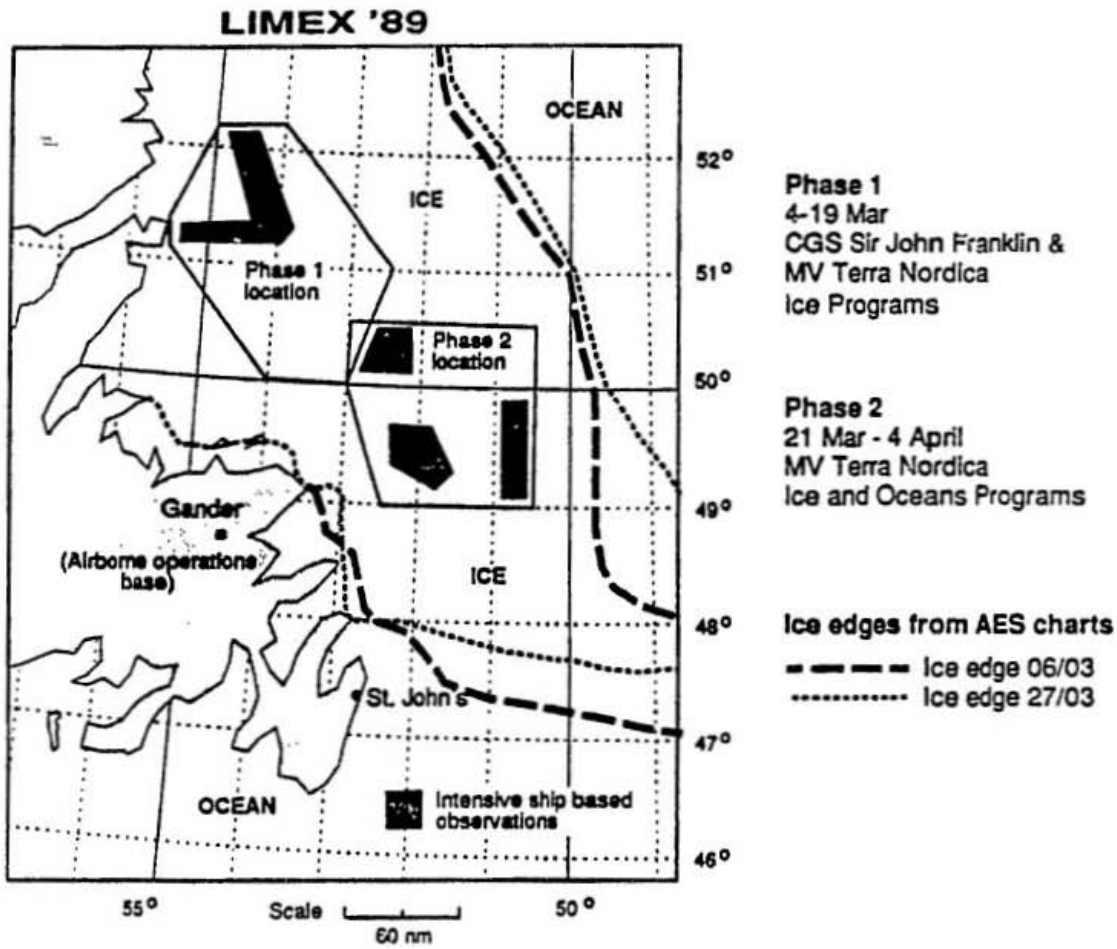

Figure 4.2: Location of LIMEX'89 experiment sites (after Raney et al, 1990)

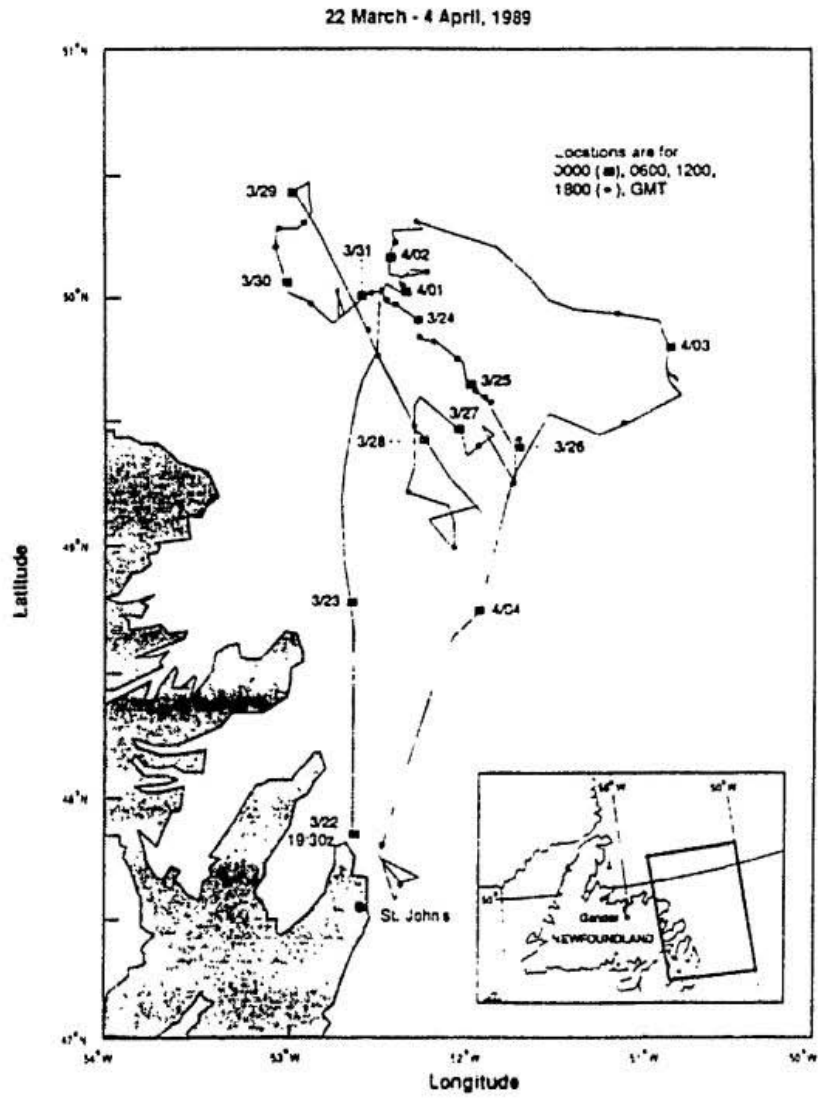

Figure 4.3: MV *Terra Nordica*'s trajectory during LIMEX'89 phase two (after Maclaren Plansearch Limited, 1990)

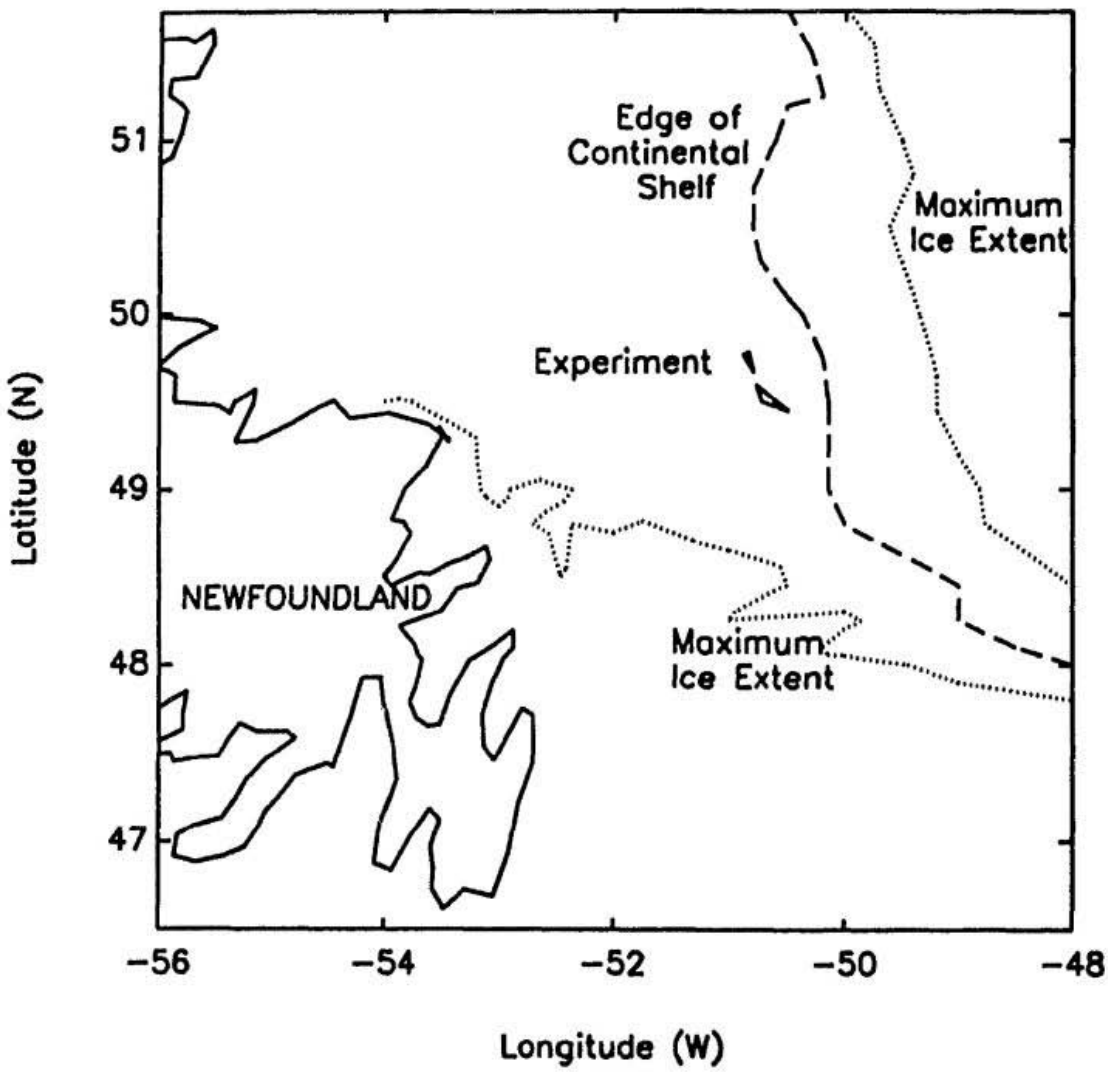

Figure 4.4: Location of experiment 6 of LIMEX'89 phase two conducted from the MV *Terra Nordica* (after Maclaren Plansearch Limited, 1990)

Figure 4.5: Slide 5400 of the aerial photographs from LIMEX'89

Slide number	Taken time Apr 2, 89 GMT	Latitude	Longitude	Altitude m	Angle of film long axis to true North
5400	20:09	49° 47' N	50°47' W	150	341°
5404	20:13	49° 46' N	50° 50' W	240	341°
5412	21:01	49° 46.23' N	50° 53.53' W	170	355°
5416	21:01	49° 46.23' N	50° 53.53' W	170	355°
5420	21:02	49° 47.51' N	50° 53.25' W	140	355°

Table 4.1: Details of the aerial photographs from LIMEX'89

4.4 Ice Floe Data from the Photographs

Before starting to measure ice floe spacing distances, a judgement must be made on what is to be considered as a floe. This judgement is necessary because many smaller ice pieces, whose sizes may range from tens of centimeters to several metres, exist among the larger floes (Figure 4.5). The criterion for this judgement must be arbitrarily chosen. For the problem of floe collisions, however, it is better to obtain the criterion from a consideration of kinetic energy. For experiment 6, the mean floe diameter $D_m = 10$ m, mean thickness $h = 0.8$ m, density $d = 0.88$, then the average floe mass M is about 55,000 kg. From the ice motion package data, it is known that during the flight period for the pictured area, the wave amplitude $a = 0.13$ m, and the wave period of the main spectral peak $T = 10$ s. The maximum water particle velocity by Airy Wave Theory is :

$$v = a\omega = 0.082 \text{ m/s}, \tag{4.5}$$

and the kinetic energy of a floe with the mean diameter of 10 m is:

$$E_m = 0.5Mv^2 = 183\text{Nm}. \tag{4.6}$$

For a small floe of $D = 3$ m, $M = 4976$ kg, its kinetic energy is $E = 16.7$ Nm. The ratio $16.7/183 = 0.09$ shows that a floe of 3 m diameter has less than ten percent of the kinetic energy of a floe with the mean diameter. We will therefore consider ice pieces of diameter less than 3 m are considered as *brash* ice but not ice *floes*.

This criterion is still somewhat artificial. We should furthermore take into account floe collision velocity which is important for predicting ice loading forces

on offshore structures. According to McKenna and Crocker (1990), the possible maximum collision velocity for a pair of floes of the same size is directly proportional to the floe diameter D. The energy lost during a floe collision is directly proportional to the mass of the floe and the square of the collision velocity, which means that the energy lost is directly proportional to D^4. Compared with the floes with mean diameter, the ratio of lost energy is smaller than the ratio of floe kinetic energy shown above. This means the ice pieces smaller than 3 m in diameter cause very small ice damage and wave energy losses when they collide with others. These small ice pieces almost do not collide with each other, because when they are close to each other, their centre distances are so small that they have negligible horizontal displacement differences and velocity differences.

Although ice pieces of diameter less than 3 m are not considered as floes, they can transfer or pass collisions between two bigger floes. In this case, take

$$L = L_1 + L_2 \tag{4.7}$$

and l as illustrated in Figure 4.6. These small ice pieces reduce the edge distance between neighbouring floes and cause more collision events. In the case of Figure 4.6, the two floes have a relatively large centre distance which makes large displacement difference between the floes. This large centre distance, together with the reduced edge distance by the small ice piece, makes equation (3.12) more easily satisfied.

In order to obtain floe centre distances, all the floe geometric centres must be first located on the photographs. This work could have been done by a digitizer.

However, after locating the geometric centres, further work still had to be done manually for measuring edge distances and centre distances. Since an ice floe is usually surrounded by several other floes and some small ice pieces in random directions, two neighbouring floes have to be defined as those which will most possibly collide with the floe of interest. The principles for defining the two neighbouring floes for the floe of interest are that the two neighbouring floes have the largest centre distances and the smallest edge distances with the floe of interest in the wave propagation direction. In this procedure, small ice pieces among the floes should be taken into account. Their diameters should be deducted from the edge distances as illustrated in Figure 4.6. The photographic slides were projected onto grid tracing paper and the work was carried out on these projected pictures. The calibration is shown in Appendix B and the results are shown in Table 4.2. In the table, v is the length of a project; *Length projected*, F_1 and F_2 refer to the sizes of the projected pictures; and S is the real length per unit length of the projected pictures.

The number of floes of diameter larger than 3 m were marked on the projected picture of each slide. For a big floe, as illustrated in Figure 4.7, the stripe heights were $H_i = en_i$, ($i = 1, 2, 3, \ldots, N$), where n_i was the grid number in the y direction at $x = i$, e was the grid dimension of 1 mm, and N was the maximum grid number of the floe in x direction. N and n_i were counted for each floe, then the x coordinate of a floe's geometric centre was obtained by

$$\begin{aligned} \bar{x} &= \frac{\sum_{i=1}^{N} e^2 H_i (i - 0.5)}{\sum_{i=1}^{N} e H_i} \\ &= e \frac{\sum_{i=1}^{N} n_i (i - 0.5)}{\sum_{i=1}^{N} n_i} \end{aligned} \tag{4.8}$$

After this, the process was repeated by rotating 90 degrees from $\bar{x}$ direction to obtain $\bar{y}$. The cross point of $\bar{x}$ and $\bar{y}$ was the geometric centre of the floe. For small floes, their geometric centres were located by eye. Since they were small, the errors were thought not significant.

After the geometric centres were located, the ice floe edge distance L and centre distance l in the wave propagation direction were measured manually. These distances were measured in millimeters and multiplied by the scales S of Table 4.2 to obtain the real distances. These sample observations of the floe spacing distances were analysed later. Two groups of sample observations were then obtained for edge distance and centre distance respectively. In order to test if the floe spacing distributions changed in different directions, the same measuring procedure was repeated in two directions: long axis direction of the frames and the Tp direction in which the waves had peak energy at wave spectra. The long axis direction was also the helicopter flight direction. These two directions were 77 degrees (slides 5400, 5404) and 63 degrees (slides 5412, 5416, 5420) apart. The probability distribution plot test in the next section is then composed of two subsets in the two directions.

It should be mentioned that in the floe spacing distance measurements, arbitrariness was sometimes not able to be avoided. This came mainly from the fact that a decision had to be made, among several neighbouring floes, for choosing the *adjacent* floe for the floe we were working on. Because it was assumed before that one floe could at most hit two adjacent floes in the forward and backward wave propagation direction, only one floe could be chosen as an adjacent floe in one di-

rection. This decision was sometimes arbitrary according to individual judgement. Another problem in the measuring work was the resolution of the photographic slides. The resolution of the projected pictures was about 0.5 mm, which restricted the precision of measuring work for very closely neighbouring floes. This resolution gave about 10 to 15 cm of real distance. It will be discussed later that the resulting ice floe collision probability changes quite sensitively with floe edge distance distribution when the distance is small. Floe edge distances are small for a closely packed ice floe field. The mean of floe edge distance of the present study is 0.85 and 0.93 metres for the two directions respectively. The resolution of 10 to 15 cm therefore has a significant influence on the floe collision probability. A detailed discussion is in chapter 7.

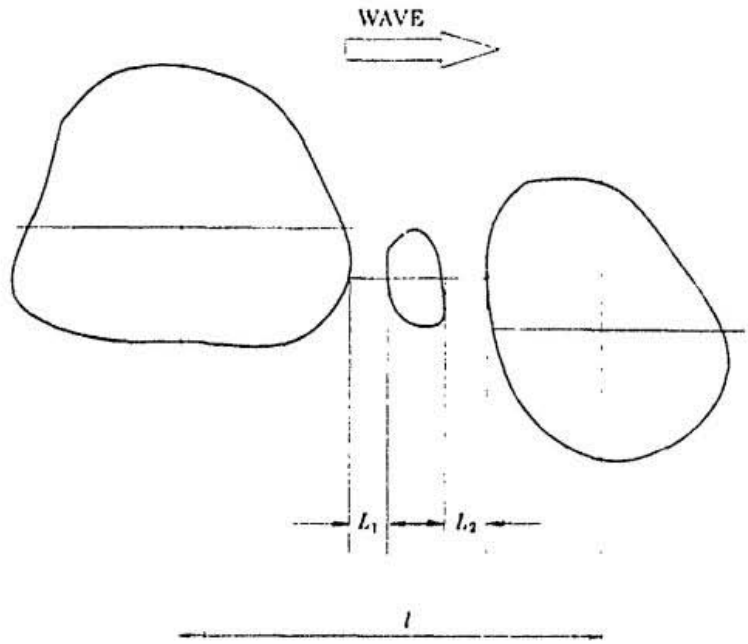

Figure 4.6: Definition of floe edge and centre distances

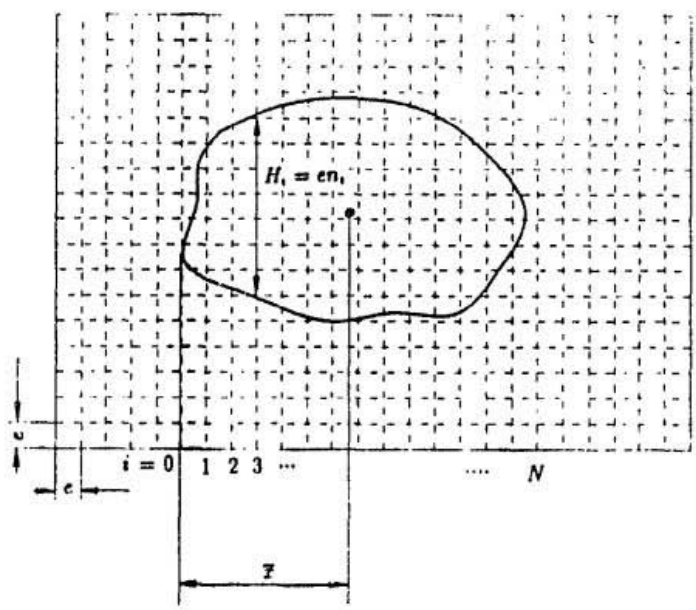

Figure 4.7: Determination of floe geometric centre

Slide number	A Altitude m.	$o = A/0.05$	Length projected F_1 mm.	Length projected F_2 mm.	Ratio R $F_1/23$, $F_2/35$	$S = o/R$
5400	150	3000	234	356	10.17	295
5404	240	4800	235	358	10.22	470
5412	170	3400	237	361	10.29	330
5416	170	3400	234	356	10.17	334
5420	140	2800	234	356	10.17	275

Table 4.2: Calibration of the aerial photographs

4.5 Probability Plot Test

Two groups of sample observations of ice floe edge distance L and centre distance l were obtained from the aerial photographs of LIMEX'89. As demonstrated before, L and l are two random variables. Such data of random ice floe spacing distances did not exist before, and their physical properties and probabilistic characteristics are not readily amenable to theoretical deduction or formulation. Therefore, probabilistic models have to be determined empirically based on the available observations. It is to be determined whether or not the observational data can be appropriately modelled by a specific probability distribution.

A probability plot technique was used to carry out this research. One of the methods used to find a suitable probability distribution for given sample observations is the probability graph paper. Probability paper is constructed such that a linear graph between the cumulative probabilities of the underlying distribution and the corresponding values of the variate is obtained if the variate follows the underlying distribution. Cumulative distribution functions plotted on the probability graph paper are commonly called frequency curves. The linearity, or lack of linearity, of a set of sample data plotted on a particular probability paper, therefore, can be used as a basis for determining whether the distribution of the underlying population of the sample is the same as that of the probability paper. A statistical test for the goodness-of-fit of an assumed probability distribution to the observed data must be applied to see if the fit is good enough. This test, called probability plot coefficient test, provides an objective way of testing the linearity of the plotted points on probability graph paper. Both the goodness-of-fit test and the probability

plot test can be easily carried out using a spreadsheet (Lye, 1990). The software of Quattro.Pro (Borland International, 1990) was used in the present study to do the probability plot test and the goodness-of-fit test.

Four kinds of probability distributions were tested to see which one fitted the sample data best. Normal, Gamma and Lognormal distributions were tested by the similar Normal Probability Paper, since Gamma and Lognormal distributions might be obtained if the data could be transformed to fit Normal Probability Paper. For simplicity, the threshold was not used to test the full form of Lognormal distribution, although it might achieve a better fit. The data were transformed to another form to fit the Weibull Probability Paper. Details of the transformations are shown in Appendix C.

The most important step in the procedure of drawing the frequency curve of a random variable is that each observation must be plotted at the appropriate location, called plotting positions, on probability graph paper. For a relatively small sample of available observations, many plotting positions have been proposed. For construction of Normal probability plots, Blom's plotting position is usually recommended by statisticians. In the present study Blom's plotting position

$$\frac{\gamma - 0.375}{\Omega + 0.25} \tag{4.9}$$

was used for drawing frequency curves, where γ is the rank, smallest value is ranked 1, largest value is ranked Ω; Ω is the number of values.

After plotting data on probability graph paper, we must test how the assumed

distribution fits the data. A powerful and simple test called probability plot correlation coefficient test was used to judge the goodness-of-fit. The resulting coefficient R provides an indication whether to accept the tested distribution under a certain significance level. The results of probability plot tests are shown in Table 4.3 to Table 4.6 and Figure 4.8 to Figure 4.11. The figures show only the Lognormal distribution probability plots. The values of the *Means* and *S.D.* in the figures are those of $\ln(L)$ and $\ln(l)$. In the Tables, η and ξ are the scale and shape parameters of a Weibull distribution respectively; μ and σ are, respectively, the mean and standard deviation of x for a Normal distribution, the mean and standard deviation of $x^{1/3}$ for a Gamma distribution, and the mean and standard deviation of $\ln(x)$ for a Lognormal distribution.

The critical point of the correlation coefficient R based on Blom's plotting position is 0.987 for sample size 100, and 0.959 for sample size 25 under 5 percent significance level. By checking Rs in Table 4.3 to Table 4.6, it is clear that a Lognormal distribution fits the data best. The values of R for a Lognormal distribution of the whole data are 0.9749, 0.9936, 0.9949, and 0.9946, which means that the fit is very good. The results obtained from the data of individual photograph also show that a Lognormal distribution fits the data best. The exception is photo 5416 whose correlation coefficients are smaller than those of other photographs for all the tested probability distributions in both directions.

From the above probability plot test and correlation coefficient test, it is clear that both the floe centre distance and the edge distance can be considered to be

Lognormally distributed at a 5 percent significance level. The probability density function (PDF) of a Lognormal distribution is:

$$p(x) = \frac{1}{\sqrt{2\pi}x\sigma}\exp[-\frac{(\ln(x)-\mu)^2}{2\sigma^2}] \qquad (4.10)$$

$$0 < x < \infty$$

where μ and σ are, respectively, the mean and standard deviation of $\ln(x)$. The mean μ_x and standard deviation σ_x of the variate x are:

$$\mu_x = \exp[\mu + 0.5\sigma^2] \qquad (4.11)$$

$$\sigma_x^2 = \mu_x^2[\exp(\sigma^2) - 1] \qquad (4.12)$$

It should be noted from the above equations that $\ln(\mu_x)$, the logarithm of the mean of x is not equal to the mean of $\ln(x)$. In the above expressions, x represent either floe edge distance L or centre distance l. $p_1(L)$ and $p_2(l)$ refer to the Lognormal probability density functions of floe edge distance and centre distance respectively. Under the assumptions demonstrated before, $p_1(L)$ and $p_2(l)$ are regarded as mean one-dimensional distributions which do not change with time within an individual space subset and an individual time period. The values of the parameters of these Lognormal distributions and the probability plot correlation coefficients R obtained from the probability plot test are shown in Table 4.7. The graphs of Lognormal probability density functions (PDF) of floe edge and centre distance distributions in two directions (long axis direction and Tp direction) are shown in Figure 4.12 to Figure 4.15.

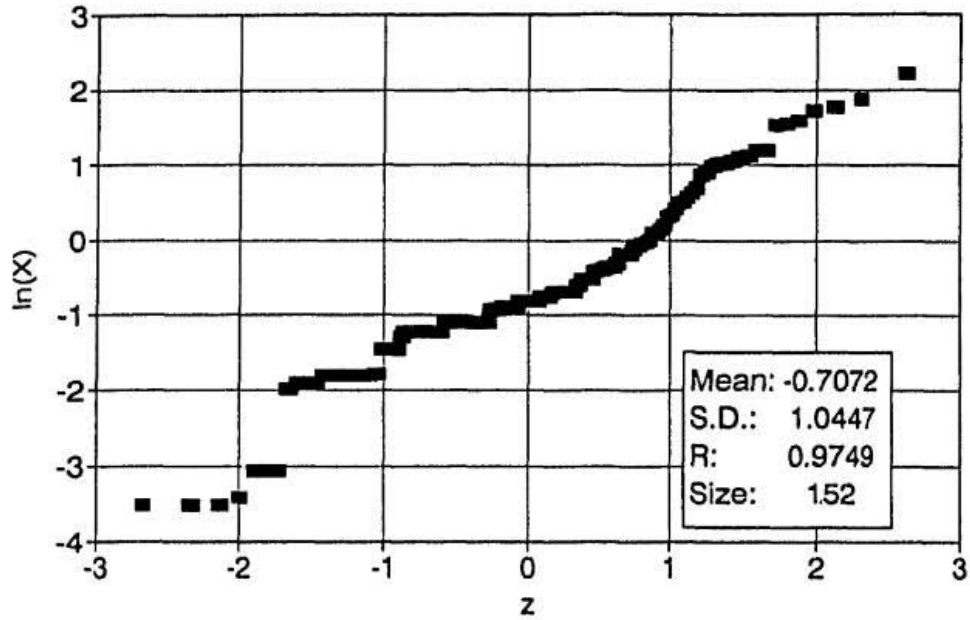

Figure 4.8: Lognormal distribution plot of edge distance in long axis direction

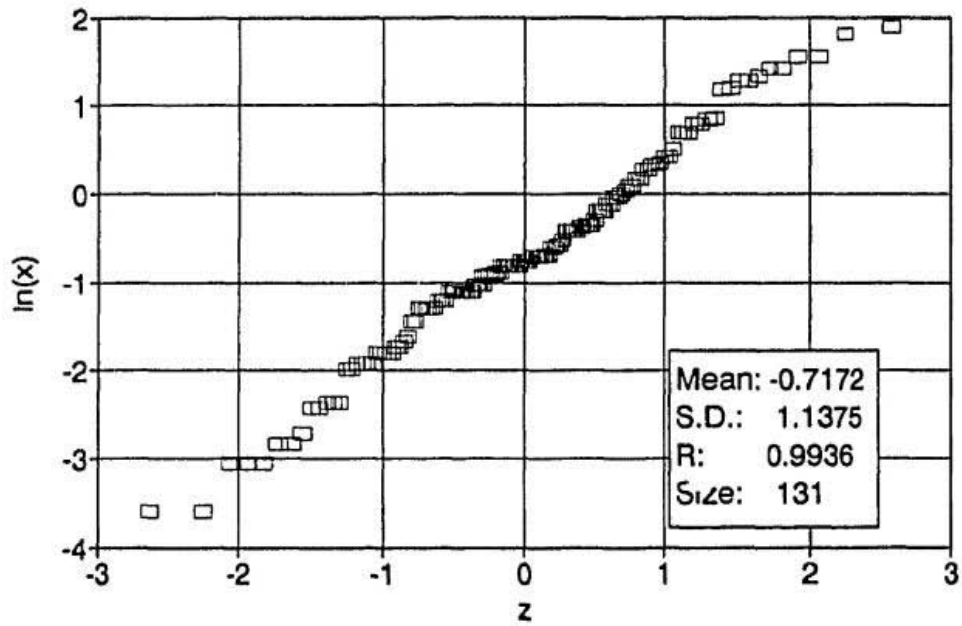

Figure 4.9: Lognormal distribution plot of edge distance in Tp direction

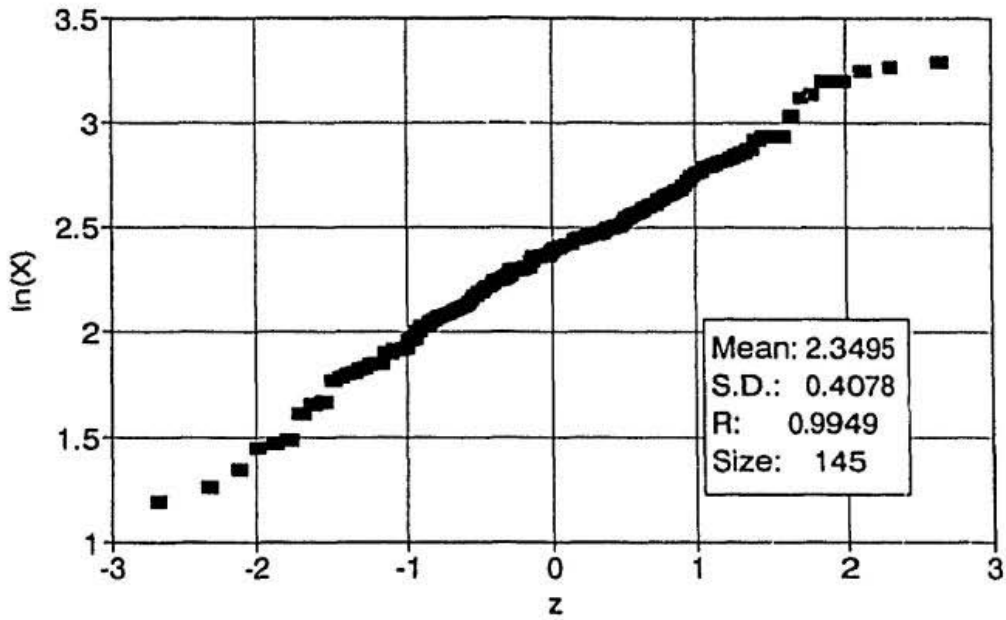

Figure 4.10: Lognormal distribution plot of centre distance in long axis direction

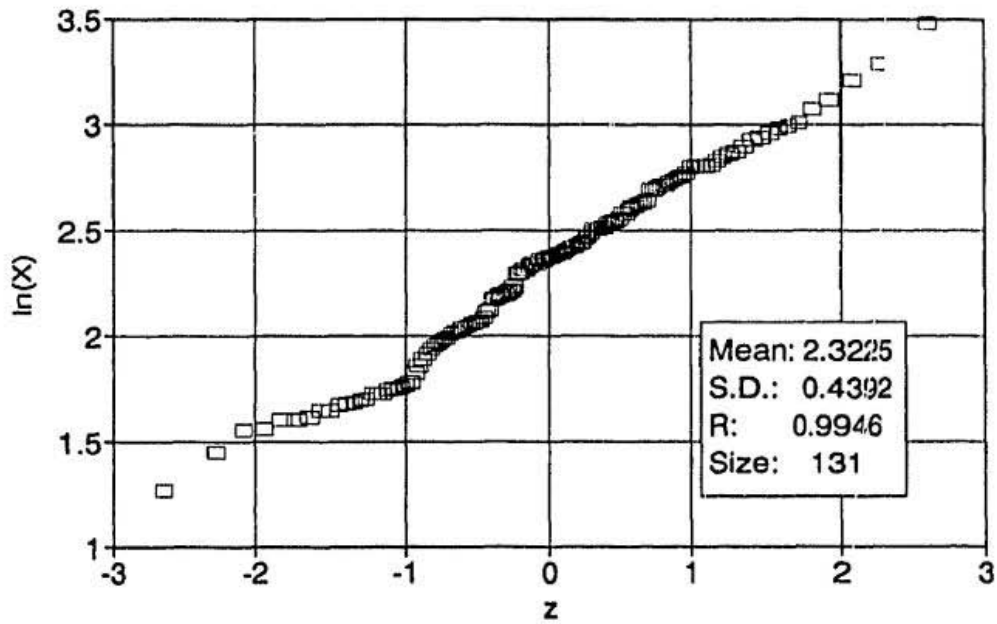

Figure 4.11: Lognormal distribution plot of centre distance in Tp direction

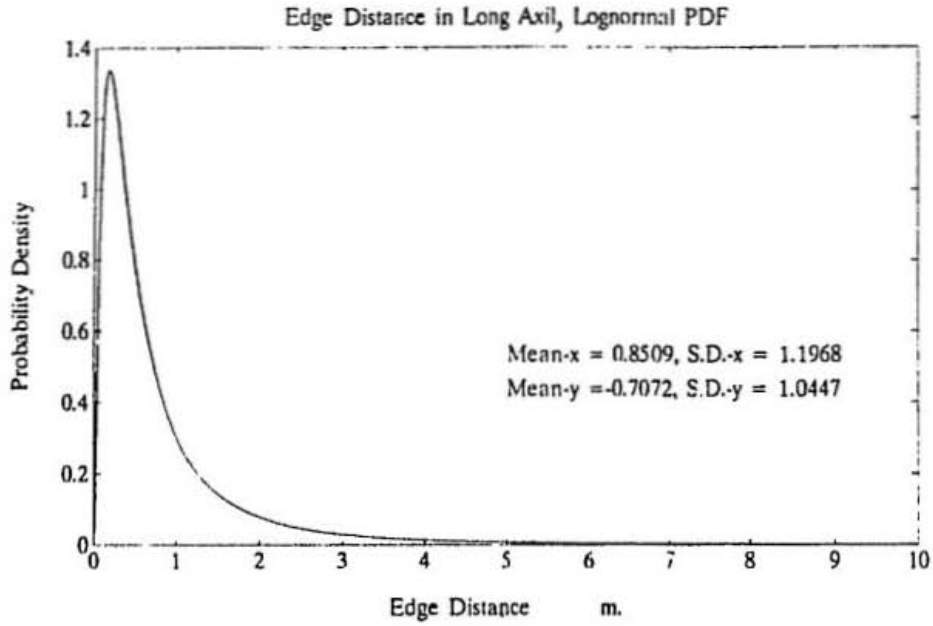

Figure 4.12: Lognormal PDF of edge distance in long axis direction

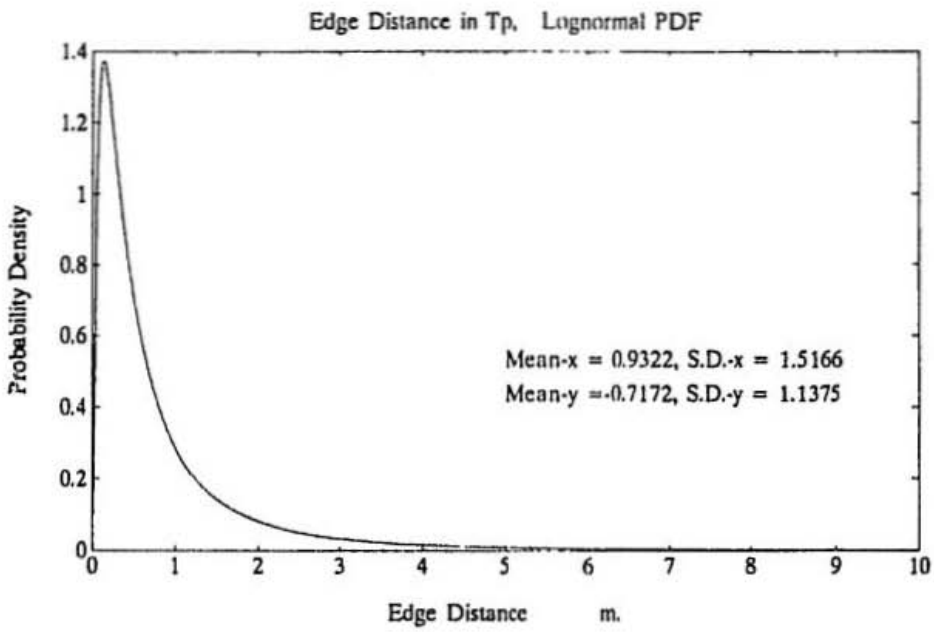

Figure 4.13: Lognormal PDF of edge distance in Tp direction

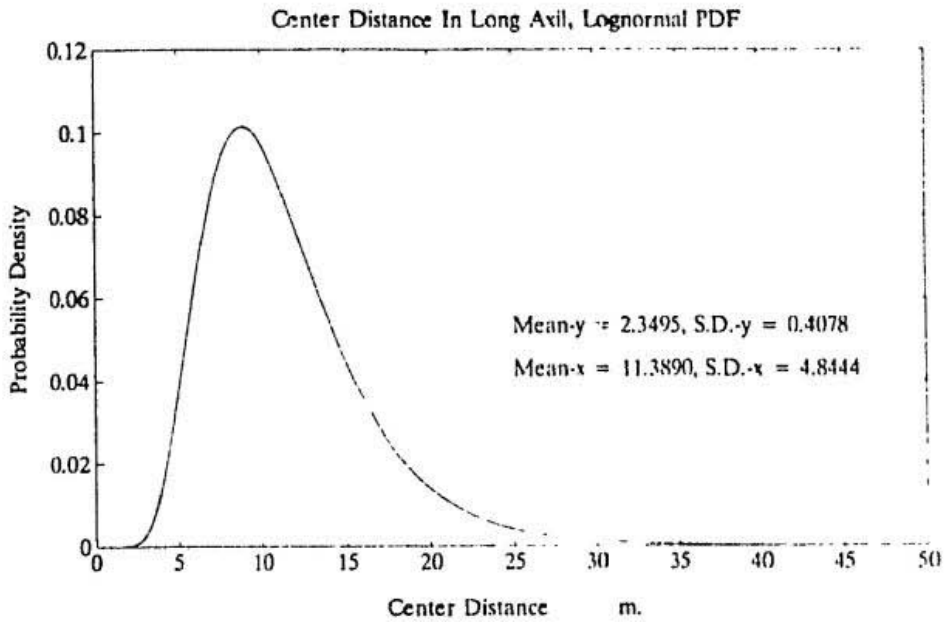

Figure 4.14: Lognormal PDF of centre distance in long axis direction

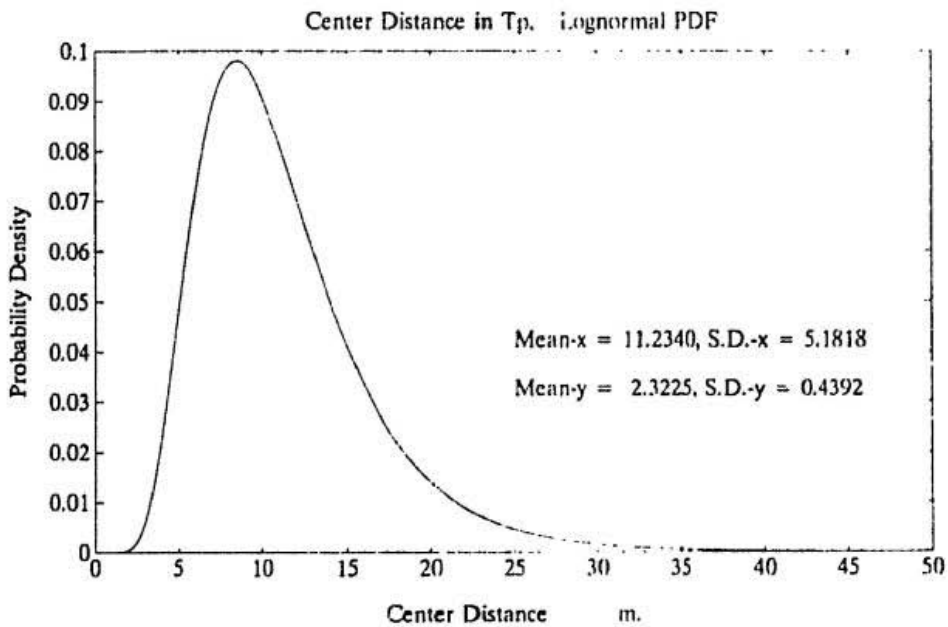

Figure 4.15: Lognormal PDF of centre distance in Tp direction

PHOTO	SAMPLE	WEIBULL DISTR.			NORMAL DISTR.			GAMMA DISTR.			LOGNORMAL DISTR.		
#	SIZE	η	ξ	R	μ	σ	R	μ	σ	R	μ	σ	R
5400	37	2.0421	0.7043	0.9320	0.4688	0.3713	0.7663	0.7210	0.1946	0.9275	-1.1091	0.8645	0.9129
5404	31	0.6178	1.1710	0.9729	1.9149	2.0844	0.8811	1.0521	0.4797	0.9754	-0.1726	1.4738	0.9795
5412	28	2.3127	0.6308	0.8786	0.6793	0.5304	0.6120	0.7028	0.2089	0.8466	-1.1897	0.8252	0.9209
5416	30	1.7960	0.3721	0.8665	0.5299	0.3109	0.7736	0.7797	0.1354	0.8807	-0.7932	0.4928	0.9186
5420	26	0.8057	0.6648	0.9546	1.2111	1.0156	0.8745	0.9873	0.2837	0.9647	-0.1535	0.8543	0.9838
TOTAL	152	1.2868	0.7950	0.9423	0.9076	1.0146	0.7496	0.8423	0.3023	0.9293	-0.7072	1.0447	0.9749

Table 4.3: Probability plot test of edge distance in long axis direction

PHOTO	SAMPLE	WEIBULL DISTR.			NORMAL DISTR.			GAMMA DISTR.			LOGNORMAL DISTR.		
#	SIZE	η	ξ	R	μ	σ	R	μ	σ	R	μ	σ	R
5400	30	2.3267	0.6198	0.9768	0.3963	0.2809	0.9366	0.6918	0.1807	0.9836	-1.2071	0.8143	0.9796
5404	27	0.8971	1.2189	0.9565	1.4918	1.7397	0.8542	0.9365	0.4650	0.9533	-0.5698	1.5563	0.9789
5412	27	1.3475	0.6626	0.9585	0.7236	0.6126	0.8376	0.8314	0.2349	0.9557	-0.6670	0.8431	0.9777
5416	28	2.1496	0.6604	0.8989	0.4915	0.4605	0.7838	0.7163	0.2137	0.9043	-1.1332	0.8591	0.9372
5420	19	1.0424	1.0016	0.9808	1.0074	1.0364	0.8678	0.8840	0.3479	0.9772	-0.5922	1.2129	0.9814
TOTAL	131	1.2422	0.8753	0.9700	0.9107	0.9791	0.8075	0.8452	0.3185	0.9623	-0.7172	1.1375	0.9936

Table 4.4: Probability plot test of edge distance in Tp direction

PHOTO #	SAMPLE SIZE	WEIBULL DISTRIBUTION			LOGNORMAL DISRTIBUTION		
		η	ξ	R	μ	σ	R
5400	37	0.0947	0.3178	0.9893	2.1768	0.3936	0.9746
5404	30	0.0640	0.3876	0.9850	2.5305	0.4844	0.9821
5412	28	0.0772	0.2498	0.9667	2.4211	0.3157	0.9758
5416	29	0.0854	0.2513	0.9898	2.3186	0.3113	0.9785
5420	21	0.07997	0.3292	0.9362	2.3425	0.4312	0.9837
TOTAL	145	0.0795	0.3179	0.9811	2.3495	0.4078	0.9949

Table 4.5: Probability plot test of centre distance in long axis direction

PHOTO #	SAMPLE SIZE	WEIBULL DISTRIBUTION			LOGNORMAL DISTRIBUTION		
		η	ξ	R	μ	σ	R
5400	30	0.1059	0.2913	0.9652	2.0796	0.3755	0.9872
5404	27	0.0595	0.3185	0.9620	2.6263	0.4443	0.9800
5412	27	0.0811	0.2873	0.9820	2.3513	0.3581	0.9780
5416	28	0.0828	0.3304	0.9563	2.3051	0.4168	0.9632
5420	19	0.0867	0.3358	0.9670	2.2588	0.4248	0.9829
TOTAL	131	0.0809	0.3353	0.9652	2.3225	0.4392	0.9946

Table 4.6: Probability plot test of centre distance in Tp direction

	Long Axis		Tp Direction	
	Edge	Center	Edge	Center
R	0.9749	0.9949	0.9936	0.9946
μ	-0.7072	2.3495	-0.7172	2.3225
σ	1.0447	0.4078	1.1375	0.4392
μ_x	0.8509	11.3890	0.9322	11.2340
σ_x^2	1.4324	23.4682	2.3001	26.8508

Table 4.7: Lognormal distribution parameters of the edge and centre distances

Chapter 5

Collision Probability

5.1 Joint Probability Distribution of Floe Spacing Distances

Ice floe edge distance L and centre distance l have been shown to be described by a Lognormal distribution quite well as $p_1(L)$ and $p_2(l)$. The two random variables L and l certainly depend on each other. Generally speaking, they should be somewhat directly proportional to each other when the floes are loosely packed. However, when there is a large number of floes and they are closely packed, this conclusion becomes doubtful. Between neighboring floes, large centre distance does not necessarily mean large or small edge distance, and vice versa, since most of the floe centre crossing lines are not in the wave propagation direction, and floe concentration and size also influence the distances (recall that the measurements of floe spacing distances were made in the direction of wave propagation). Furthermore, if the floe shapes are very irregular, L and l would be less dependent on each other. For the ice field of the present study, where the ice floes were closely packed and

their shapes were irregular or , say, randomly distributed, it could be assumed that l and L are independent random variables. Then one obtains the joint probability density function of floe edge distance and centre distance as:

$$\begin{aligned} p(l, L) &= p_1(L)p_2(l) \\ &= \frac{1}{2\pi\sigma_1\sigma_2 Ll} \exp[-\frac{(\ln(L) - \mu_1)^2}{2\sigma_1^2} - \frac{(\ln(l) - \mu_2)^2}{2\sigma_2^2}] \end{aligned} \tag{5.1}$$

$$0 < L < \infty, 0 < l < \infty$$

where μ_1 and σ_1 are the mean and the standard deviation of $\ln(L)$ respectively; μ_2 and σ_2 are the mean and the standard deviation of $\ln(l)$ respectively; whose relations with the means and standard deviations of L and l are as equation (4.11) and (4.12).

Figure 5.1 shows the joint probability density function $p(l, L)$ of floe edge and centre distances. The graph is from equation (5.1), and the means and the standard deviations of the equation are from the values in the long axis direction of Table 4.7. From the figure it is clear that the joint probability density function is concentrated at a small area. The peak is at the position where edge distances L is near zero and centre distance l is about 10. This joint probability density function, together with the floe collision criterion, will give the ice floe collision probability.

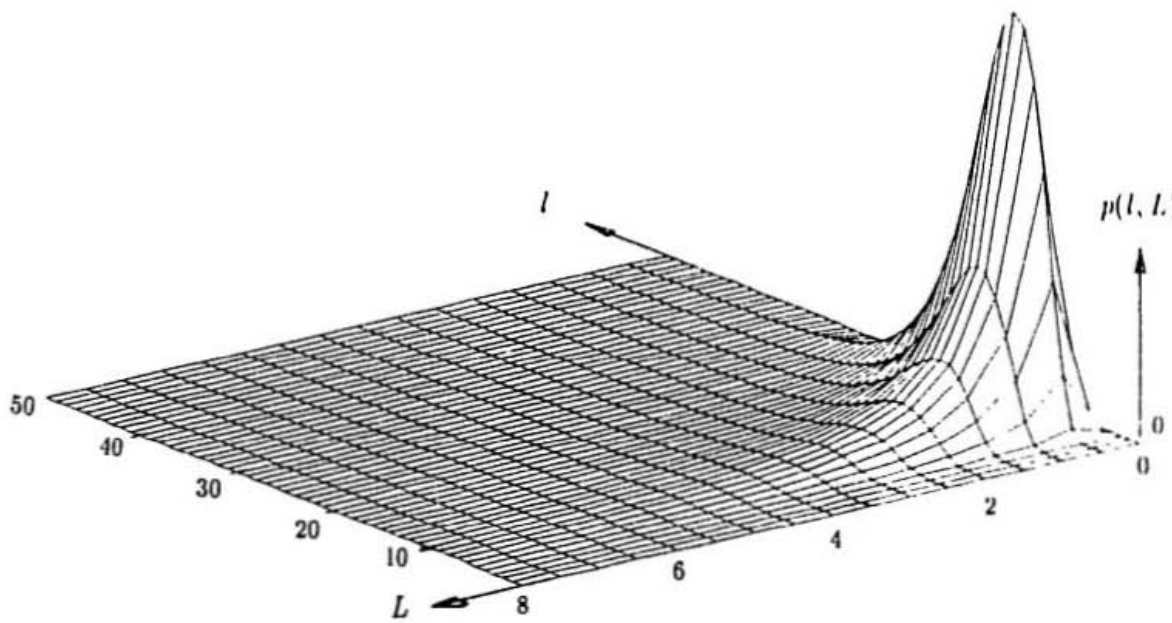

Figure 5.1: Joint probability density function of the Lognormal distributions of floc edge and centre distances

5.2 Collision Probability

So far, the floe collision criterion has been obtained as equation (3.12), where ak represents wave conditions and L/l represents floe spacing conditions. Floe collision occurrence depends on whether the criterion $L/l \leq ak$ is satisfied. L and l have been defined as random variables and assumed independent from each other, and their joint probability distribution has also been obtained as equation (5.1). Now the problem has been turned into how to find the probability of L/l less than ak. This probability is the desired collision probability. From probability theory, the collision probability for two adjacent floes can be described as:

$$\begin{aligned} G(ak) &= P(\frac{L}{l} < ak) \\ &= \int_0^{\infty} \int_{-\infty}^{lak} p(L,l)\mathrm{d}L\mathrm{d}l + \int_{-\infty}^{0} \int_{lak}^{\infty} p(L,l)\mathrm{d}L\mathrm{d}l \qquad (5.2) \\ & \qquad 0 < L < \infty, 0 < l < \infty \end{aligned}$$

From the sketch of this integration in Figure 5.2, it can be seen that the integration has non-zero value only at the area between $L = akl$ and $L = 0$, considering $l > 0$ and $L > 0$.

Substitution of equation (5.1) into (5.2) gives:

$$\begin{aligned} G(ak) &= \frac{1}{2\pi\sigma_1\sigma_2} \int_0^{\infty} \mathrm{d}l \int_0^{lak} \\ & \frac{1}{Ll} \exp[-\frac{(\ln(L)-\mu_1)^2}{2\sigma_1^2} - \frac{(\ln(l)-\mu_2)^2}{2\sigma_2^2}]\mathrm{d}L \qquad (5.3) \\ & \qquad 0 < L < \infty, 0 < l < \infty \end{aligned}$$

where μ_1 and σ_1 are the mean and the standard deviation of $\ln(L)$ respectively, μ_2

and σ_2 are the mean and the standard deviation of $\ln(l)$ respectively. $G(ak)$ is the collision probability of two adjacent floes during one wave cycle.

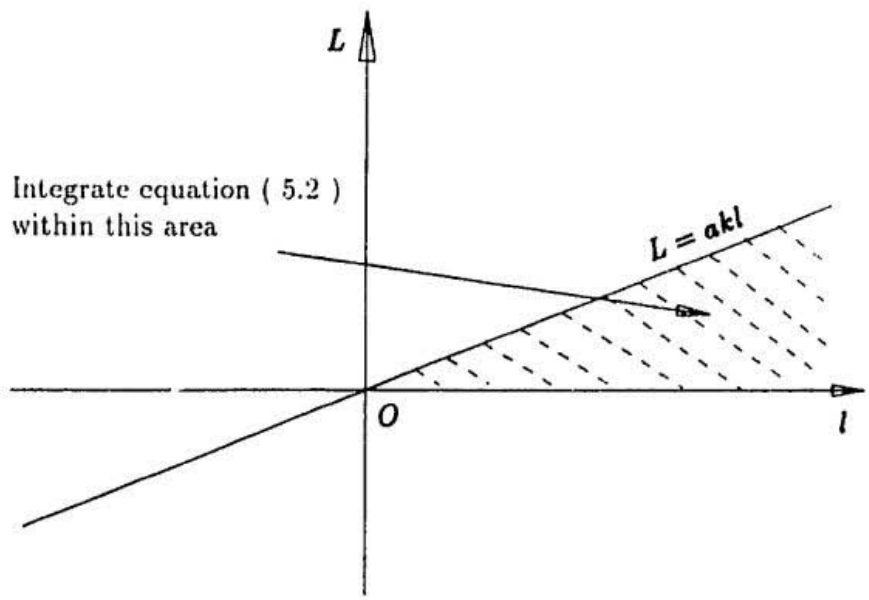

Figure 5.2: Sketch of probability integration

5.3 Numerical Integration and Potential Extension of the Collision Probability

The collision probability , $G(ak)$, of two adjacent ice floes during one wave cycle can be obtained by numerical integration of equation (5.3). The means and the standard deviations were from Table 4.7. From the ice motion package data of experiment 6 of LIMEX'89 phase two conducted from the MV *Terra Nordica*, the significant wave height was 0.26 metres, and the wave period of the main spectral peak was 10.0 seconds at 22:30 GMT for package 6. The choice of package 6 was due to the fact that the area, where the photographs were taken, was near package 6. Then the results from numerical integration of equation (5.3) were $G(ak) = 0.02126$ in the long axis direction, and $G(ak) = 0.03009$ in Tp direction. A Fortran program for the numerical integration is shown in Appendix D. These values should not be rashly used to get the number of collisions for any special individual floe. However, valuable results can be derived from these probabilities. Further discussion is presented in chapter 7.

If the number of ice floes in an area is known as N, the possible collision number during one wave cycle in that area can be expressed as $NG(ak)$. From $NG(ak)$, wave energy lost due to floe collisions can be obtained (for this purpose, collision velocity distribution and duration distribution are required). Of course, to do this one should not use the same $G(ak)$ throughout, because the waves will be attenuated as they pass through the area covered by ice floes. The ice floe spacing characteristics may also change in different areas. The area should be further divided into a number of subareas, and attenuated wave parameters and local floe

spacing distributions should be used in each subarea.

Now we consider the floe collision problem during a selected time period t_0. The time period t_0 should be long enough compared with wave period T, which is necessary for obtaining practical floe collision numbers from the collision probability. If the wave period is T, the possible number of collisions in an area with N pieces of floes is:

$$m = \frac{t_0}{T} NG(ak) \tag{5.4}$$

Ice floe collisions are thought as one of the major sources of ocean noise in the Marginal Ice Zone. The obtained collision number can provide insight to the investigation of under-sea acoustic noise, which is important for remote sensing some of the physical processes of the ocean. The possible collision number for one floe in that period is:

$$n = 2\frac{t_0}{T} G(ak) \tag{5.5}$$

where the coefficient 2 occurs because of the assumption that one floe may collide with two other adjacent floes forward and backward of wave direction during one wave cycle. See Figure 5.3 for the sketch of this concept. From the above results, it is known that one floe may collide n times during time period t_0, so that floe size reduction and energy losses may be derived from this number. This knowledge is important for predicting ice loading forces on offshore structures.

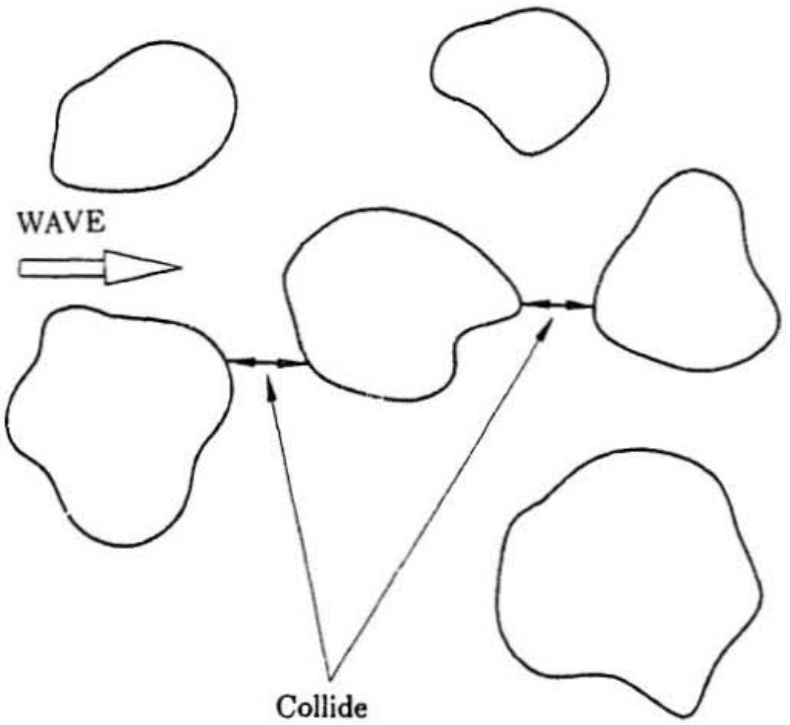

Figure 5.3: One floe may collide with two others during a wave cycle

Chapter 6

Collision Analysis from Ice Motion Data

6.1 LIMEX'89 Ice Motion Data

Three ice motion packages, numbered 3, 5, and 6 were used for experiment 6 of LIMEX'89 phase two conducted from the MV *Terra Nordica*. Each motion package consisted of three accelerometers mounted in orthogonal directions, a gyro measuring tilt and a compass, allowing for the measurement of the translational and rotational motions of the floes. Acceleration, tilt and compass data were collected for 30 minute periods each hour for a total of about 20 hours on April 2 and 3 of 1989. While the interpretation of floe collisions from the motion package data was not the primary goal of the LIMEX'89 experiment, the evidence of collision in the data provides an opportunity to investigate the behaviour of ice floes under wave action. The data were filtered and resampled at 1.33 Hz and recorded in blocks of 200 seconds. Translational accelerations were resolved into N-S and E-W components in the horizontal plane, and into a vertical component. Tilt angles were also resolved to N-S and E-W components. The resolution of the accelerations was

about 0.001 ms^{-2}, the tilt angles were recorded to ± 0.01 degrees and compass bearings were resolved to ± 0.3degrees. See McKenna and Crocker (1991) for detailed descriptions.

The motion package data gave measurements of wave-induced floe motions and provided information to establish whether collision had actually taken place. The data had a frequency responses of up to about 0.5 Hz, which was only sufficient to identify deviations from regular floe motion, but not high enough to characterize the nature of the collisions. This becomes clear from looking at the acceleration traces shown in figure 6.1. From the acceleration traces, collision events can be identified during that period by identifying the abnormal acceleration traces or the smoothness of the traces. The information about the ice motion packages is in Table 6.1 and Figure 4.4.

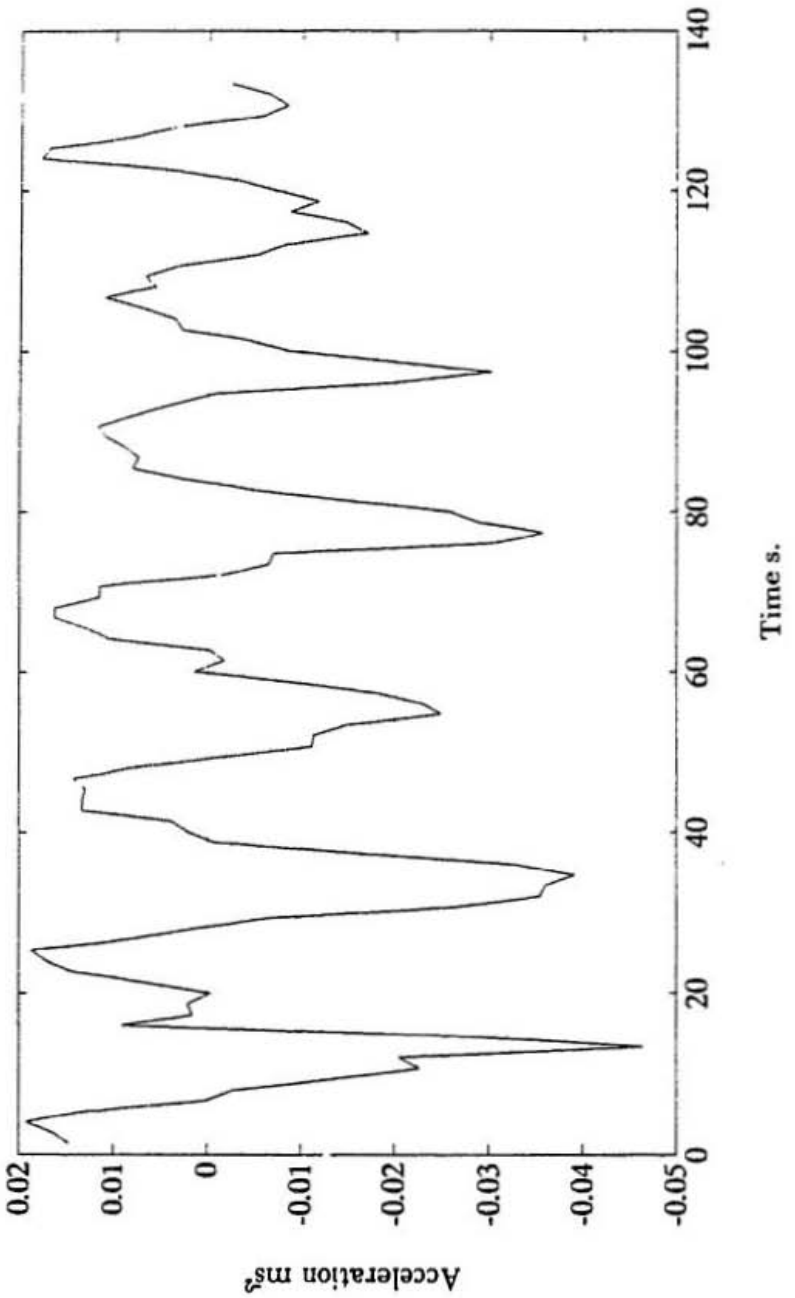

Figure 6.1: An example of the acceleration traces from ice motion package 6

Package #	Deployment Time (GMT)	Recovery Time (GMT)	Floe Avr. Thickness (m)	Floe Dimension (m×m)	Initial Position	Final Position
3	21:00 Apr 2	16:40 Apr 3	1.13	28 × 25	49°40.2′N 50°48′W	49°27′N 50°28.8′W
5	22:15 Apr 2	16:15 Apr3	0.89	13 × 11	49°46.8′N 50°53.3′W	49°35.4′N 50°46.2′W
6	22:00 Apr 2	16:00 Apr 3	0.89	20 × 15	49°46.2′N 50°53.4′W	49°30′N 50°43.2′W

Table 6.1: Information about ice motion package

6.2 Collision Events Obtained from the Acceleration Data

In order to identify collision events from the abnormal acceleration traces, a Fortran program was completed (Appendix E). It used the zero crossing of the acceleration traces to define a half wave cycle. As demonstrated before, in the present study waves were thought to be the only dominant factor which excited ice floes and governed their movements. By the assumption of water particle-like motion of ice floes, the floes moved as water particles on a wave surface. The acceleration traces of a floe therefore had only one maximum and one minimum during one wave cycle. This meant that the derivation of acceleration traces changed sign once during a half wave cycle. Within any individual half wave cycle, if the derivative of the acceleration traces changed sign twice or more, which meant one or more extra troughs existed, it was considered that a collision had occurred. It should be noted that this statement was true only for a virtually monochromatic swell. A better criterion for collisions could be established if ice acceleration data with higher frequency are available. As mentioned by McKenna and Crocker (1991), most of the evidence for collisions was found in the horizontal accelerations; only a few was transferred to the heave cycle.

The same procedure was carried out on all three acceleration time series. A collision event might be shown on all three acceleration traces and it might be shown on only two or one traces. However, only one collision event was counted even though extra troughs might be found on two or even all three acceleration traces at the same time. Multiple collisions within half wave cycle were thus ignored.

This treatment was because: 1) it could not be identified that the simultaneously abnormal traces of more than one acceleration were caused by one single collision event or by two or three events; 2) in Chapter 5 floe spacing distances were measured on the assumption of one floe hitting at most two other floes in the forward and backward wave propagation direction during one wave cycle, which meant no more than one single collision event existed during a half wave cycle. The results of collision events are shown in Table 6.2, 6.4, and 6.6. In the Tables, the ' CYCLES ' is the arithmetical average of wave cycle numbers from the three accelerations during half an hour; the ' COLLISION NUMBER ' is the sum but without the repeated events from the three accelerations; the ' COLLISION PROPORTION ' is the quotient of collision number over wave cycles.

When ice floe spacing distances were worked out from the aerial photographs in Chapter 5, it was demonstrated that floe collisions occurred in the wave propagation direction, and the floe spacing distances were measured in that direction. A group of floe spacing distances were also measured in the so called long axis direction, which was the flight direction of the helicopter. The long axis direction was about 70 degrees from Tp direction, depending on individual photographic slide. This group of data was for the purpose of comparison. (See Chapter 5 and Chapter 7 for details). In order to see how collision events were reflected on acceleration data of different directions, the horizontal data were resolved into Tp direction and its orthogonal direction, here Tp direction was the direction with peak wave energy on the wave spectra. Tp direction, being 58 degrees from the true North and about 70 degrees from the long axis (flight) direction, may still be called wave propagation

direction. The results of collision events in Tp direction are shown in Table 6.3, 6.5, and 6.7.

For part of the data from ice motion package 3, floe collision events were also identified visually by the same principle used in the program and recorded manually for the purpose of comparison. The results are shown together with the results by the program in Table 6.8. In the table, A_x A_y, and A_Z refer to the two horizontal and the vertical accelerations respectively. Note that the values here from the program are somewhat different from those in Table 6.2. This is because more than one event might be recorded during a half wave cycle, if the abnormal acceleration traces were found from the data of two or three directions . The comparison result shows a good agreement between the two approaches.

TIME	CYCLES	COLLISON NUMBER	COLLISION PROPORTION
21:30-22:00	195.0	71.0	0.3559
22:30-23:00	196.3	68.0	0.3529
23:30-24:00	204.7	44.0	0.2148
00:30-01:00	201.7	47.0	0.2334
01:30-02:00	201.0	52.0	0.2673
02:30-03:00	201.7	60.0	0.3132
03:30-04:00	206.0	58.0	0.2828
04:30-05:00	206.3	64.0	0.3122
05:30-06:00	204.3	56.0	0.2749
06:30-07:00	196.7	51.0	0.2619
07:30-08:00	177.7	99.0	0.5712
08:30-09:00	172.3	130.0	0.7847
09:30-10:00	149.3	131.0	0.9373
10:30-11:00	148.7	123.0	0.9488
11:30-12:00	126.7	137.0	1.2261
12:30-13:00	137.7	151.0	1.2739
13:30-14:00	134.7	146.0	1.3498
14:30-15:00	147.7	176.0	1.3523
15:30-16:00	145.7	158.0	1.1541
16:30-17:00	165.0	191.0	1.1360

Table 6.2: Collision events from acceleration data of package 3

TIME	CYCLES	COLLISON NUMBER	COLLISION PROPORTION
22:30-23:00	187.7	101.0	0.5512
23:30-24:00	192.0	72.0	0.3831
00:30-01:00	200.0	72.0	0.3648
01:30-02:00	205.0	75.0	0.3673
02:30-03:00	201.0	70.0	0.3583
03:30-04:00	200.3	114.0	0.5644
04:30-05:00	210.0	118.0	0.5587
05:30-06:00	232.7	255.0	1.0976
06:30-07:00	263.7	355.0	1.3381
07:30-08:00	265.3	339.0	1.3343
08:30-09:00	330.0	270.0	0.8927
09:30-10:00	328.3	222.0	0.7203
10:30-11:00	386.7	121.0	0.3321
11:30-12:00	263.3	257.0	1.0201
12:30-13:00	305.0	206.0	0.6917
13:30-14:00	266.7	270.0	1.0556
14:30-15:00	220.0	317.0	1.4808
15:30-16:00	192.3	300.0	1.5994

Table 6.3: Collision events from acceleration data of package 3 (in Tp direction)

TIME	CYCLES	COLLISON NUMBER	COLLISION PROPORTION
21:30-22:00	182.7	116.0	0.6286
22:30-23:00	179.0	89.0	0.5097
23:30-24:00	183.0	149.0	0.8273
00:30-01:00	184.0	84.0	0.1764
01:30-02:00	191.3	99.0	0.5296
02:30-03:00	186.0	116.0	0.6467
03:30-04:00	181.3	102.0	0.5767
04:30-05:00	183.7	140.0	0.7778
05:30-06:00	161.0	176.0	1.1459
06:30-07:00	151.3	178.0	1.2219
07:30-08:00	139.7	178.0	1.2973
08:30-09:00	127.3	163.0	1.3188
09:30-10:00	143.7	217.0	1.1292
10:30-11:00	143.7	217.0	1.4292
11:30-12:00	163.7	224.0	1.3265
12:30-13:00	149.3	243.0	1.6125
13:30-14:00	142.7	226.0	1.5386
14:30-15:00	156.0	145.0	1.2238
15:30-16:00	112.3	141.0	1.4373

Table 6.4: Collision events from acceleration data of package 5

TIME	CYCLES	COLLISON NUMBER	COLLISION PROPORTION
21:30-22:00	197.3	101.0	0.4995
22:30-23:00	200.3	82.0	0.4180
23:30-24:00	202.7	42.0	0.2078
00:30-01:00	203.7	57.0	0.2790
01:30-02:00	205.0	39.0	0.1909
02:30-03:00	205.3	39.0	0.1898
03:30-04:00	198.7	74.0	0.3827
04:30-05:00	203.3	53.0	0.2635
05:30-06:00	198.3	65.0	0.3322
06:30-07:00	201.0	50.0	0.2502
07:30-08:00	185.3	90.0	0.4963
08:30-09:00	167.0	124.0	0.8048
09:30-10:00	160.7	149.0	0.9548
10:30-11:00	138.0	132.0	1.0658
11:30-12:00	141.7	136.0	1.1048
12:30-13:00	118.0	92.0	1.2663
13:30-14:00	124.0	125.0	1.3003
14:30-15:00	128.0	134.0	1.3534
15:30-16:00	145.0	131.0	1.0248
16:30-17:00	165.3	207.0	1.2115

Table 6.5: Collision events from acceleration data of package 5 (in Tp direction)

TIME	CYCLES	COLLISON NUMBER	COLLISION PROPORTION
22:30-23:00	185.0	100.0	0.5766
23:30-24:00	185.3	79.0	0.4581
00:30-01:00	199.7	82.0	0.4243
01:30-02:00	200.7	92.0	0.4653
02:30-03:00	199.3	85.0	0.4457
03:30-04:00	200.0	140.0	0.7040
04:30-05:00	207.7	134.0	0.6453
05:30-06:00	237.0	311.0	1.2813
06:30-07:00	256.3	419.0	1.6196
07:30-08:00	266.3	324.0	1.2912
08:30-09:00	342.3	258.0	0.7993
09:30-10:00	337.3	247.0	0.7640
10:30-11:00	380.0	137.0	0.3898
11:30-12:00	256.7	271.0	1.1332
12:30-13:00	294.0	207.0	0.7848
13:30-14:00	275.0	255.0	1.0046
14:30-15:00	234.0	313.0	1.3881
15:30-16:00	187.0	309.0	1.6948

Table 6.6: Collision events from acceleration data of package 6

TIME	CYCLES	COLLISON NUMBER	COLLISION PROPORTION
21:30-22:00	171.3	115.0	0.7007
22:30-23:00	177.0	89.0	0.5194
23:30-24:00	174.7	109.0	0.6506
00:30-01:00	177.0	73.0	0.4539
01:30-02:00	182.3	118.0	0.6750
02:30-03:00	180.0	106.0	0.6003
03:30-04:00	170.7	102.0	0.6469
04:30-05:00	177.0	139.0	0.8216
05:30-06:00	159.3	161.0	1.0971
06:30-07:00	158.7	155.0	1.0245
07:30-08:00	157.7	186.0	1.1978
08:30-09:00	111.0	121.0	1.3827
09:30-10:00	124.3	175.0	.5233
10:30-11:00	124.3	175.0	1.5233
11:30-12:00	135.7	185.0	1.3899
12:30-13:00	124.0	188.0	1.5406
13:30-14:00	128.7	156.0	1.3277
14:30-15:00	122.3	108.0	1.0599
15:30-16:00	111.3	106.0	1.4024

Table 6.7: Collision events from acceleration data of package 6 (in Tp direction)

	22:30-23:00		23:30-24:00		00:30-01:00		01:30-02:00		02:30-03:00	
	Observ.	Program	Observ.	Program	Observ.	Program	Observ.	Program	Observ.	Program
A_x	17	16	27	30	18	20	15	19	28	29
A_y	47	49	41	38	20	22	23	24	21	21
A_z	16	15	4	6	5	6	8	7	7	7
Sum	80	80	72	74	43	48	46	50	56	57

Table 6.8: Collision events obtained by the program and by visual judgement

Chapter 7

Discussion

7.1 Comparison of Collision Frequencies and Discussion of Errors

The acceleration data in Chapter 6 gave the number of collisions for Package 6 during 21:30-22:00 GMT of April 2, 1989. The numbers of collisions were 116 from the original data and 115 after the horizontal data were resolved into Tp and its perpendicular directions. Numerically integrating equation (5.3) gave the value of $G(ak)$ of 0.02126 for floe spacing distances measured in the long axis direction, and 0.03009 for distances measured in Tp direction. The predicted collision numbers for one floe during half an hour were then 7.75 and 10.83 respectively by equation (5.5). These numbers were one order of magnitude less than those obtained from the acceleration data.

The discrepancy was thought to be caused by several reasons. First, as mentioned before, $G(ak)$ should not be used directly to describe the collision events of any specific floes. It was from the view of statistical average that the collision probability of one floe with an adjacent floe in one wave cycle was obtained as $G(ak)$.

Floes with different sizes and shapes have different collision probabilities. Figure 7.1 shows the floe diameter distribution obtained from the aerial photographs of LIMEX'89, the mean diameter of the floes was 10.26 metres, if the floes were circles, while the dimension of the floe on which package 6 was mounted was about 20 metres. This meant that the floe of package 6 was far from representative of the floes in that area. Larger floes were surrounded by more floes than smaller ones, so they had more chances to collide with others. From the aerial photographs, it was also found that larger floes usually had larger centre distances with their neighbors than small ones did, while their edge distances with others did not have significant differences from those of small ones. This meant that larger floes had larger displacement differences and velocity differences with others, and therefore had a greater probability of colliding with adjacent floes than smaller ones did. Rottier (1990) indicated that the collision probability was greater for floes of large size. He addressed the reason as that large floes were driven by the low frequency component of the wave field, whose amplitude was greater in a typical ocean wave spectrum. The mean μ_x of the floe centre distances was 11.234 metres in the Tp direction. This value was near the mean diameter 10.26 metres of the floes, which was expected for a closely packed ice floe field. In order to check the size effects on collision probability, we took the floe diameter of 20 metres as μ_x and kept the standard deviation the same as in table 4.7 (The standard deviation of the floe centre distance has little influence on the collision probability. Refer to Figure 7.9). Then the integration program was run again and the resulting collision numbers were 22 and 28 respectively in the long axis and Tp directions. However, the above treatment is only a qualitative analysis, and the quantitative relation between the

floe size and the collision probability is to be found out in the future studies.

Secondly, only wave action was considered as a cause of floe collisions when the problem was analysed by the collision criterion and floe spacing distributions. In the real ice floe field, several other factors also influence floe collisions, although waves were thought the dominant factor in the present research. Winds and ocean currents certainly influenced floe collision behaviour. Temperature might also contribute to the collisions (McKenna and Crocker 1990). Particularly, the wave amplitude of 0.13 metres during experiment 6 was quite small (although it was the largest among the six experiments). Its effects on floe collisions might be the same order as that of other environmental factors. The collision number obtained from package acceleration data represents the combined effect of all the environmental factors, this number is therefore greater than that from one factor alone.

Thirdly, the method of judging floe collisions from acceleration data might overestimate collision events. Because the data were heavily filtered and resampled at 1.33 Hz, some significant points on the acceleration traces might be lost. The details of the interactions between ice floes could not be obtained from these acceleration data. Therefore, some floe interactions other than collisions, for example shearing contacts between floes, were also recorded on the acceleration data and could not be distinguished from floe collisions. Rottier (1990) reported that this shearing contact might occur in a quite high frequency. However, the probabilistic model of the present study did not include this shearing process. Furthermore, it is reasonable to believe that some of the collision events found from the acceleration data

were caused by small ice pieces other than by the ice floes defined in the present study. These small ice pieces were not considered as floes in the work of obtaining floe spacing distances, but they did collide with the packaged floes, although the collision energy and forces were thought very small. We could not find the detailed characteristics of the collisions from the acceleration data. The number of collisions from the acceleration data included all the collision events recorded on the ice motion data, but the collision number from the probabilistic model included only the collision events between floes larger than 3 m in diameter.

Finally, some errors in obtaining floe spacing distances affected the calculated floe collision probability. As mentioned before, the resolution of projected pictures was about 0.5 mm, which gave 0.10 to 0.15 m of real distance. It will be shown later that the floe collision probability is sensitive to the floe edge distance distribution. The mean of the floe edge distance from LIMEX'89 was 0.85 and 0.93 metres for the long axis and Tp directions respectively. The resolution of 10 to 15 cm therefore had a significant influence on floe collision probability. Another possible error was caused by the precision of the flight altitude of the helicopter. The flight altitude was the object distance A in the calibration of the photographs (Refer to Figure B.1 of Appendix B). It affected the determination of the floe spacing distances directly. The flight altitudes were obtained from the audio reports on the video tapes which were taken during the flight. It was also reported on the tapes when photographs were taken. Unfortunately, sometimes the flying altitudes were not reported at the same time as the photographs were taken, which meant the altitudes of some aerial photographs had to be estimated from the nearest altitude

reports. These estimations might be some different from the real altitudes. For example, the report of taking the photograph of number 5404 was 57 seconds from the nearest altitude report. The altitude of the photograph had to be estimated as this altitude of 240 metres. It was learnt by checking the video tapes that the flight altitude might change as much as 40 metres in one minute during the operation. Therefore, the estimated altitude might be as much as 20 percent from the real value. This difference would affect the resulting values of the means directly.

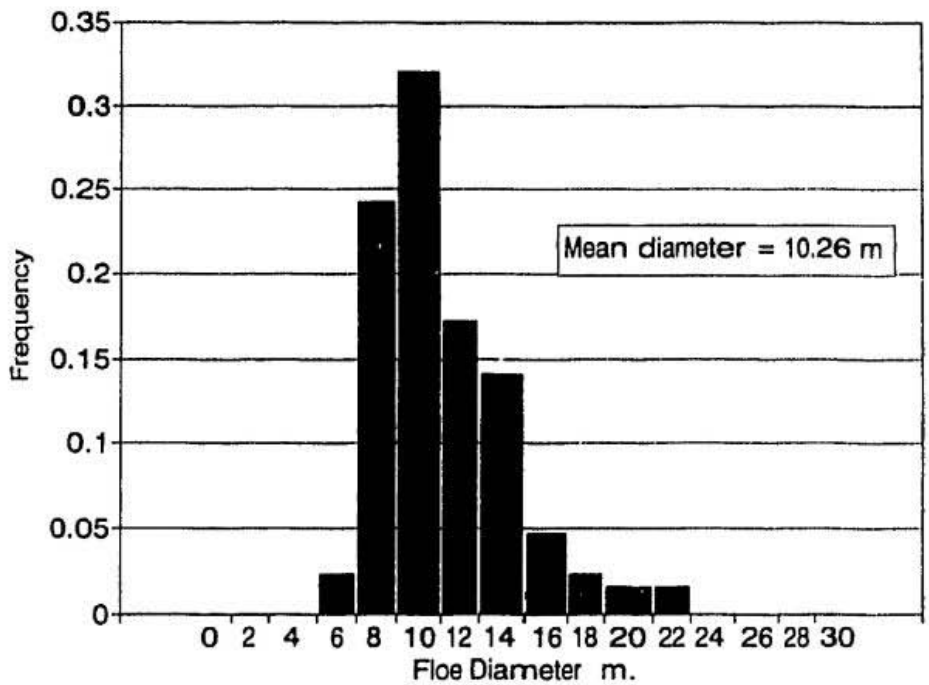

Figure 7.1: Floe diameter distribution

7.2 Collision Probability with Wave Conditions and Floe Spacing Distribution

Equation (5.3) gives the floe collision probability under wave action. Some interesting conclusions can be obtained from this expression. Plots of equation (5.3) are shown in Fig 7.2 to Figure 7.9. The collision probability $G(ak)$ is not only a function of wave amplitude a and wave period T , but also a function of floe spacing distributions, i.e. mean edge distance μ_{xe} and standard deviation σ_{xe}, and mean centre distance μ_{xc} and standard deviation σ_{xc}. In the following discussion, the means and standard deviations are as above, while the logarithms of the means and standard deviations are expressed as μ_e, μ_c, σ_e, and σ_c. The relations among means, standard deviations, and the logarithms of a Lognormal distribution are as equation (4.11) and (4.12). It should be noted that the mean μ of logarithmic distance $\ln(x)$ is not equal to the logarithm of the mean $\ln(\mu)$ of the distances x.

Figure 7.2 and Figure 7.3 show that the collision probability $G(ak)$ changes with different wave amplitude a and period T (Some values may violate the Linear Wave Theory and some combinations of a and T may not be found in nature). The ice floe spacing conditions used here are: $\mu_e = -0.7$, $\mu_c = 2.0$, $\sigma_e = 1.0$, and $\sigma_c = 0.4$ (e refers to edge distance and c refers to centre distance). These values are very near those obtained from the photographs of LIMEX'89. From these figures, it is clear that collision probability $G(ak)$ is directly proportional to wave amplitude a and inversely proportional to wave period T. Figure 7.2 shows that when a is very small, G changes very sharply with T for short waves, and slowly with long waves. There exists a transition between the two distinct parts. As a becomes larger, the

curves become smooth and finally almost a straight line for $a = 5.5$ metres. It can be found from Figure 7.3 that when T is small, $G(ak)$ changes sharply with a for the portion of small a, while the curve is very flat for large a. A transition also exists between these two parts. However, for long waves, the curves are smooth and almost a straight line for the longest one ($T = 20$ seconds). The tendency is clear that $G(ak)$ changes dramatically with small T and a. This means that we should be more careful when dealing with the results obtained from wave conditions of small amplitude and short period.

Figure 7.4 to Figure 7.7 show that the collision probability changes with the various means of the floe spacing distributions. Here the probabilities were calculated with $\sigma_e = 1.0$ and $\sigma_c = 0.4$. In these figures, the means are represented by μ_{xe} and μ_{xc}, and they are related to μ_e and μ_c by equation (4.11) and (4.12). From these figures, it is clear that the mean μ_{xe} of the edge distribution has a great influence on the collision probability. When μ_{xe} is small, $G(ak)$ increases sharply as μ_{xe} decreases. As μ_{xe} becomes larger (say larger than 2), its influence on collision probability becomes quite small. This is because the separation distances among floe edges are large enough that the floes rarely collide with each other.

Compared with the means of the edge distance, the means of the centre distance have less influence on collision probability $G(ak)$. For large μ_c, $G(ak)$ has an almost linear relation with μ_c. But when μ_e is very small, $G(ak)$ also becomes sensitive to μ_c. When the concentration of ice floes is very high, i.e. the floes are very close to each other, there is a high collision probability and it greatly depends on the mean

μ_{xe} of edge distribution. This is to be expected: the closer the floes , the greater the probability of collisions . The higher collision probability with larger μ_c reflects the fact that two floes with larger centre distances have greater phase differences and produce bigger displacement differences. Higher collision probabilities are then obtained.

Figure 7.8 and Figure 7.9 show the influence of the values of variance of floe spacing distance on the collision probability. The means used to calculate $G(ak)$ are $\mu_e = 2.35$ and $\mu_c = -0.71$, which are the values from the photographs of LIMEX'89. The values in the figures for variance are σ^2_{xe} and σ^2_{xc}. Their relations with σ_e and σ_c are as in equation (4.11) and equation (4.12). The figures clearly show that the variance of centre distance has little influence on collision probability. When σ^2_{xc} changes from 5 to 50, $G(ak)$ only changes slightly. $G(ak)$ increases as the variance of edge distance increases, which can be found on both Figure 7.8 and Figure 7.9. However, it is clear that the influence of σ_{xe} on $G(ak)$ is not as great as μ_{xe}.

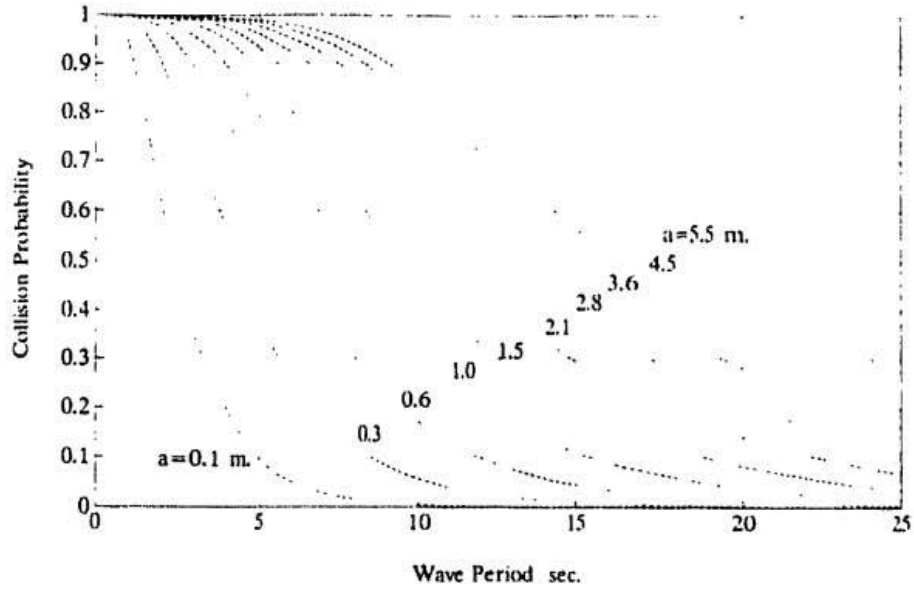

Figure 7.2: Collision probability with wave period

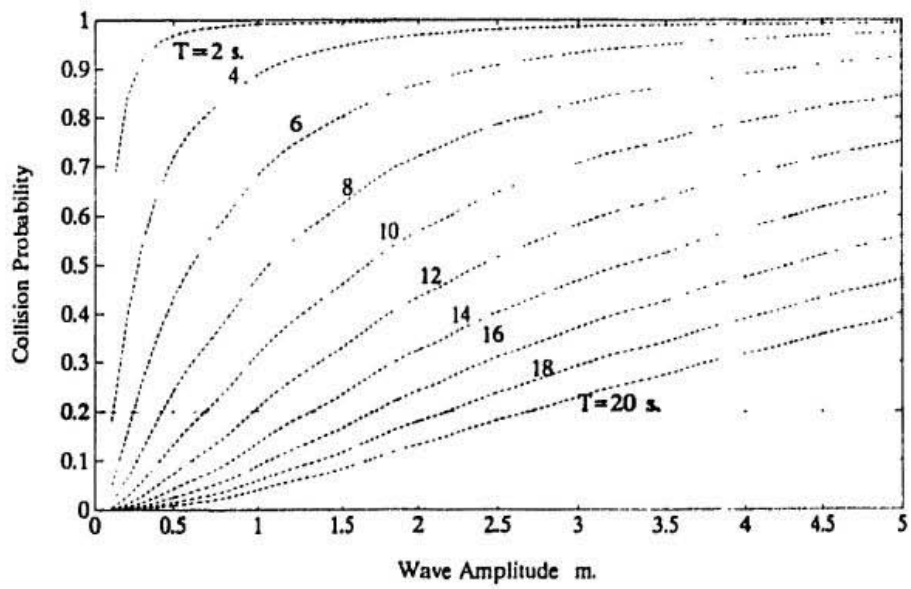

Figure 7.3: Collision probability with wave amplitude

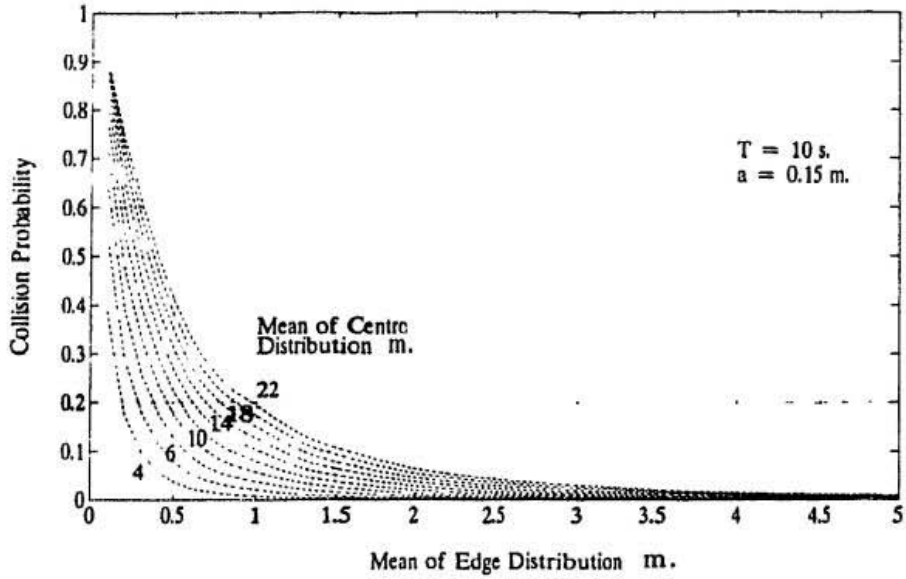

Figure 7.4: Collision probability with the mean of edge distance distribution (a = 0.15 m.)

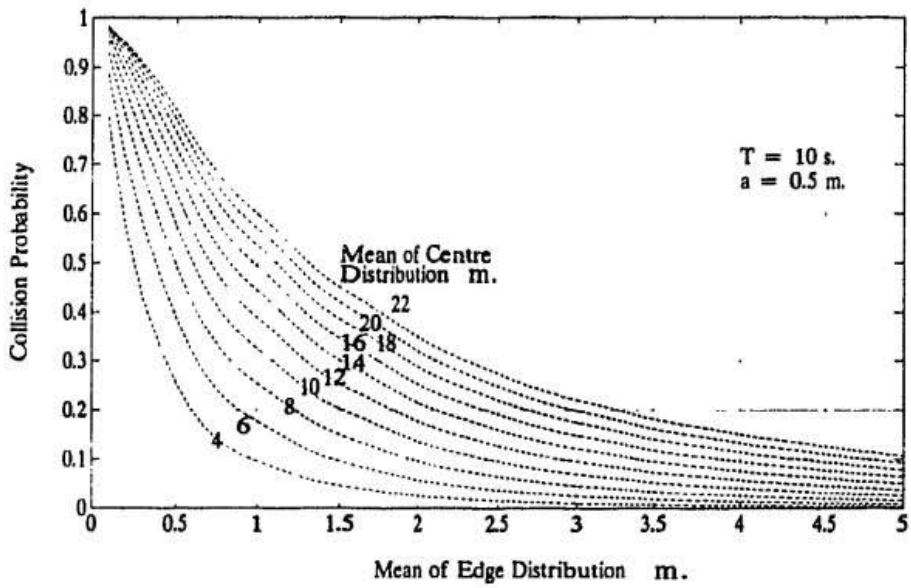

Figure 7.5: Collision probability with the mean of edge distance distribution (a = 0.5 m.)

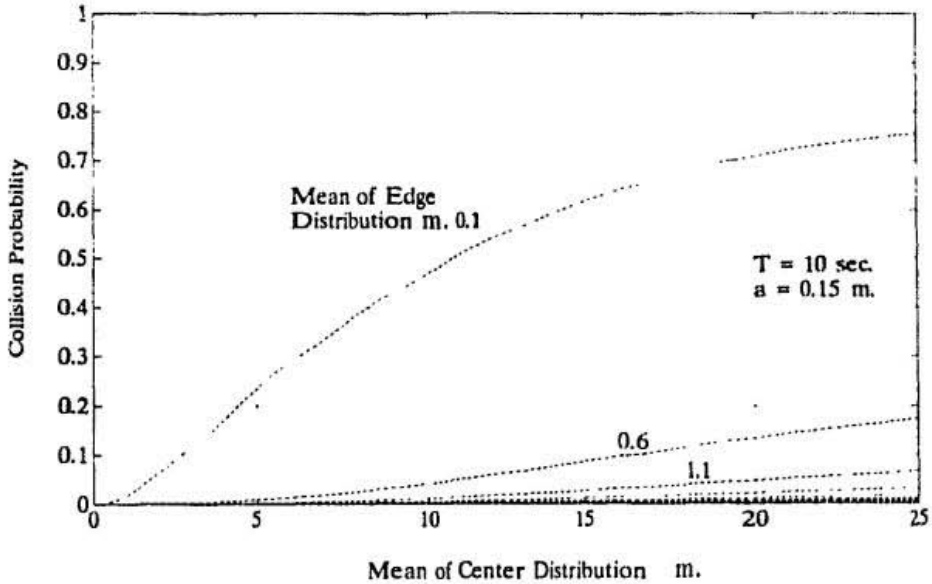

Figure 7.6: Collision probability with the mean of centre distance distribution (a = 0.15 m.)

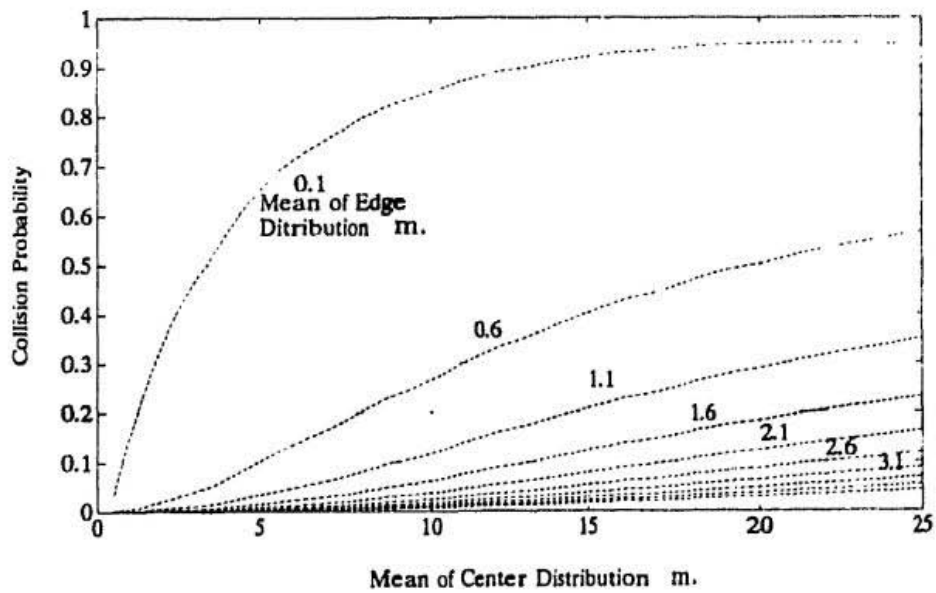

Figure 7.7: Collision probability with the means of centre distance distribution (a = 0.5 m.)

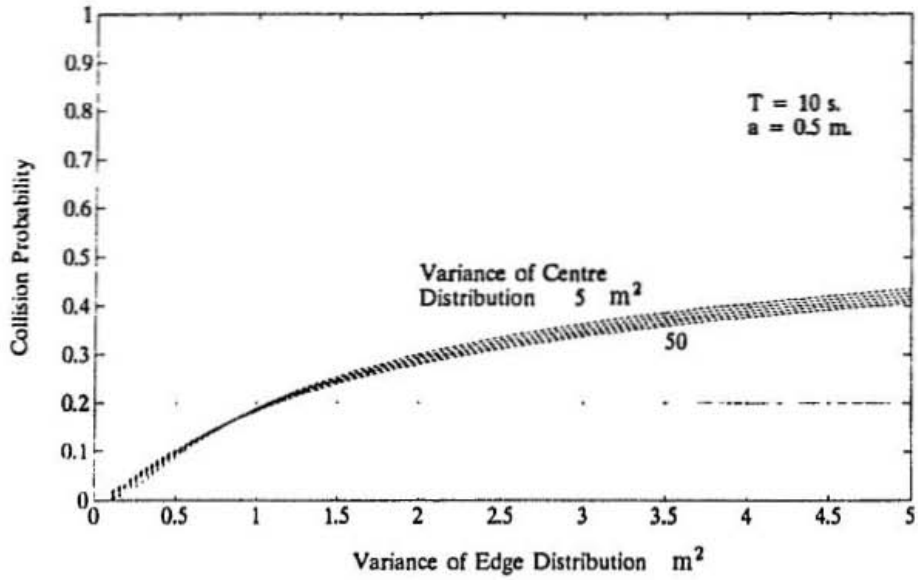

Figure 7.8: Collision probability with the variance of edge distance distribution

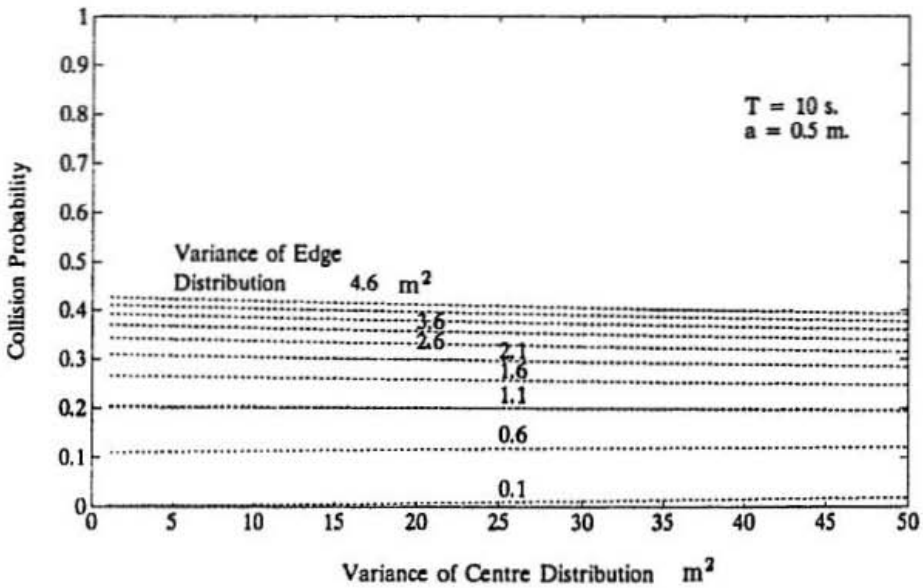

Figure 7.9: Collision probability with the variance of centre distance distribution

7.3 The Frequency of Collision Events from the Acceleration Data

Figure 7.10 to Figure 7.12 show the collision proportions obtained from the acceleration data of the three ice motion packages during experiment 6 of LIMEX'89 phase two conducted from the MV *Terra Nordica*. The time series of the acceleration data can be divided into two fundamental segments. The first period began at 22:30 GMT on April 2 and lasted until about 08:00 GMT on April 3. There was a significant swell, westerly winds and falling air temperature. The collision proportion was quite low and stable . Wave amplitudes became smaller subsequent to 08:00, and until 16:00 GMT on April 3. During this interval, temperatures were at their lowest $-4°C$ and the winds were veering to the northwest. The collision proportion obtained from the acceleration data became very high. Contrary to expectations, there was not a positive relation between collision frequency and wave amplitude. McKenna and Crocker (1990) explained that because of the small wave amplitudes during the second period, there was less resolution in the accelerations and less certainty that variations in the translational components in the horizontal plane were due to ice processes rather than due to noise and to the digitization process.

Two additional processes may also account for this phenomenon. When the wave amplitude is large, it is reasonable that the waves are considered as the dominant factor for floe collisions. When the wave amplitude is small, however, other environmental factors may have the same or even a higher order of influence on floe collisions. In this case, the waves may still be considered as the most important

factor because they are the driving forces which cause ice floes to oscillate at the predominant wave frequency. This floe movement itself may be not strong enough to cause severe floe collisions when the wave amplitude is small. But when floes are oscillating under wave action, other environmental factors such as winds and ocean currents can cause floe collisions. For example, the vortices and turbulence of wind boundary layers near the oscillating ice cover would disturb the regular water particle-like movement of the floes and cause greater phase differences between adjacent floes than that without winds. These greater phase differences will increase floe collision frequencies. The winds may also push floes close to each other but with little collision, if waves do not exist at all. McKenna and Crocker (1991) reported that the frequency of floe collisions increased with an increase in local wind speed during LIMEX'89. Further studies are needed to learn the constitutional relationship between ice floes and wave-wind driving forces.

Figure 7.13 and Figure 7.14 (after Maclaren Plansearch Limited, 1990) show the directional spectra and wave energy density spectra in the open water near the ice floe field , at about 20:00 GMT April 2 and 13:00 GMT April 3, in the first and the second period respectively. The wind vectors and the corresponding wind speeds are shown in Figure 7.15 (after McKenna and Crocker, 1991). From the figures it is clear that during the first period, there were small westerly winds and significant swells. The swells were thought to be the dominant factor causing floe collisions. During the second period from about 8:00 to 16:00 GMT on April 3, the winds veered to the northwest and the speed increased up to more than 10 m/s . These winds should be responsible for the high frequency northwest waves

and the double peaks of wave spectral density in the open water near the ice floe field. The high frequency part of the spectral density was obviously from local wind-generated waves. Inside the ice floe field, however, wave amplitude became smaller which caused the confusing effect that small waves produced high collision frequency.

Masson and LeBlond (1989) indicated that in the Marginal Ice Zone, the ability of an offshore wind to generate a significant wave field was severely limited. The ice cover appeared to be very effective in dispersing the energy; the wave spectrum tended to isotropy, a tendency which prevented the normal growth of wave energy and the decrease in peak frequency. Therefore, winds can not generate waves in an ice floe field as large as those in the open water. From Figure 7.14, it could be found that the total wave energy in the second period was significantly greater than that in the first period, although the 0.1 Hz swell was the inverse situation. The ice floe field might receive the same order of wind energy as the open water. This energy, not being able to generate large waves inside the ice floe field, must be dissipated through the mechanisms of wave scattering, accelerating the floes and causing an increase in floe drift, and causing floe collisions. During the second period, the stronger winds were then thought to be the cause of the higher collision frequency with the smaller wave amplitude inside the ice field.

McKenna and Crocker (1991) identified collision events visually from the same data of experiment 6 of LIMEX'89 phase two conducted from the MV *Terra Nordica*. Their results are shown together with those of the present study in Figure

7.10 to Figure 7.12. In the figures, the vertical axis is the proportion of wave cycles in which collision events occurred; the horizontal axis is time in hours. A tendency is clear from the figure. For small values, the results of the present study are smaller than those of McKenna and Crocker. For the later part of the experiment where collision proportion is large, the results of the present study are larger than those of McKenna and Crocker. Their results never exceed 1.0 while the values of the present study can be as large as 1.6. An explanation of this discrepancy is that they ignored multiple events within *one* wave cycle, while in the present study multiple events were ignored within a *half* wave cycle. As discussed before, one floe was thought to collide at most twice within a wave cycle, during the forward and backward of the wave propagation directions. When the floe collision frequency is low, a floe rarely collides in both the forward and backward directions. In the case of high collision frequency, a floe may often collide twice in a wave cycle. This is considered as the cause of the discrepancy in the high collision frequency. If at most one event is counted within a wave cycle, the results of the present study will be smaller than those of McKenna and Crocker over the whole entire measurement period. More work is needed to explain this discrepancy. However, a reliable identification of floe collision events demands data with higher frequency of sampling, while the present available data do not contain information above 0.5 Hz.

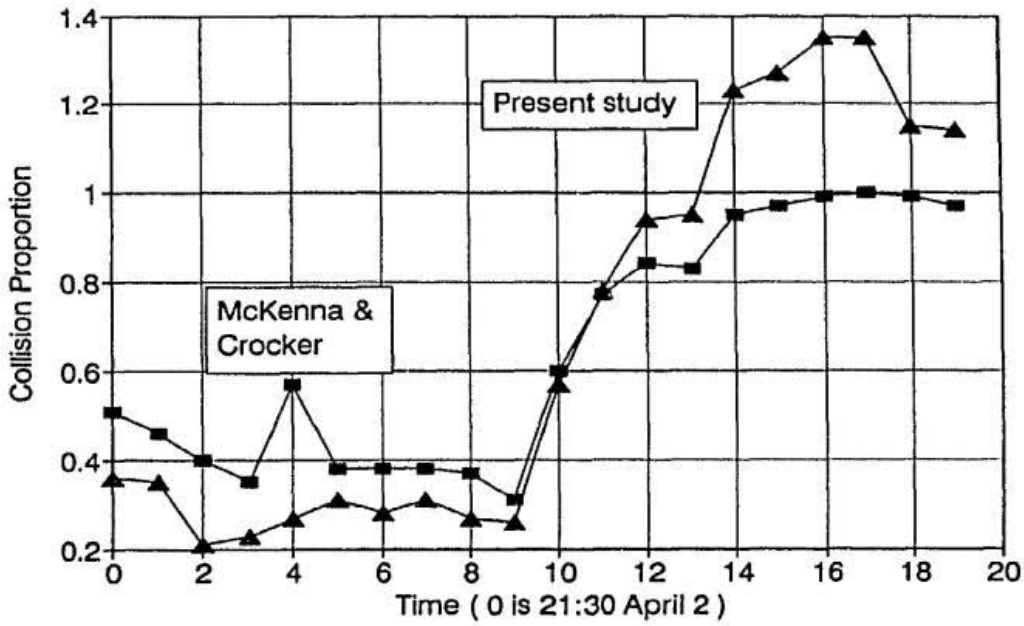

Figure 7.10: Collision proportion from acceleration data of ice motion package 3

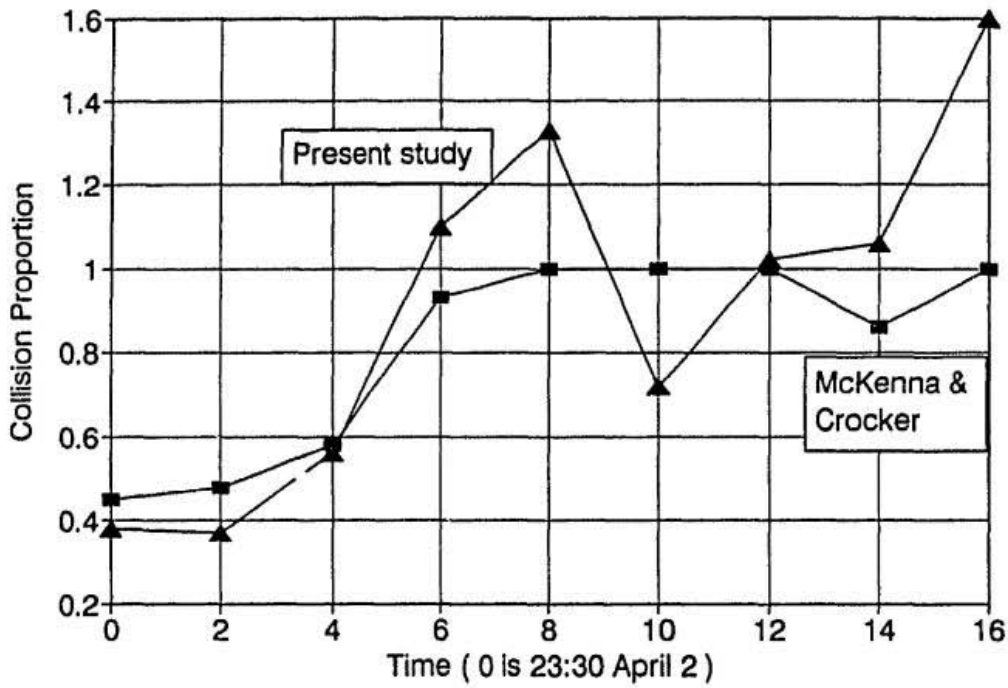

Figure 7.11: Collision proportion from acceleration data of ice motion package 5

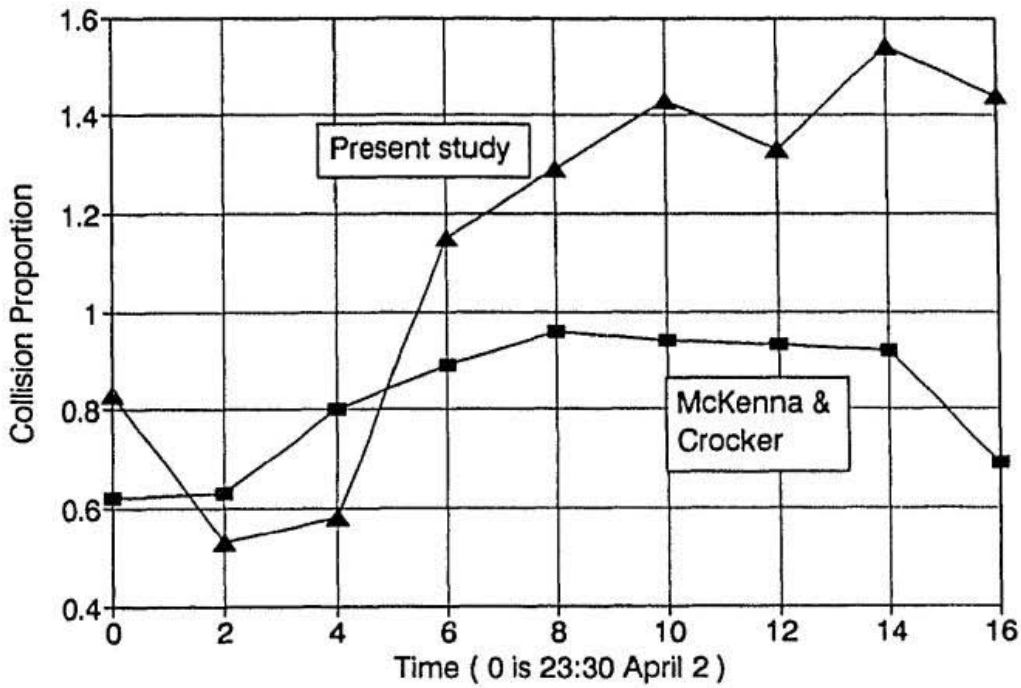

Figure 7.12: Collision proportion from acceleration data of ice motion package 6

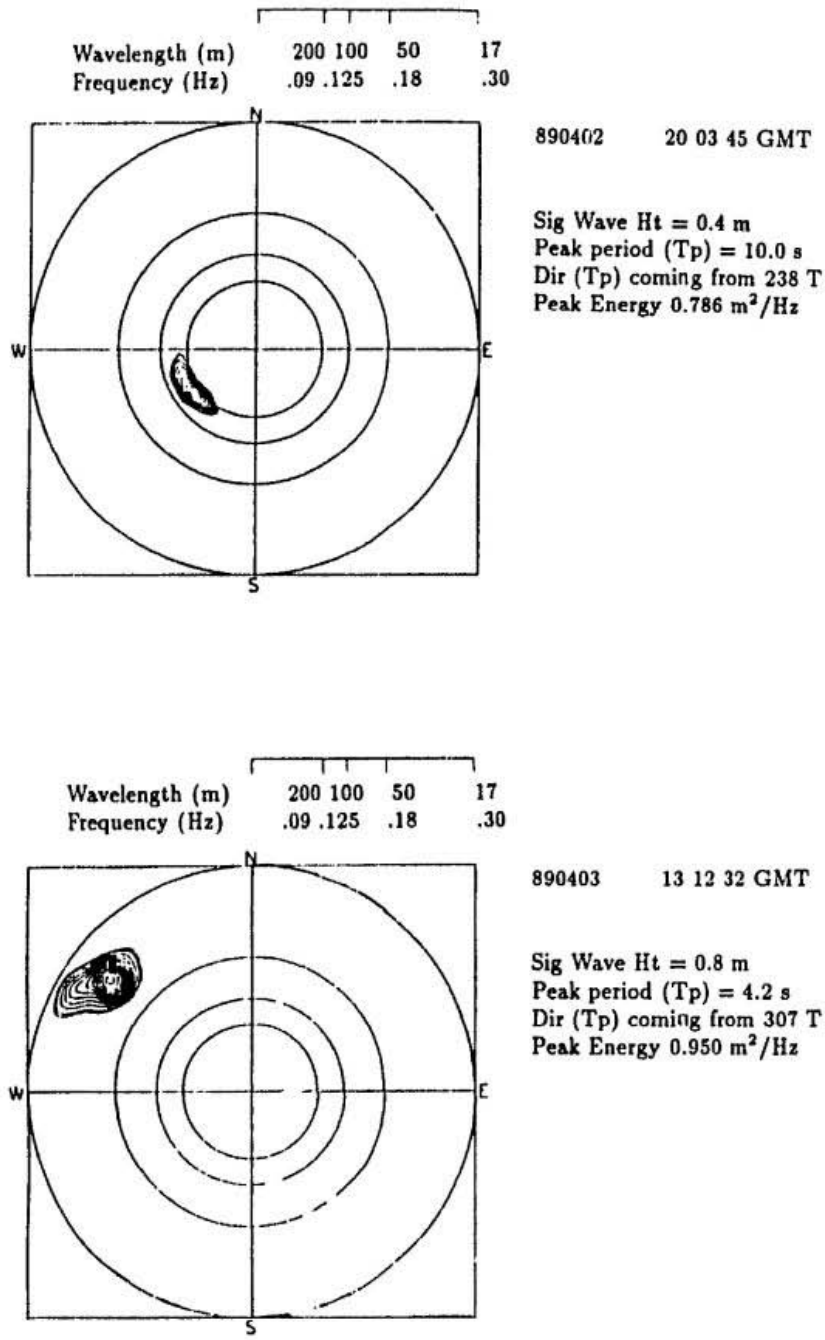

Figure 7.13: Directional spectra during experiment 6 of LIMEX'89 phase two conducted from the MV *Terra Nordica* (after Maclaren Plansearch Limited, 1990)

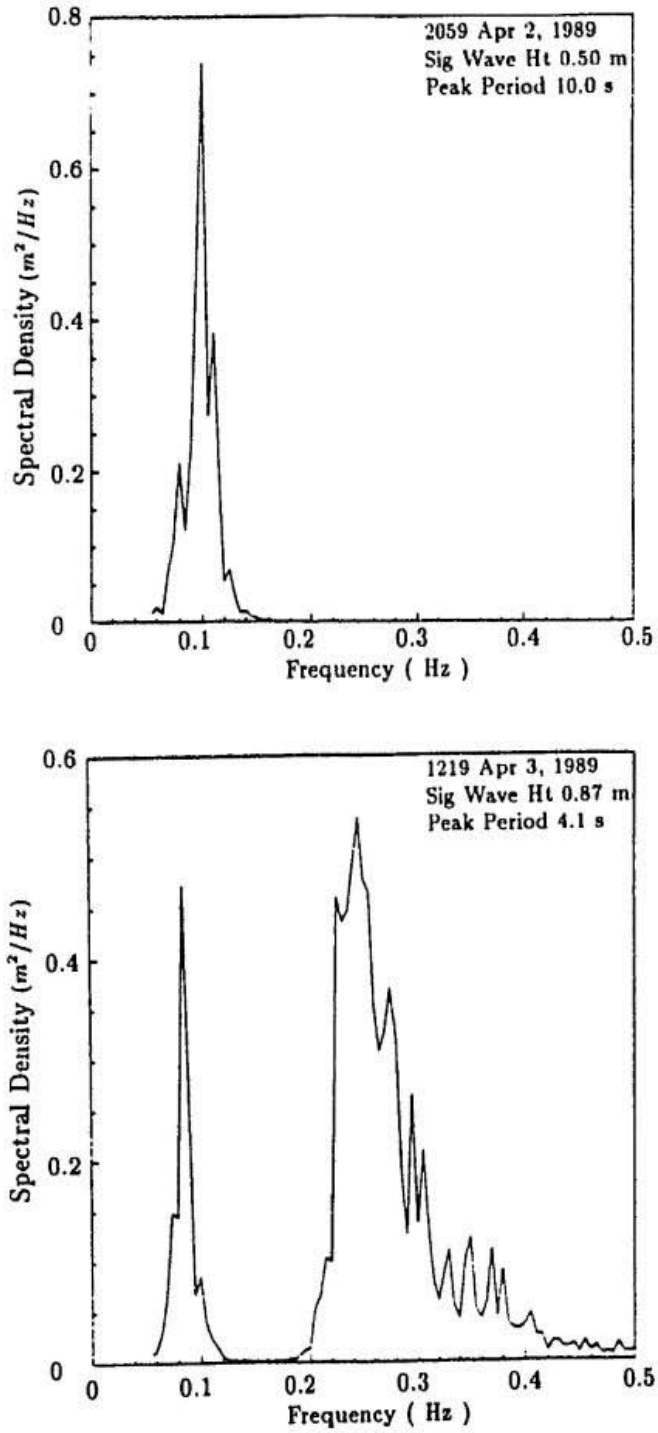

Figure 7.14: Wave energy spectra during experiment 6 of LIMEX'89 phase two conducted from the MV *Terra Nordica* (after Maclaren Plansearch Limited, 1990)

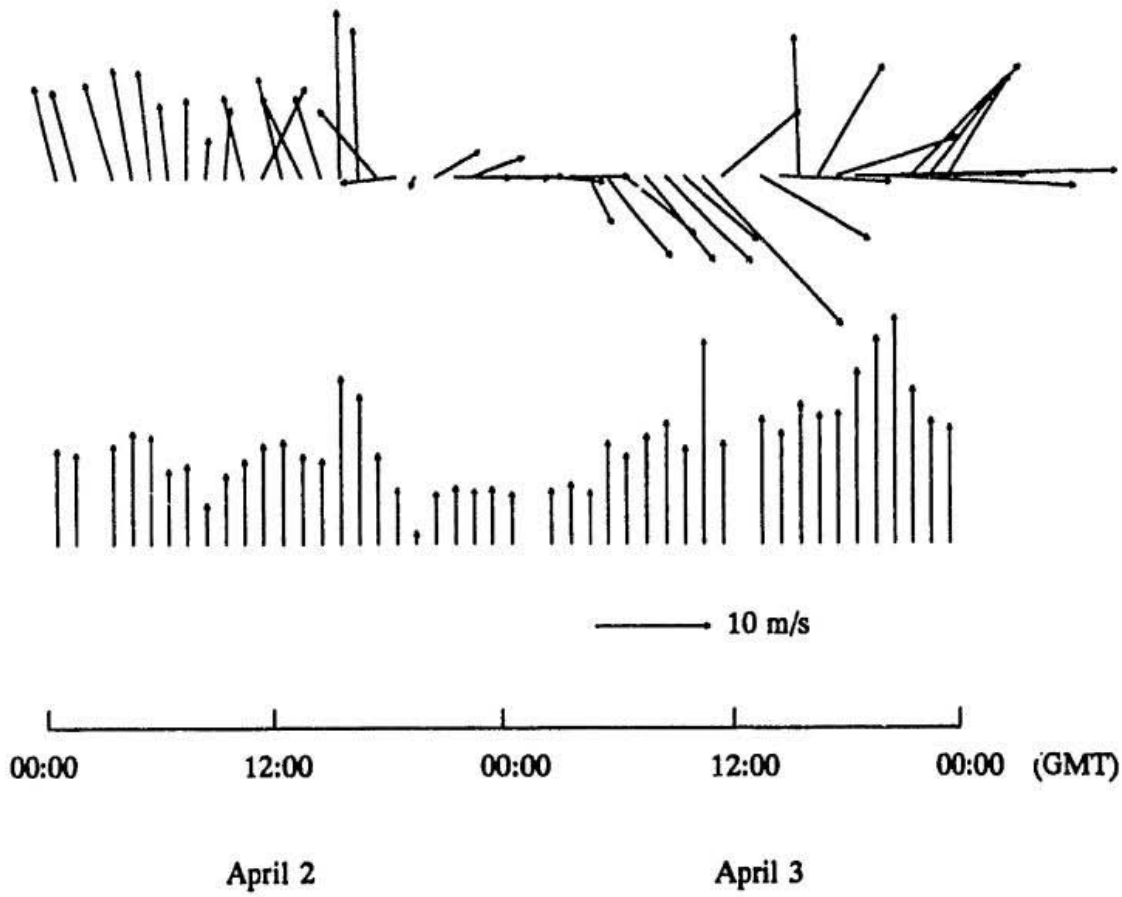

Figure 7.15: Wind vectors and wind speeds during experiment 6 of LIMEX'89 phase two conducted from the MV *Terra Nordica* (after McKenna and Crocker, 1990)

7.4 Collision Type and Direction

It was supposed that floes collided in the wave propagation direction. In order to test this assumption and its effect on floe spacing distributions and collision probability, the spacing distances were measured in two directions: Tp direction and long axis direction, which were about 77 and 63 degrees different from each other. The results show that the relevant floe spacing distributions were only slightly different (Table 4.7). The collision probabilities obtained from these distributions were also not significantly different. Table 6.2 to Table 6.7 show that the numbers of collisions in the two horizontal directions are not very different, in either the N-S and E-W directions or in Tp and its orthogonal directions.

The above results are real but do not necessarily violate the assumption of floe collisions occurring in the wave direction, since observers have shown with confidence that the floe collisions were not random but related to the predominant waves (Martin and Becker,1988; Rottier, 1990; McKenna and Crocker, 1991). The probable explanation is that most of the floe pairs' centre lines were not in the wave directions at the moments of collisions, or say, most collisions were eccentric. By the assumption of water particle-like movement, ice floes move in the wave direction when they are not colliding with other floes. When a floe is colliding with another one eccentrically, the collision force acting on the floe is in the wave propagation direction but does not go though the floe centre. Shen (1987) proposed an elastic floe collision model to study ice floe collision behaviour, while other researchers (Rottier, 1990; McKenna and Crocker, 1991) concluded from field observations that ice floe collisions presented inelastic characteristics. Intensive work has not been

done to study ice floe collision mechanism from the view of ice mechanics. Although the floe collision mechanisms are not well understood, it is still reasonable to assume that the eccentric collision force will make the floes rotate and move in a direction somewhat different from the wave propagation direction. This mechanism causes floe spacing distances to be evenly distributed and less directional in the horizontal plane. It also causes the collision events obtained from the horizontal acceleration data not to present a significantly directional tendency. It is the floe collision that dissipates wave energy, transfers energy among floes, and makes floes tend to be evenly distributed. It can be imagined that without collisions, floe distributions would present more clear directional properties. However, a conclusive statements can not be made without more and better data.

7.5 Floe Concentration, Size Distribution and Spacing Distributions

The floe spacing distributions were obtained by directly measuring floe spacing distances and using the probability plot test. The parameters of floe size distribution and ice floe concentration were not involved in the probabilistic model. Among these three things, some relations must exist. It can be expected that floe size changes directly with floe centre distance. Generally speaking, the bigger the floes are, the larger the floe centre distance is. This is especially apparent for a closely spaced ice floe field. The relation between floe size and floe edge distance is not easily demonstrated, since ice concentration has greater influence on floe edge distances than floe size does. It is clear that ice concentration has an inverse relation with floe spacing distances. Higher concentration means floes are more closely packed, which leads to smaller floe spacing distances.

Efforts have been made to determine these relations. However, the author was unable to establish them, because the floe shapes were irregular and the floes were randomly distributed in the horizontal plane, while the floe spacing distances were defined before as in the wave propagation direction. Nevertheless, it is still worth trying more to find these relationships in further research work, since size distribution and floe concentration are two of the concepts that are used most often for describing an ice floe field.

Another difficult thing to deal with is the brash ice between floes. This brash sometimes occupies a large proportion of water surface between floes. As described

in Chapter 4, the brash ice influences the measurements of floe edge distances. In the present study, ice pieces of diameter less than 3 metres were not treated as floes. Although this definition was based on the magnitude of the kinetic energy of ice floes, some arbitrariness existed. The choice of this critical value of floe size influences the measurements of both the floe edge and centre distances.

Chapter 8

Summary and Suggestions

8.1 Summary

To study the movement of small ice floes under wave action, the assumption of water particle-like movement was made. This led to the investigation of floe motion by analysing water particle motion using Airy Linear Wave Theory. The relative distance change between neighbouring floes was demonstrated to be the key parameter determining whether or not a floe collision occurred. A floe collision criterion was then derived. With this criterion, the floe collision likelihood was related to floe centre distance, floe edge distance, wave amplitude, and wave period.

An ice floe field was considered to be random while the floe motion was treated as a stochastic process. A new concept of floe spacing distributions was proposed in order to study collision behaviour using probability theory. These floe spacing distributions were assumed to be wide stationary stochastic processes, which meant that their mean functions did not change with time and could be obtained from the data from a specific instant in time. From the five aerial photographs of the LIMEX'89 field experiments, and by means of a probability plot test, ice floe edge

distance and centre distance distributions were obtained. Both were shown to display a Lognormal distribution. Although these Lognormal distributions of floe spacing distances were from the data of a particular ice floe field, they formed a basis of floe collision studies.

Combining the floe collision criterion and the floe spacing distributions, the collision probability for a floe during one wave cycle was obtained. This collision probability changed directly with wave amplitude and floe centre distance, inversely with wave period and floe edge distance. Valuable results such as the collision frequency within an ice floe field and the number of collisions of a floe during a time period could be derived from this collision probability.

The acceleration data from LIMEX'89 were analysed to find the frequency of collision of the measured ice floes by recognizing the abnormalities in the acceleration traces. Because the data were heavily filtered and resampled at 1.33 Hz, no collision details other than the frequency of collision could be obtained. Predictions of collision frequency from the probabilistic approach and from the acceleration data were significantly different. The discrepancy, however, became smaller after the dimensional effects of floes were taken into account. The influence of winds was discussed and thought as the another primary contribution to this discrepancy. The uncertainty in the process of defining collisions from the acceleration data, the influences of wave scattering and reflecting, and other environmental factors such as temperature and ocean currents affected the results.

The same procedures for obtaining floe spacing distributions and for judging collision events from acceleration data were repeated in two horizontal directions about 70 degrees apart. The results showed that the differences between the floe spacing distributions and between the collision frequencies in the two horizontal directions were not significant. This meant that the ice floe field was evenly distributed and floe collisions occurred without a dominant direction. Wave scattering mechanisms and eccentric floe collisions were considered as the primary causes for these phenomena.

This probabilistic approach is promising for studying ice floe collision in the Marginal Ice Zone where the discrete ice floes are randomly distributed and face complicated environmental conditions. It can give collision frequency that is thought to be a major source of ocean noise. Ice floe size reduction rates can be derived using this approach. From the collision frequency, wave energy losses due to floe collisions may also be obtained, which is important for determining environmental loading forces on offshore structures. It will also be helpful for studying the dispersal of an oil slick in an ice floe field. However, more work is needed to achieve the above practical applications.

8.2 Suggestions for Further Study

It is my belief that more and valuable results can be obtained if the wave spectra are introduced into the analysis. Rottier (1990) pointed out that collision events between floes of similar size are most easily driven by a relatively narrow band of wave lengths of around 2 to 4 times the floe length. McKenna and Crocker (1990) proposed that since waves are a factor in moving the floes relative to each other and changing the local ice concentration, then surely the different frequency components of the directional wave spectrum influence this process. By floe collision criterion of equation (3.12), wave amplitude and frequency are the most important parameters for floe collision occurrence. For a given ice floe field, amplitude spectrum of waves can be obtained from ice motion data, and floe spacing distributions can be acquired from aerial photographs or video. The wave amplitude spectrum and floe spacing distributions are to be related by equation (3.12), which will lead to a more real picture of ice floe collisions in a sea covered by ice floes.

It is important in further studies to consider different floe collision scenarios and the influence of the brash ice between ice floes. To establish floe collision scenarios, the basic understanding of collision mechanism from the view of mechanics and hydrodynamics is essential. Intensive work is needed to learn: the mechanical process during floe impact of different types of collisions, how collisions change the impacted floes' movement, how the response amplitude operator and added mass influence floe motion in waves, and so on. The quantitative classification of brash ice between floes is also important for establishing floe collision scenarios and their mechanical process, since brash ice plays a significant role in the interactions

between ice floes.

Collision velocity and duration distributions are required for the problem of determining the energy attenuation and ice loading forces on offshore structures. Ice floe collision velocity and duration should be random variables, even though linear wave theory is used. This is because they are influenced by floe spacing distances as well as wave motions. Some relations must exist among these random variables. If wave spectrum is also introduced into the analysis, together with the knowledge of mechanical process of floe collisions, wave energy attenuation and ice loading forces on offshore structures due to floe collisions can be obtained.

More and better ice motion data are one of the keys for further study. The data should be sampled with higher frequency, which is essential for better estimation of collision events and better understanding of collision and floe damage mechanisms. It will be valuable if the data can be collected in a heavy and random sea, because it is believed that severe floe collisions and the critical ice loading forces on offshore structures occur under harsh environmental conditions. A technique of obtaining floe geometric and spacing parameters automatically from aerial video images is also very important to establish a floe data base for a given marginal ice zone, since aerial video tapes contain much more information about the ice floes over a large area in an ice floe field than aerial photographs.

References

Bai, K.j. (1977). " The Added-Mass of Two-Dimensional Cylinders Heaving in Water of Finite Depth," *J. Fluid Mechanics*, Vol. 81, pp.85-105.

Borland International (1990). " QUATTRO PRO, " Version 2.00, Scotts Valley, CA, USA.

Carstens, T. and Rosdal, A. (1987). " Wave Reflection from an Ice Edge, " *POAC'87, Proceedings*, Vol.1, pp.253-261.

Crocker, G.B. (1990). " Ice Characteristics, " *LIMEX'89 Data Report*, AERDE Environmental Research, Halifax, N.S., Section 8.8.

Crocker, G.B., and Wadhams, P. (1988). " Observations of Wind Generated Waves in Antarctic Fast Ice, " *J. Physical Oceanography*, Vol.18, No.9, pp. 1292-1299.

Eid, B. M., Morton, C. M., Windsor, W. D., and Cardone, V. J. (1989). " Wave-ice Interaction Study during LIMEX'87, " *International Workshop on Hindcasting and Forcasting*, preprints, 2nd, Vancouver, BC, pp. 213-223.

Fox, C. and Squire, V. A. (1990). " Reflection and Transmission Characteristics at the Edge of Shore Fast Sea Ice, " *J. Geophysical Research*, Vol. 95, No. C7, pp. 11,629-11,639.

Henry, G.J. (1968) *Wave-ice Interaction: Model Experiments*, Davidson Lab, Stevens Inst. of Tech., Hoboken, New Jersey, Report 1314, 34 p.

Lever, J.H., Reimer, E. and Diemand, D. (1984). " A Model Study of the Wave Induced Motion of Small Icebergs and Bergy Bits, " *3rd International Symposium on Offshore Mechanics and Arctic Engineering*, Vol.3, pp. 282-290.

Liu, A. K., and Mollo-Christensen, E. (1988). " Wave Propagation in a Solid Ice Pack, " *J. Physical Oceanography*, Vol. 18, pp. 1702-1712.

Lye, L.M. (1990). *An Introduction to Probabilistic Modelling for the Water Resources Engineer*, Course Notes, Memorial U. of Newfoundland.

MacLaren Plansearch Limited (1990). " Buoy Program, " *LIMEX'89 Data Report*, AERDE Environmental Research, Halifax, N.S., Section 8.2.

Martin, S., and Becker, P. (1988). " Ice Floe Collisions and Their Relation to Ice Deformation in the Bering Sea During February 1983, " *J. Geophysical Research*, Vol. 93, pp. 1303-1315.

Masson, D. , and LeBlond, P.H. (1989). " Spectral Evolution of Wind-generated Surface Gravity Waves in a Dispersed Ice Field, " *J. Fluid Mechanics*, Vol. 202, pp.43-81.

McKenna, R.F. (1990). " Ice Mechanical Properties, " *LIMEX'89 Data Report*, AERDE Environmental Research, Halifax, N.S., Section 8.7.

McKenna, R.F., and Crocker, G.B. (1990). " Wave Energy and Floe Collisions in Marginal Ice Zones, " *Ice Technology for Polar Operations*, ed. T.K.S. Murthy et al, Computational Mechanics Publications, pp. 33-45.

McKenna, R.F., and Crocker, G.B. (1991, in press). " Ice Floe Collisions Interpreted from Acceleration Data During LIMEX'89, " *Atmosphere Oceans.*

Mollo-Christensen, E. (1983). " Edge Waves as a Cause of Ice Rideup On Shore, " *J. Geophysical Research*, C, Vol.88, No. 1-6, pp. 2967-2970.

NORDCO Limited (1989). *Hydrodynamic Interaction of Fixed and Floating Bodies*, Contract Report for IMD, NRC, CR-1989-21, 26 p.

Ofuya A.O., and Reynolds, A.J. (1967). " Laboratory Simulation of Waves in an Ice Floe, " *J. Geophysical Research*, 72: pp. 3567-3583.

Rancy, K., Werle, D., and Mcnutt, L. (1990). " Executive Summary, " *LIMEX'89 Data Report*, AERDE Environmental Research, Halifax, N.S., Canada, Section 2.

Rao, G.L., and Vandiver, J.K. (1987). " Wave Attenuation in Ice, " *OTC*, Vol.4, pp.403-411.

Rottier, P.J. (1990). *Wave/Ice Interactions in the Marginal Ice Zone and the Generation of Ocean Noise*, Ph.D. Dissertation, U. of Cambridge.

Shen, H., Hibler, W., and Lepparanta, M. (1987). " The Role of Floe Collision in Sea Ice Rheology, " *J. Geophysical Research*, Vol. 92, No. C7, pp. 7085-7096.

Squire, V.A. (1983a). " Dynamics of Ice Floe in Sea Waves, " *J. Society for Underwater Technology*, 9 (1), pp. 20-26.

Squire, V.A. (1983b). " Numerical Modelling of Realistic Ice Floes in Ocean Waves, " *Annals of Glaciology*, 4, pp. 277-282.

Squire, V.A. and Allan, A.J. (1977). " Propagation of Flexural Gravity Waves in Sea Ice, " *C-CORE Report*, 77-22, Centre for Cold Ocean Resources Engineering, Memorial University of Newfoundland, St. John's, Nfld, 14p.

Squire, V.A., and Martin, S. (1980). *A Field Study of the Physical Properties, Response to Swell and Subsquent Fracture of a Single Ice Floe in the Winter Bering Sea*, Scientific Report No. 18, Department of Atmospheric Sciences and Oceanography, U. of Washington, Seattle, 56p.

Squire, V.A., and Moore, S.C. (1980). " Direct Measurement of the Attenuation of Ocean Waves by Pack Ice, " *Nature*, London, 283, pp. 365-368.

Wadhams, P. (1972). " Measurement of Wave Attenuation in Pack Ice Inverted Echo Sounding, " *Sea Ice*, ed. T. Karlsson, National Research Council of Iceland, Reykjavik, pp. 255-260.

Wadhams, P. (1973). *The Effect of a Sea Ice Cover on Ocean Surface Waves*, Ph.D. Thesis, U. Cambridge.

Wadhams, P. (1975). " Airborne Laser Profiling of Swell in an Open Ice Field, " *J. Geophysical Research*, 80: pp. 4520-4528.

Wadhams, P. (1978). " Wave Decay in the Marginal Ice Zone Measured from a Submarine, " *Deep-Sea Research*, 25: pp. 23-40.

Wadhams, P. (1986). " The Seasonal Ice Zone, " *The Geophysics of Sea Ice*, ed. N. Untersteiner, Plenum Press, New York, pp. 825-992.

Wadhams, P., and Cowan, A.M. (1984). *Wave-Ice Interactions and Floe Flexure of Pack Ice of the Labrador Current*, SPRI report 84-1, Scott Polar Research Institute, U.of Cambridge.

Wadhams, P. and Kristensen, M. (1983). " The Response of Antarctic Icebergs to Ocean Waves, " *J. Geophysical Research*, Vol.88, No. C10, pp. 6053-6065.

Wadhams, P. , Squire, V.A. , Ewing, J. A., and Pascal, R.W. (1986). " The Effect of the Marginal Ice Zone on the Directional Wave Spectrum of the Ocean, " *J. Physical Oceanography*, 16 (2), pp358-376.

Wadhams, P., Squire, V.A., Goodman, D., Cowan, A.M., and Moore, S.C. (1988). " The Attenuation Rates of Ocean Waves in the Marginal Ice Zone, " *J. Geophysical Research*, Vol.93, No. C6, pp.6799-6818.

Weber, J.E. (1987). " Wave Attenuation and Wave Drift in the Marginal Zone, " *J. Physical Oceanography*, Vol.17, pp. 2351-2361.

Winsor, W.D. (1990). " Ice Photography and Video, " *LIMEX'89 Data Report*, AERDE Environmental Research, Halifax, N.S., Section 8.9.

Winsor, W.D., Clark, J.I. , Eid, B.M. and Morton, C.M. (1989). " Role of Ice Properties in Wave-ice Interaction During LIMEX'87, " *IGARSS'89, Canadian Symposium on Remote Sensing*, Proc. 12th, Vol. 4, pp. 2350-2354.

Winsor W.D., Crocker, G.B., McKenna, R.K., and Tang, C.L. (1990). *Sea Ice Observations during LIMEX, March-April 1989*, Department of Fisheries and Oceans, Dartmouth, NS, 44 p.

Appendix A

Aerial Photographs of LIMEX'89

Two 35 mm cameras, mounted onto the floor of the Bell 206 helicopter, were used to take photographs during experiment 6 of LIMEX'89 phase two conducted from the MV *Terra Nordica*. During Experiment 6, ten aerial photographs were taken vertically downwards onto the ice floe field, while others were taken obliquely downwards. The vertical photographs are better for the purpose of measuring the ice floe spacing distances. Among these ten vertical photographs, five of them are suitable for the use of determining the ice floe spacing distance distributions, while the others contain either an open water or only a few ice floes because of low flight altitude. These five slide ID numbers are 5400, 5404, 5412, 5416, and 5420 (Winsor, 1990). The details of these aerial photographs are shown in Table 4.1.

The cameras were mounted on the helicopter so that the long axis of the frames were parallel to the flight direction, which gave the directions of the photographs as in Table 4.1. These directions are necessary for measuring floe edge distance and floe centre distance in the wave propagation direction. The photographs were taken at the area near Package 6. The flight altitudes for these photographs are

also shown in Table 4.1. These altitudes provide the objective distance A in the calibration of the photographs (Refer to Figure B.1 of Appendix B). Both the positions and the altitudes were from the audio reports on the video tapes which were taken during the flight. Sometimes the flying altitudes or the positions were not reported at the same time as the photographs were taken. The time difference might be as big as 57 seconds. This factor affected the accuracy of measuring floe spacing distances. More discussions of this problem are in Chapter 7. If the ice floe spacing distributions obtained from individual frames are not significantly different from each other and not significantly different from those obtained from the frames as a whole, it can be concluded that ice floe spacing distances in this area may be described by identical floe spacing distributions.

Appendix B

Calibration of the Photographs

From optics of photography, the position of an object can be determined using the relationship:

$$\frac{1}{f} = \frac{1}{A} + \frac{1}{B} \tag{B.1}$$

where f is the focal length of the camera lens, A is the distance from the object to the lens, and B is the distance from the image to the lens (see Figure B.1). A convenient number to use in describing image size is the linear magnification m_o, defined as:

$$m_o = \frac{i}{o} = \frac{B}{A} \tag{B.2}$$

where i is the height of the image and o is the height of the object (Figure B.1).

Combining the above two equations gives the following:

$$m_o = \frac{f}{A - f} \tag{B.3}$$

If the object distance A is large compared with f, which is the case in the present study, then:

$$m_o \simeq \frac{f}{A} \tag{B.4}$$

The length of an object is then derived as:

$$o = \frac{Ai}{f} \tag{B.5}$$

For unit image length $i = 1$, the relevant object length is:

$$o = \frac{A}{f} \tag{B.6}$$

The slide dimension is 23×25 mm. These slides were projected onto grid paper to obtain projected pictures. These projected pictures were used to determine floe centres and to measure the floe spacing distances. The length ratio of the projected pictures to the slides was set as R, a scale S of real length on the sea and image length on the projected pictures would be:

$$S = \frac{o}{R} \tag{B.7}$$

The focal length f of the camera used in the experiment was 0.05 metres. The object distance A were provided by the helicopter flight altitudes which were obtained from the audio reports of the operator on the video tapes taken during the flight. The calibration results are shown in Table 4.2. In the table the *Length projected* F_1 and F_2 refer to the size of the projected pictures. The resulting S is the real length per unit length on the projected pictures.

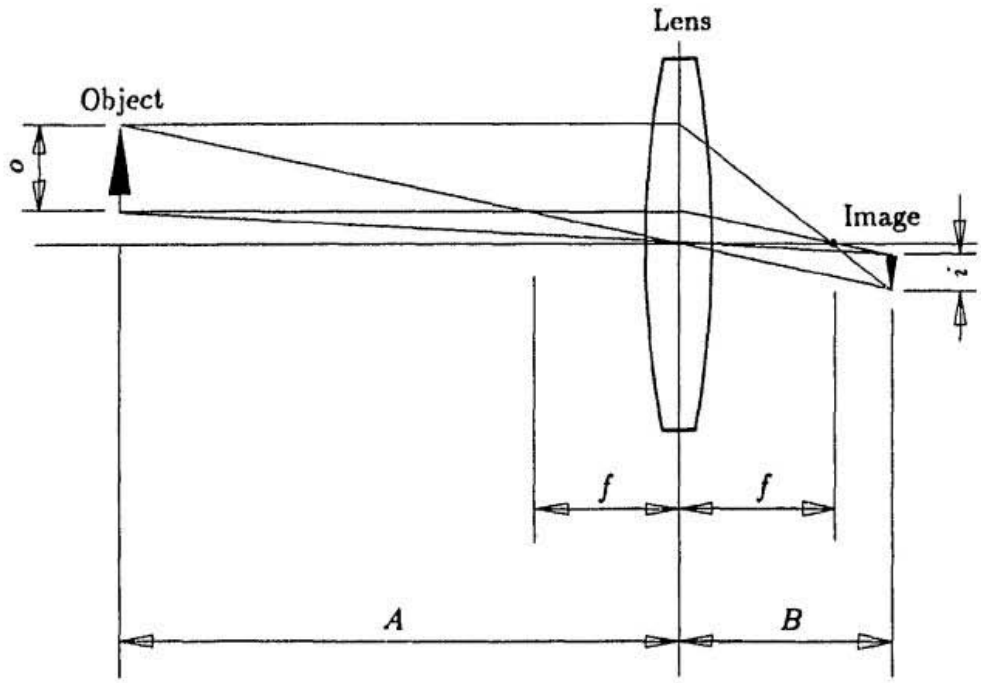

Figure B.1: Optic relation between object distance, image length and focal length

Appendix C

Transformations to the Normal Distribution

After a suitable transformation, some theoretical probability distributions approximately follow the Normal distribution. This transformation is necessary because few of these other distributions are as well known or as widely tabulated as the Normal distribution. The use of the Lognormal distribution is very similar to the regular Normal distribution. The only difference is that the logarithm of the variable, $\ln(x)$, is approximately normally distributed rather than the ' original ' random variable x. The standardization transformation is:

$$z = \frac{\ln(x) - \mu}{\sigma} \tag{C.1}$$

where z is the standard normal variate. Then the probability of any event associated with x can be found in terms of z using the standard normal table. If the random phenomenon can be modelled approximately with a Lognormal distribution, the observed data obtained should plot approximately a straight line on the Lognormal probability graph paper. This straight line passes through $F(z)$=0.5 and $\ln(x) = \mu$ with slope $\sigma = (\ln(x_P) - \mu)/z$; where $\ln(x_P)$ is the value of $\ln(x)$ at probability

$P = F(z)$. In particular, at $P = 0.84$, $z = 1$; hence the slope is:

$$\sigma = \ln(x_{0.84}) - \mu \tag{C.2}$$

Blom's plotting formula was used to obtain the plotting positions P in the present study. The standard normal variate z could be related by a standard normal table, however, it was derived for the present study from an empirical formula expressed as:

$$z = 5.0633 \times (P^{0.135} - (1 - P)^{0.135}) \tag{C.3}$$

where P is the Plom's plotting position as equation (4.9). After plotting the points of z and $\ln(x)$ on the Lognormal graph paper, a probability plot correlation coefficient test was used to test the linearity of the plotted points for judging the goodness-of-fit.

If the random variable x is Gamma distributed, the cube-root transformation, $x^{1/3}$, will produce an approximately normally distributed variate. By the same probability plotting positions and standard normal variate z but changing $\ln(x)$ into $x^{1/3}$, the probability plot test and goodness-of-fit test were carried out for the Gamma distribution using the same procedure as for the Lognormal distribution.

The probability function of a Weibull distribution is expressed as:

$$P = 1 - \exp(-\frac{x^{\xi}}{\eta}) \tag{C.4}$$

Taking the logarithm of both sides of the expression, one obtains:

$$\ln(-\ln(1 - P)) = -\ln(\eta) + \xi \ln(x), \tag{C.5}$$

where ξ is the shape parameter and η is the scale parameter of the distribution. Let $w = -\ln(1-P)$, then $\ln(w)$ and $\ln(x)$ have a linear relation. The probability P was determined by Blom's plotting position. The probability plot test and the probability plot correlation coefficient test were conducted to show the linearity between $\ln(w)$ and $\ln(x)$. If they had a linear relation on the Weibull probability paper under a certain level of confidence, it was said that variate x was approximately distributed by a Weibull distribution.

Appendix D

Fortran Program for Numerical Integration of Equation (5.3)

```
*****************************************************************
********                FORTRAN PROGRAM                  ********
*                                                               *
*            Integration of Collision Probability               *
*_______________________________________________________________*

*                        file: INT.FOR                          *

      DIMENSION L(2), U(3), W(3), C(2), X(2), KK(2,2), DD(2,3)
      EXTERNAL FUN, FUPP, FLOW
      COMMON UP,CA0,CA1,EA0,EA1,DOG1,DOG2
      CHARACTER*20 FILE1, DIR
      TYPE*,'input result file name ???????'
      ACCEPT88, FILE1
      TYPE*,'input collision direction ???????'
      ACCEPT88, DIR
88    FORMAT(A20)
      OPEN(UNIT=10, FILE=file1, STATUS='NEW')
      PRINT*,'upper limit of center distance ??????'
      READ*,UP
      TYPE*,'center distribution s MEAN ?????? '
      READ*,CA0
      TYPE*,'center distribution s S.D ?????? '
      READ*, CA1
      TYPE*,'edge distribution s MEAN  ?????? '
      READ*,EA0
      TYPE*,'edge distribution s  S.D ?????? '
      READ*, EA1
      WRITE(10,111) DIR, FILE1
111   FORMAT(///15X,'Collision Probability in',2X,A20
     1       /20X,'Program file: INT.FOR'
     1       /20X,'Output  file:',1X,a20
     1      ///3X,'C-Mean', 8x,'C-SD',8X,'E-Mean',8X,'E-SD',
     1        4X,'Blocks',3X,'Prob.'/)

      U(1)=0.7745967
      U(2)=0.
      U(3)=-U(1)
      W(1)=0.5555556
      W(2)=0.8888889
      W(3)=0.5555556
      DO 2 I=1,10
      LL=2**I
      L(1)=LL
      L(2)=LL
      CALL MULG(2,L,3,U,W,C,X,KK,DD,3,GSI,FUN,FUPP,FLOW)
      GSI=GSI/2/3.141592/CA1/EA1
      WRITE(10,112) CA0, CA1, EA0, EA1, LL, GSI
2     PRINT*, LL,GSI
112   FORMAT(/1X,f8.5,5X,f8.5,5X,f8.5,5X,f8.5,2X,i4,5X,f8.6)
      STOP
      END
```

```
**************
      SUBROUTINE MULG(N,KS,MP,U,W,C,X,KK,DD,NM,GSI,FUN,
     1  FUPP,FLOW)
      DIMENSION KS(N), U(MP), W(MP), C(N), X(N), KK(2,N),
     1  DD(2,NM)
      COMMON UP,CA0,CA1,EA0,EA1,C1,E1
      C1=2*CA1*CA1
      E1=2*EA1*EA1
      M=1
      DD(1,NM)=1.
      DD(2,NM)=1.

300   DO 100 J=M,N
      A=FLOW(J,X)
      B=KS(J)
      DD(1,J)=0.5*(FUPP(J,X)-A)/B
      C(J)=DD(1,J)+A
      X(J)=DD(1,J)*U(1)+C(J)
      DD(2,J)=0.
      KK(1,J)=1
100   KK(2,J)=1
      J=N
301   F=FUN(J,X)
      KB=KK(1,J)
      DD(2,J)=DD(2,J+1)*DD(1,J+1)*F*W(KB)+DD(2,J)
      KK(1,J)=KK(1,J)+1
      IF(KK(1,J).LE.MP) GOTO 303
      IF(KK(2,J).LT.KS(J)) GOTO 302
      J=J-1
      IF(J.NE.0) GOTO 301
      GSI=DD(2,1)*DD(1,1)
      RETURN
302   KK(2,J)=KK(2,J)+1
      C(J)=C(J)+DD(1,J)*2.
      KK(1,J)=1
303   KC=KK(1,J)
      X(J)=DD(1,J)*U(KC)+C(J)
      IF(J.EQ.N) GOTO 301
      M=J+1
      GOTO 300
      END
```

```
**************
      FUNCTION FUN(J,X)
      DIMENSION X(2)
      COMMON DOG1,CA0,DOG2,EA0,DOG3,C1,E1
      IF(J.LT.2) GOTO 3
      FUN= 1.0/X(1)/X(2)*EXP(-(ALOG(X(1))-CA0)**2/C1
     1                       -(ALOG(X(2))-EA0)**2/E1)
      RETURN
3     FUN=1.0
      RETURN
      END

**************
      FUNCTION FUPP(J,X)
      DIMENSION X(2)
      COMMON UP
      GOTO(1,2), J
1     FUPP=up
      RETURN
2     FUPP=X(1)*0.0048369
      RETURN
      END

***************
      FUNCTION FLOW(J,X)
      DIMENSION X(2)
      GOTO(3,4), J
3     FLOW=0.00000001
      RETURN
4     FLOW=0.00000001
      RETURN
      END
```

Appendix E

Fortran Program for Collision Judgement

```
*************************************************************************
*******                    FORTRAN PROGRAM                        ********
*                                                                       *
*          FLoe Collision Events from Acceleration Data                 *
*                                                                       *
*                                                                       *
*                         file: JUDGE.FOR                               *


      INTEGER DI, N1, N2, P, X, Y, Q, Y1,   H, H1, H2,
     1          J1, G1, G2
      DIMENSION A(50000,3), S(50000,3), T(5), U(5), V(5)
      CHARACTER*20 file1, file2, dirc
      TYPE*,'Input data file name1'
      ACCEPT88,file1
      TYPE*,'Input output file name2'
      ACCEPT88,file2
      TYPE*,'Input direction: Original or Tp ????'
      ACCEPT88,dirc
      TYPE*,'Input the program the data got from ?'
      ACCEPT88,via
88    FORMAT(A20)
      OPEN (UNIT=5, FILE=file1, STATUS='OLD')
      OPEN (UNIT=6, FILE=file2, STATUS='NEW')
      TYPE*,'from which row of the data ?????'
      READ*, N1
      TYPE*,'to which row of the data ???????'
      READ*, N2

      WRITE(6,1001)   DIRC, FILE1, VIA, FILE2
      WRITE(6,1002)
1001  FORMAT(//10X,'ICE FLOE COLLISION JUDGEMENT FROM',
     1       1X,A9,'ACCELERATIONS'//
     1       22X,'Program File: JUDGE.FOR'/
     1       22X,'Data    file:',1X,A20,'via ',A20/
     1       22X,'Result  File:',1X,A20//
     1       17X,'Directions : ',1X,'1--North; 2--West;
     1                              3--Vert.'/
     1       17X,'Cycles MEAN: ',1X,'SUM/3'/
     1       17X,'Collis MEAN: ',1X,'SUM'/
     1       17X,'Prop.      : ',1X,'Collis/Cycles'/
     1       17X,'CCollis    : ',1X,'1 Coll. Half Cycle
     1                              at Most'/
     1       17X,'CProp      : ',1X,'1 Coll. Half Cycle
     1                              at Most'//)
1002  FORMAT(4X,'Data Block',2X,' AccDir.',3X,' Cycles',3X,
     1 ' Collis',3X,' Prop.',3X,' CCollis',3X,' CProp.'/
     1 '    ----------------------------------------
     1 ----------------------------'//)
```

```
1       DO I=N1, N2
        READ (5,*) A(I,1), A(I,2), A(I,3)
        END DO
        G1=(N1-1)/2430
        G2=N2/2430-1
        DO 520 J1=G1,G2
        H1=2430*J1+1
        H2=2430*(J1+1)
        CYCLES=0
        COLLIS=0
        PROPOR=0
        COLCOM=0
        PROCOM=0

        DO 510 DI=1,3
        X=0
        Y=0
        K=0
        J=0
        L=0
        Q=0
        Y1=0

        DO 500 I=H1,H2
        IF (A(I,DI)*A(I-1,DI)) 10, 500, 500
10      K=K+1
        IF (K.EQ.2) GOTO 100
        J=I
        GO TO 500
100     L=I-1
        X=X+1

        DO 300 M=J+1, L
        S(M,DI)=A(M,DI)-A(M-1,DI)
        IF (S(M,DI)*S(M-1,DI)) 150, 300, 300
150     P=P+1
300     CONTINUE

        DO 400 M=J+1,L
        IF (S(M,DI)*S(M-1,DI)) 340, 400, 400
340     GO TO (350,360,370), DI
350     Q=P
        GOTO 400
360     IF (S(M,DI-1)*S(M-1,DI-1).GE.0) Q=Q+1
        Q=Q
        GO TO 400
```

```
370     IF (S(M,DI-1)*S(M-1,DI-1)) 377,375,375
375     IF (S(M,DI-2)*S(M-1,DI-2).GE.0) Q=Q+1
377     Q=Q
400     CONTINUE

        IF (P.GE.2) Y=Y+1
        IF (Q.GE.2) Y1=Y1+1
C       PRINT*, J, L, X, Y
        P=0
        Q=0
        K=1
        J=L+1
500     CONTINUE
        T(DI)=X/2
        U(DI)=Y
        V(DI)=Y1
        WRITE(6,1000) H1, H2, DI, T(DI), U(DI), U(DI)/T(DI),
     1                V(DI), V(DI)/T(DI)
1000    FORMAT(I7,' -',I7,1X,I4,6X,F6.1,4X,F6.1,4X,F7.4,3X,
     1         F6.1,3X,F7.4)
        CYCLES=CYCLES+T(DI)
        COLLIS=COLLIS+U(DI)
        PROPOR=PROPOR+U(DI)/T(DI)
        COLCOM=COLCOM+V(DI)
        PROCOM=PROCOM+V(DI)/T(DI)
510     CONTINUE

        CYCLES=CYCLES/3
        WRITE(6,3000)  CYCLES, COLLIS, PROPOR, colcom, procom
3000    FORMAT(5X,' MEAN',18X,F5.1,5X,F5.1,4X,F7.4,4X,F5.1,
     1         3X,F7.4//)
520     CONTINUE
        STOP
        END
```

Appendix F

Fortran Program for Transformation of Acceleration Direction

```
**********************************************************************
**********              FORTRAN PROGRAM                      *********
*                                                                    *
*            Accelerations Transformed into Tp Wave                  *
*            Direction from Two Original Horizontal                  *
*                          Accelerations                             *
*____________________________________________________________________*

*                          file: PKG6.FOR                            *


      INTEGER ROW
      DIMENSION A(50000, 6), B(50000), C(50000, 2)
      CHARACTER*32 FILE1, FILE2
      TYPE*, 'Input data file name1'
      ACCEPT88,file1
      TYPE*, 'Input output file name2'
      ACCEPT88,file2
88    FORMAT(A32)
      OPEN (UNIT=10, FILE=FILE1, STATUS='OLD')
      OPEN (UNIT=11, FILE=FILE2, STATUS='NEW')

      TYPE*, 'How many data rows ?'
      READ*, ROW
      READ (10,*) ((A(I,J), J=1,6), I=1,ROW)

      DO K=1,ROW
      B(K) = SQRT( A(K,1)**2 + A(K,2)**2  )
      END DO

      BT=-58
      PI=3.14159
      BT1=BT/360*2*PI

      DO K=1,ROW
      S=A(k,2)/A(k,1)
      AL=ATAN(S)
      IF (S) 10,100,30
C     S<0: AL<0;   A(K,1)<0: 2nd;   A(K,1)>0: 4th
10    IF (A(K,1)) 15,100,17
15    AL=PI+AL
      GO TO 100
17    AL=2*PI+AL
      GOTO 100
C     S>0: AL>0;   A(K,1)<0: 3rd;   A(K,1)>0: 1st
30    IF (A(K,1)) 35,100,100
35    AL=PI+AL
      GO TO 100
```

```
100     AL1=AL-BT1
        C(K,1)=B(K)*COS(AL1)
        C(K,2)=B(K)*SIN(AL1)
        AL=AL/PI/2*360
        AL1=AL-BT
        WRITE (11,*) C(K,1), C(K,2), A(K,3), AL, AL1
        END DO

        STOP
        END
```

Bibliography

Bjorkenstam, U., and Lindgren, M. (1989). " Wave Interaction between Two Floating Bodies, " *POAC'89, Proceedings* , pp.627-637.

Cammaert, A.B., and Muggeridge, D.B. (1988). *Ice Interaction with Offshore Structure*, Van Nostrand, New York, 432 p.

Carter, D., Ouellet, Y. , and Pay, P. (1981). " Fracture of a Solid Ice Cover by Wind-induced or Ship-generated Waves, " *POAC'81, Proceedings*, Vol.2 , pp.843-851.

Chatfield, C. (1983). *Statistics for Technology*, 3rd ed., Chapman and Hall, New York, 380 p.

Dean, R.G. and Dalrymple, R.A. (1984). *Water Wave Mechanics for Engineers and Scientists*, Prentice-Hall Inc., Englewood Cliffs, New Jersey, 353 p.

Goodman, D.J., Wadhams, P., and Squire, V.A. (1980). " The Flexural Response of a Tabular Ice Island to Ocean Swell, " *Annals of Glaciology*, 1, pp. 23-27.

Harms, V.W. (1986). " Ice-floe Wave Drift Experiments, " *OTC*, Vol.1, pp. 9-15.

Hastings, N.A., and Peacock, J.B. (1976). *Statistical Distributions*, Butterworth *and* Co., London, 130 p.

Kannan, D. (1979). *An Introduction to Stochastic Processes*, North Holland, New York, 296 p.

Kristensen, M., and Squire, V.A. (1984). " Modeling of Antarctic Tabular Icebergs in Ocean Waves, " *Annals of Glaciology*, 4, pp. 152-157.

Martin, S., and Kauffman P. (1981). " A Field and Laboratory Study of Wave Dumping by Grease Ice, " *J. Glaciology*, 27 (96): pp. 283-314.

McCormick, M.E. (1983). *Ocean Engineering Wave Mechanics*, John Wiley *and* Sons, New York, 179 p.

Murray, J.J., Guy, G.B., and Muggeridge, D.B. (1983). " Response of Modelled Ice Masses to Regular Waves and Regular Wave Groups, " *Oceans'83, Proceedings*, Vol.2, pp.1048-1052.

Newman, J.N. (1977). *Marine Hydrodynamics*, MIT Press, 402 p.

Sachs, L. (1982). *Applied Statistics*, 2nd ed. , Translated by Reynarowych, Z., Springer-Verlag, New York, 707 p.

Sanderson, T.J.O. (1988). *Ice Mechanics*, Graham *and* Trotman, London, 253p.

Sarplaya T. and Isaacson, M. (1981). *Mechanics of Wave Forces on Offshore Structures*, Van Nostrand Reinhold Co., New York, 651 p.

Shapiro, A., and Simpson, S. (1953). " The Effect of a Broken Icefield on Water Waves, " *Oceanography*, Vol. 34, No.1, pp.36-42.

Squire, V.A. (1989). " Super-critical Reflection of Ocean Waves; A New Factor in Ice-edge Dynamics ? " *Annals of Glaciology*, 12, pp. 157-161.

Yuen, C., and Lasca, N.P. (1989). " Fracturing of an Ice Sheet by Ship-induced, Ice-coupled Waves, " *Cold Regions Science and Technology*, Vol.16, pp.75-82.